THE PROCEEDINGS OF THE PHYSICAL SOCIETY

Section A

VOL. 65, PART 1 1 January 1952 No. 385 A

EDITORIAL

Fellows of the Physical Society will realize that during the last few years the size of the *Proceedings* has significantly increased. The Papers Committee and Council have had to decide that this continued expansion must now be checked, both because of increases in the cost of paper, of printing and of the other services ancillary to publishing, and also because of the increasing difficulty of obtaining, for example, sufficiently large allocations of paper.

In the matter of actual presentation of papers assistance can be given by the way in which diagrams and mathematics are prepared. Diagrams should be displayed in such a way as to take a minimum of space, e.g. a shallow, wide diagram is preferable to a long, narrow diagram, and individual single curves can often be superposed in one framework. In general no elementary mathematical steps should be included in a paper, and every effort should be made to reduce tables to a minimum, and to replace any series of values, wherever possible, by the mean and a standard deviation. The co-operation of Fellows of the Society can materially assist in procuring these small but necessary economies.

Papers are still sometimes written in an unduly verbose style. If the referees of such a paper have made no objections and the paper is accepted, its undue length makes inroads into the publication space available. If the referees do object, the typing of referees' reports and additional communications to authors and referees places an extra burden on the secretarial staff. If authors ensured that their papers were written in a concise style, considerable advantage would result: submitting a manuscript to a critical colleague can be a useful check.

Recently an increasing tendency has been noticed for authors, both individual and in research establishments, to submit for publication papers which contain interim experimental results, or tentative conclusions from their work. It is felt that the value of such articles would be greatly increased if their publication were withheld until more final results and conclusions were established. Moreover, much valuable time on the part of the referees of the papers, and of the office staff, could be saved if authors would consider this point more seriously before submitting papers for publication.

H. H. HOPKINS,
Honorary Papers Secretary.

A Spectroscopic Investigation into the Structure of Diffusion Flames

By H. G. WOLFHARD and W. G. PARKER
Royal Aircraft Establishment, Farnborough, Hants.

Communicated by A. C. Egerton ; MS. received 15th May 1951

ABSTRACT. Ammonia–oxygen, ethylene–oxygen and other diffusion flames were examined spectroscopically using the flat flame technique described in a previous paper. Each flame is shown to consist of a main reaction zone where the temperature is a maximum. The emission from this zone is thermal, and the component gases are in chemical equilibrium. On either side of the main reaction zone there is a region with a steep temperature gradient which constitutes a pre-heating zone. Fuels such as hydrocarbons or ammonia and oxidizers such as nitric oxide undergo chemical change in these pre-heating zones. On the fuel side the change is principally a thermal decomposition because the main reaction zone presents a barrier to oxygen penetration. Thus carbon formation in hydrocarbon diffusion flames is essentially a pyrolytic process. The application and value of absorption spectroscopy are discussed and quantitative measurements of the concentrations of molecular oxygen and OH radicals are recorded which could not have been otherwise obtained. These results and a number of qualitative observations clearly show that diffusion flames with oxygen at atmospheric pressure have the structure predicted for a flame in which diffusion is the rate determining process. A number of differences are described between the characteristics of diffusion and pre-mixed gas or Bunsen flames.

§ 1. INTRODUCTION

A new technique for the investigation of diffusion flames which was developed by the authors has been described in a previous paper (Wolfhard and Parker 1949). The principal feature of the technique is the very full use of absorption spectroscopy which can be made with it. It has now been applied in a more quantitative way and from a detailed study of one particular problem, viz. the diffusion flame with oxygen, a number of new facts have been obtained which are considered in relation to the structure of the flame. These facts help to show the essential differences between diffusion flames and those of the pre-mixed gas or Bunsen type.

§ 2. DISCUSSION OF THE MECHANISM OF DIFFUSION FLAMES

In order to obtain a mental picture of the physical processes in a diffusion flame let us suppose that we have two gases such as hydrogen and oxygen enclosed in a box and separated by a diaphragm. If the diaphragm can be removed and the gases lit instantaneously at their interface then the temperature will rise at this interface by the production of heat. After a very short interval of time the gases close to the interface will reach equilibrium and will have a definite composition of H_2O, H_2, H, O_2, O and OH, which will not change unless the temperature changes. Two processes will now occur:

(*a*) Heat will flow towards the unburnt hydrogen and oxygen, and will raise the temperature of these gases. The velocity with which this heat travels is governed by known laws of conductivity and is essentially an error function, i.e. the heat travels rapidly at first on account of the steep temperature gradient near the source and then more slowly as the distance increases. Since the thermal conductivity changes markedly with temperature it is not feasible to calculate this heat flow.

(*b*) The unburnt hydrogen and oxygen will diffuse into the zone of burnt gases where their partial pressures are low. This diffusion process will be rather rapid near the hot burnt gases and slower in the colder layers outside because the diffusion coefficients increase with increasing temperature.

The entry of fresh gas into the zone of burnt gases would raise the partial pressures of the hydrogen and oxygen above the equilibrium amount. At the high temperature involved however the velocity of the chemical reaction is so great that equilibrium is achieved at once and the heat released in the process replaces the heat lost by conductivity.

Thus our conception of a diffusion flame is that of a mass of hot burnt gas formed at the centre. Diffusion, which is a relatively slow process, tends to change the composition of this gas but chemical reaction follows very rapidly and does not allow any chemical potential (i.e. non-equilibrium condition) to develop. The mass of hot burnt gas grows thicker and the gradient of partial pressures of the hydrogen and oxygen away from the centre becomes less steep. The overall velocity of combustion therefore slows down until the final flame temperature is reached and the partial pressure of each constituent of the burnt gas is uniform.

Gases at the centre which are at 2000° c or higher should begin to radiate especially if carbon monoxide, oxygen and OH molecules are present. Some ionization will take place and the recombination of ions and electrons will cause emission of weak continuous light in the visible region of the spectrum. The light emitted by the flame comes from regions of sufficiently high temperature for gas radiation and does not necessarily indicate the point of combustion. In this respect diffusion flames contrast with pre-mixed gas flames where the radiation of the inner cone comes directly from the reacting molecules. Thus the OH, C_2 and CH radiations of the inner cone of a pre-mixed hydrocarbon–air flame are not those of molecules in thermal equilibrium (Gaydon and Wolfhard 1948).

The conditions on ignition of the gases in the hypothetical case of the box are brought about in effect in the flat diffusion flame mentioned previously. If the burner (Wolfhard and Parker 1949) is supplied with hydrogen and oxygen at carefully controlled rates, two parallel streams of these gases emanate with equal velocities and laminar flow from the two internal rectangular tubes of the burner. When the flame is lit a series of events similar to those described for the box occurs in a vertical direction. Thus a stationary flame is obtained which has an end-view similar to that shown in the photographs, figs. 1 and 2.

This concept of what may be termed the ideal diffusion flame is certainly an extreme case and is based on the assumption that the diffusion of the reactants and not the reaction velocity is the rate determining process in the flame. This assumption is believed to be valid for the following reason.

A pre-mixed stoichiometric flame of ethylene and oxygen has a flame velocity of about 600 cm/sec and a reaction zone of only 0·005 cm thickness. Thus the mean rate of conversion is about 4 mole of oxygen burnt per cm^3

per second. The final flame temperature which may be calculated is only reached after the gases have passed through the inner cone of the flame. It appears therefore that this very high reaction velocity is achieved in a part of the flame where the temperature is probably below the final temperature.

In the diffusion flame combustion is rapid at first and then slows down until everything has been burnt but the reaction always takes place at a temperature close to the final temperature. At this temperature the activation energy of the reaction can be overcome and a high concentration of free radicals is presumably present to assist combustion. In spite of these advantages the reaction velocity is small compared with that of the pre-mixed gas flame. For example the rate of combustion in a diffusion flame of ethylene and oxygen was measured on our burner. With 50 cm^3/sec of each gas emanating from the two parallel tubes (each 5 cm × 1 cm) the flame had a height of 7 cm and a reaction zone about 1 cm thick. The mean rate of conversion was therefore of the order 6×10^{-5} mole of oxygen burnt per cm^3 per second. This rate is nearly five orders lower than that of the corresponding pre-mixed gas flame alhtough conditions of temperature and radical concentration should be favourable to the diffusion flame. It must be concluded therefore that the rate of combustion is not fixed by the reaction velocity but by the rate of diffusion of the reacting molecules. In such cases it is probably justifiable to regard the diffusion flame as a zone of hot gases in chemical equilibrium where diffusion processes create small concentration and temperature changes which are very quickly brought back into equilibrium by chemical reaction.

This conception of the diffusion flame only holds in ideal cases, however, such as those of the oxygen flames investigated here. In flames which have a lower temperature and a lower reaction velocity pre-mixing may occur in the reaction zone and some chemical potential may develop there. Diffusion will then cease to be the sole rate determining process. It is possible that air flames will come into this category but the question has not yet been investigated. Low pressure conditions may also change the relative rates of diffusion and chemical reaction. Thus if we imagine that the pressure of hydrogen and oxygen in our box is only 1 mm Hg instead of 760 mm Hg the reaction velocity assuming a second order reaction will be only $(1/760)^2$ but the diffusion rate will be 760 times greater. Mixing by diffusion will be almost instantaneous whereas reaction will take an appreciable time. We shall have in fact a pre-mixed gas flame. Experiments in support of this argument are mentioned later.

§3. APPLICATION OF ABSORPTION SPECTROSCOPY TO DIFFUSION FLAMES

Up to the present spectroscopic studies of flames supported on a round tube have been limited by the geometry of the flame. Thus the important reaction zone presents a three-dimensional problem in which it is impossible to locate the emitters exactly or to apply absorption spectroscopy satisfactorily. The emission spectrum which is obtained is only a measure of the concentration of the unexcited atoms or molecules when these are in thermal equilibrium and there is no self-absorption. Moreover the correlation of the strength of emission and concentration is a difficult matter, and can only be used in a few special cases to get an approximate value of the number of unexcited molecules. In the flat diffusion flame the reaction zone at ordinary pressure is 5–10 mm thick and has an optical depth of 5 cm or more. The thickness of the reaction zone may be seen in the photographs of the end-view of the ammonia and ethylene flames, figs. 1 and 2 respectively. It is therefore practicable to get absorption as well as emission spectra of reacting molecules. This is an important advance since the strength of the absorption gives a direct measure of the number of molecules involved and thus the concentration, as well as the exact location, of some of the molecules may be obtained.

As regards the general optical arrangement which is used for investigations with flat flames, it is essential to have quartz-fluorite achromatic lenses otherwise it is impossible to focus light of all wavelengths from the flame on to the slit of the spectrograph. The lens used between the flame and the spectrograph had a focal length of 40 cm and a diameter of 2·4 cm. It was stopped down to 0·8 cm in a direction parallel to the direction of gas flow. A very small aperture was employed in order that the different light zones of the 5 cm long flame would not overlap appreciably in the image. By placing the lens 80 cm from the flame unit magnification was obtained and the overlapping in the image of the flame was not greater than ± 0·01 cm.

Figure 1. Photograph of NH_3–O_2 flame; end view, actual size.

Figure 2. Photograph of C_2H_4–O_2 flame; end view, actual size.

In absorption experiments a spurious absorption effect was noticed which was caused by refraction. Light from the background light source had to pass through the flame and therefore through regions with steep temperature gradients. In doing so it was refracted (as in a Schlieren system) away from the lens and was partially or wholly missing from the image on the slit. The impression of a continuous absorption was thus obtained from the photographic plate. This effect was troublesome at first until the reason was established. Fortunately, it only occurred outside the main flame in regions of lower temperature. Schliere develop in regions of rapid change in refractive index, i.e. where $1/T$ changes rapidly in hot gases, and are therefore strongest at rather low values of the absolute temperature T.

.A
5
2

Interpretation of Absorption Spectra

The spectrographs used gave strong and measurable absorption but did not truly resolve the lines of band spectra. The measured strength of such an absorption is a complicated function and depends *inter alia* on whether the line width consists mainly of Doppler broadening or of collision broadening. Van der Held (1931) has considered the problem and has concluded that for pure collision broadening the absorption strength is proportional to the number of absorbing centres. For pure Doppler broadening on the other hand, the strength of the absorption increases proportionally at first but quickly approaches a saturation value. Practically there is a combination of these two effects, and in the present investigation it was found that the absorption increased proportionally at first but that the rate of increase subsequently became smaller with increasing numbers of absorbing centres.

These results indicate that the absorption coefficient is not proportional to the number of absorbing centres, i.e. Beer's law does not hold. To overcome this difficulty we compared the strength of absorption in the flame under investigation with the absorption in another flame where conditions were known. A number of precautions were necessary which are best described in relation to a particular system. In the OH system we used the (0, 0) band with its head at 3064 Å. The absorption is only slightly affected at different temperatures by the changing population in different vibrational levels because most of the molecules are in the lowest vibrational state at the temperatures encountered. Within this band some Q lines in front of the second head ($Q\,3\frac{1}{2}$, $4\frac{1}{2}$, $5\frac{1}{2}$, $6\frac{1}{2}$) are most sensitive. The strength of absorption for the rotational levels changes with temperature and the change in population may be calculated. These changes inside the rotational population were small for the temperature range covered by our measurements, viz: 2200° c–2800° c, and could be disregarded because the overall accuracy of measurement of the OH and O_2 concentrations was estimated to be about 20–30%.

The strength of the absorption could be calibrated in terms of the OH concentration by the use of a pre-mixed gas flame of similar optical depth. Pre-mixed gas flames are in chemical equilibrium above the inner cone and a pre-mixed gas flame of ammonia–oxygen or ethylene–oxygen was burned on a thin burner of about 0·3 mm width which had a length of 5 cm, similar to the optical depth of the flat diffusion flame. The flame velocity of the pre-mixed gases is high and it is reasonable to assume that at a distance of 1–2 mm above the inner cone where the flame width is 8–10 mm the temperature reaches the theoretical flame temperature corresponding to the mixture strength. The theoretical flame temperatures and equilibrium concentrations of the gaseous products corresponding to the temperature are shown in figs. 7 and 8 plotted against the mixture strength. The latter is expressed as the ratio $n_O : n_H$. It has been assumed that there is no external heat loss and it was also ascertained that no undecomposed ammonia passed through the ammonia–oxygen flame even at very low $n_O : n_H$ ratios. Similarly in the ethylene–oxygen flames no carbon formation occurred in the $n_O : n_H$ range covered by the graph of fig. 8.

At low $n_O : n_H$ ratios, i.e. in fuel-rich mixtures, the OH concentration rises steeply towards the stoichiometric ratio and falls again more gently as the $n_O : n_H$ ratio increases above stoichiometric. Mixtures in the region of the stoichiometric and on the fuel-rich side were therefore used for getting a calibration curve of absorption strength versus the OH concentration. The absorption strength was taken as the ratio of the intensity in the absorbing line to the intensity of the unabsorbed continuum (of the light source) beside the line. The intensity in each case was estimated from the density of the plate after the latter was calibrated in the usual way. A Hilger large Littrow-type spectrograph was used for the OH system in conjunction with the anode of the carbon arc as background illumination.

In comparing the strength of the OH absorption from the pre-mixed flame with that in the diffusion flame, it is necessary to have a similar gas composition (i.e. H_2O, H_2, O_2 etc.) in each case because these gases affect the collision broadening of the OH. This was done as far as possible, though small variations would presumably cause only small errors since collision broadening itself does not contribute much to the width of the line in very hot flames.

Measurements of oxygen concentration were more restricted than those of the OH molecules. Molecular oxygen cannot be measured in its (0,0) Schumann–Runge band as this has a low transition probability and is outside the range of the quartz spectrograph. Hot oxygen absorbs, however, because higher vibrational levels are excited which permit a transition to the upper electronic state above 2000 Å. Both pre-mixed and diffusion flames using oxygen show strong oxygen absorption in the region 2200 Å and in cases of excess oxygen this absorption may be followed up as high as 2600 Å. Although this absorption has been observed before (Füchtbauer and Holm 1925), a satisfactory analysis has not been achieved up to the present. The strength of the absorption clearly depends on the temperature of the flame and it is advisable to measure as far as possible in the far ultra-violet region to minimize the temperature effect. Information on collision broadening is not available. The concentration of oxygen molecules in pre-mixed gas flames is only appreciable for lean mixtures and in the diffusion flame a high concentration occurs only on the oxygen side of the main reaction zone. The actual calibration of the strength of the absorption against the oxygen concentration was done in the manner described above using oxygen-rich pre-mixed gas flames. It was fortunate for the accuracy of the measurements that the temperature in the hottest part of the diffusion flame is close to the temperature of the stoichiometric pre-mixed gas flame and the strengths of the O_2 absorption seemed just about to match. Moving from the point of highest temperature outwards on the oxygen side the O_2 concentration increased while the temperature decreased. Pre-mixed gas flames had a similar trend as the mixture strength was weakened off. On the outside of the diffusion flame where the oygen was cold there was no absorption, and no comparison could be made. The main interest of this work, however, centred round the high temperature region of the diffusion flame. A check on the method was afforded by using two oxygen lines of different wavelength (corresponding to different vibrational levels of the ground state) and comparing the results. A Hilger medium quartz spectrograph was used for these measurements.

§4. EXPERIMENTAL RESULTS

4.1. *The Ammonia–Oxygen Flame*

Ammonia and oxygen were reacted in the flat diffusion flame. The appearance of this flame was described in our previous paper and two facts established by the earlier work were assumed in the present investigation, viz. (i) the emission in the flame is of thermal origin as proved by the fact that line reversal measurements with OH radicals and sodium atoms gave the same temperature, and (ii) the ammonia does not burn directly with oxygen but first undergoes thermal decomposition via NH_2 and NH. Quantitative measurements of the OH and O_2 molecules were made in the way described above. The results are shown graphically in fig. 3, which represents a cross section through the reaction zone 1 cm above the top of the burner. The ammonia is on the left side and the oxygen on the right. The temperature as measured by sodium line reversal method is also shown.

Fig. 4(*a*) (Plate) shows a spectrogram of the visible and near ultra-violet region of an ammonia–oxygen flat diffusion flame. It should be read with the end view of the flame in mind (figs. 1 and 2). The abscissa is the plot across the reaction zone and the ordinate is the spectral wavelength. Beginning from the fuel side (on the left) the ammonia-α bands which are attributed to NH_2 radicals can be seen first, closely followed by the NH bands. After a clear gap in emission the main reaction zone follows with a faint continuum in the visible region caused by electron–ion recombination processes, and strong OH bands. Some bands of molecular oxygen can be seen a little further towards the oxygen side.

The ammonia absorption spectrum could not be measured quantitatively because it depends strongly on temperature. It was possible however to decide where all the ammonia was used up. This is denoted by the point A (fig. 3). As the ammonia approached the hot part of the flame it was observed in regions of fairly high temperature ($>1\,000°$ c). It began to disappear rapidly at about 2 100° c at which point NH_2 and NH radicals appeared in emission. This dehydrogenation was very unlikely to be a thermal dissociation in chemical equilibrium for several reasons. The equilibrium partial pressures of ammonia are negligible at temperatures of 1 000° c and above even in an atmosphere of nitrogen and hydrogen. Moreover it is believed that the amount of NH (and probably of NH_2) which accompanied the disappearance of the ammonia in the temperature region of 2 100° c was also greater than the chemical equilibrium value. Although the NH bands are of thermal origin they are only strongly emitted in the position indicated in fig. 3. Some NH molecules may be present in equilibrium amounts all over the reaction zone and their existence is favoured in the reducing gases on the left side of the flame, but the amounts are exceedingly small as shown by Ward and Hussey (1949). The estimated partial pressure is of the order of 10^{-7} which is too low a concentration for detection by absorption. The non-equilibrium decomposition of the ammonia gas is thus established and is an important difference in the course of the reaction in this part of the flame compared with the main reaction zone where the hydrogen and oxygen react and chemical equilibrium is maintained.

How the decomposition of the ammonia occurs is a matter for speculation. It is known that ammonia is very stable in the absence of surfaces and other catalysts and does not decompose with appreciable velocity below about 2 000° c (Frank and Reichard 1936). In this flame dehydrogenation may be brought about by radicals diffusing from the main reaction zone which is some distance to the right as indicated by the peak of the temperature curve, fig. 3. It has been pointed out previously that the dehydrogenation does not involve simultaneous oxidation to water since the oxidation process is strongly exothermic and the temperature distribution would differ from that found experimentally. The actual heat liberation occurs further to the right (fig. 3). The decomposition of the ammonia therefore goes to N_2 and H_2 via NH_2 and NH.

The hydroxyl radical concentration was measured quantitatively from the absorption spectra in the way described in § 3. This is expressed as the percentage partial pressure of OH (fig. 3). The maximum concentration is on the right of the position of maximum temperature, and this is to be expected since water (the main product of combustion) and oxygen in equilibrium give a higher partial pressure of OH than the combination of water and hydrogen which exists on the left of this temperature line. The strength of the OH emission bands depends on radical concentration and temperature and the peak is therefore shifted towards the position of maximum temperature.

The oxygen concentration was measured quantitatively with two lines of different wavelengths. Below about 2% partial pressure of oxygen the absorption lines were too weak for measurement. Above about 40% of oxygen a difficulty arose from the nature of the flame. Absorption which is temperature-dependent occurred in a region of rapidly falling temperature on the outside of the flame. Reliable estimates of the oxygen concentration could not be made under these conditions. Between the limits of 2% and 40%, the results with the two lines agree quite well, and at the position of maximum temperature the partial pressure was found to be about 4%.

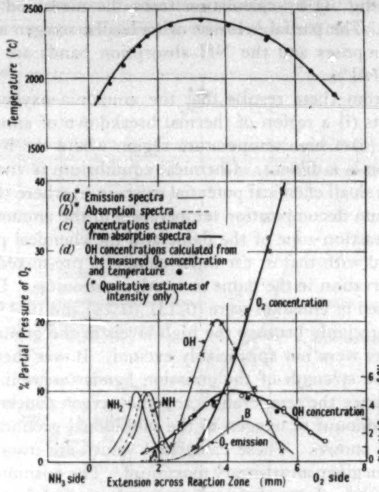

Fig. 3. Ammonia–oxygen flat diffusion flame.

These results provide measured values of the temperature, and the concentrations of OH radicals and oxygen molecules in certain parts of the main reaction zone. Although we do not know *a priori* the $n_O : n_H$ ratio across the zone we can calculate the partial pressure of every component at any point in this zone provided our conception of the diffusion flame is correct, i.e. provided chemical equilibrium is effectively maintained in this part of the flame. To calculate the concentrations of each component we need the temperature and the experimental value for the concentration of either the OH or oxygen molecules. Since the results contain measured values of both these types of molecules in various parts it is possible to cross-check this method by assuming one component and calculating the other. This was done, and the partial pressures of OH radicals calculated from the measured values of oxygen are shown as full point circles in fig. 3. Agreement is good and may be fortuitous to some extent considering the possible errors involved in the measurement of the temperature as well as in the concentrations of the molecules, but it does suggest that the assumptions about the nature of the high temperature zone are correct as regards the oxygen diffusion flame.

The partial pressure of the oxygen could not be determined experimentally below about 2% for the reasons given above. OH concentration was still high in that part of the flame however and the oxygen curve was therefore extended (dotted portion of fig. 3) by calculation from the measured temperature and OH concentration. The partial pressure of molecular oxygen at the point where the ammonia decomposes and the NH absorption bands are strongest is thus found to be about 0·01%.

We conclude from these results that the ammonia–oxygen diffusion flame consists of two parts (i) a region of thermal breakdown of ammonia to nitrogen and hydrogen and (ii) a high temperature region where the hydrogen burns in oxygen and nitrogen is a diluent. Chemical equilibrium is virtually maintained in this region but a small chemical potential exists in (i) where the temperature is above the equilibrium decomposition temperature of the ammonia. This occurs outside the main reaction zone of the flame and the chemical potential involved cannot be compared with that in the inner cone of a pre-mixed gas flame.

One other observation in the flame is worth mentioning. The oxygen bands most readily obtained in emission were (0, 13), (0, 14) and (0, 15) and these bands did not absorb appreciably because the high levels in the ground state to which the transition occurs were not appreciably excited. It was therefore possible to calculate the relative strength of the emission bands (assuming that they were of thermal origin) since the temperature and the oxygen concentration had been measured and the amount of oxygen in the vibrational ground level of the $B^3\Sigma$ state was therefore known. These calculated values are inserted in the graph (fig. 3) and have been given an arbitrary maximum. The position of the maximum is fixed by the relative effects of oxygen concentration and temperature. The graph also shows the experimental peak for the strength of the O_2 bands denoted by B. Exact measurements of the O_2 emission were rather difficult because the bands were on a strong background. The positions of the peaks of the experimental and calculated values are sufficiently close together, however, to suggest that the oxygen is really thermally excited; the implication of this is discussed later.

4.2. *The Ethylene–Oxygen Flame*

The ethylene–oxygen flat diffusion flame was similar to the methane–oxygen flame examined in our initial work and had a number of advantages for the present investigation. The reaction zone was thicker and very stable and carbon formation was more pronounced and could be readily observed in absorption. An end view of the flame is shown in fig. 2.

Fig. 4(*b*) shows the emission spectra of an ethylene–oxygen flat diffusion flame. This too should be read with the end-view of the flame in mind. Beginning on the left, i.e. on the fuel side of the flame, one can see first the carbon continuum and closely attached to that are the C_2 and CH bands. NH bands which are due to impurities are strongest in the same position as the CH bands but extend well into the main reaction zone. Between the carbon continuum and the main reaction zone there is a well marked dark space. The main reaction zone gives principally a broad continuum which has its origin presumably in an electron–ion recombination process. The OH bands are most prominent in this part but it is remarkable that some OH bands can also be seen right over on the fuel side. The oxygen bands may be seen on the oxygen side of the flame.

The temperatures in this flame were higher than those of the ammonia flame and determination of the temperature curve required the use of a carbon arc. The carbon arc was first calibrated against a standard tungsten lamp using a stepped sector. Flame temperatures determined by OH-line reversal and Na-line reversal were again identical indicating thermal equilibrium. OH and O_2 concentrations were measured as in the case of the ammonia flame and the results are plotted in fig. 5. One of the most striking things about these results is the large distance between the point at which the O_2 concentration becomes very small and the position of the luminous carbon zone. This means that little or no oxygen reaches a part of the flame where the hydrocarbon undergoes extensive chemical change. This can also be seen in fig. 4(*c*). The oxygen absorption lines fail to reach the region marked on the spectrogram which represents the beginning of the absorption by the carbon zone.

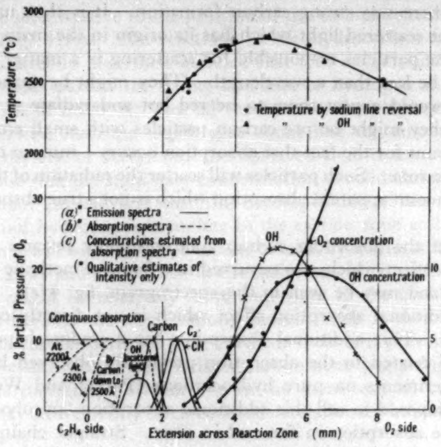

Fig 5. Ethylene–oxygen flat diffusion flame.

Again it is believed that the hot gases in the main reaction zone are in chemical equilibrium. The OH partial pressures were not calculated from the measured oxygen concentrations as a method of cross-checking the experimental results in this system for two reasons: (*a*) The calculation requires a very exact knowledge of the temperatures in the zone and the experimental temperature curve is not so accurate as in the ammonia–oxygen flame; this is because the carbon arc had to be used as the background source for the line reversal method. (*b*) An unknown proportion of the hydrocarbon is precipitated as carbon in the carbon zone. This carbon is effectively lost and the exact $n_C : n_H$ ratio is not known on which to base the calculated chemical equilibrium.

The region in which carbon formed in the flame was examined in more detail. The absorption of the carbon zone was very strong. The absorption occurred somewhat on the left of the emission because of the marked temperature gradient in that part of the flame. The width of the absorption, however, was fairly big and it is doubtful whether the whole of this absorption was due to carbon particles. On the left side of the absorption the temperature is still high and about 2 000° c according to an extrapolation of the temperature curve in fig. 5, yet no continuous radiation was observed. It may also be noted that in the position of this absorption there was a reappearance of OH emission bands. The OH bands, which were strongest in the reaction zone, had faded away before reaching the carbon zone (fig. 4(*d*)). Their reappearance on the fuel side is a curious effect which only occurred when there was strong carbon formation. It is thus unlikely to be a true radiation but scattered light which has its origin in the main reaction zone. The nature of the particles responsible for scattering is a matter of conjecture. Their size must be less than a wavelength. They might be carbon particles in which case one would expect them to be red hot and radiate at the prevailing temperature or they might be pre-carbon particles with small emissivity. The latter would account for the fact that absorption occurs 1 mm on the fuel side of the radiant carbon zone. Such particles will scatter the radiation of the background source and produce an apparent absorption which is not a true absorption obeying Kirchhoff's law.

The width of the absorbing carbon zone gradually became much greater below 2 500 Å, an effect which also occurred in a flame of methane saturated with benzene vapour and may be seen in the spectrogram, fig. 4(*e*). This certainly represents an additional absorption effect which is not directly connected with the carbon zone. This additional absorption has a wedge-shaped appearance and seems to be related to the absorption previously observed by the authors in pyrolysis experiments on pure hydrocarbons (Parker and Wolfhard 1950). It is therefore proposed to call this additional absorption 'pyrolysis absorption' in contrast to the absorption in the carbon zone. Straight chain and aromatic hydrocarbon gases showed such an absorption on heating which spread towards longer wavelengths at higher temperatures. This phenomenon was attributed to intermediate compounds which lead to carbon formation.

It is well known that hydrocarbons alone on heating to 1 000° c or over produce carbon, and the conditions in the diffusion flame in the region considered here are mainly thermal since no oxygen reaches it. Water vapour, carbon dioxide and carbon monoxide are present however and diffuse from the main reaction zone. These gases may react with the carbon particles but their influence as far as pyrolysis and carbon formation are concerned is probably small and largely a dilution effect. We therefore suggest that the carbon formation in an oxygen diffusion flame occurs in the same way as it does in the pyrolysis of a hydrocarbon.

Analysis of spectra was limited on the fuel side of the flame because ethylene does not absorb in the visible and ultra-violet regions. It was not possible therefore to follow its thermal changes in the same way as with ammonia. Acetylene and more especially benzene respond in these regions and, since their reactions in the diffusion flame are probably similar, a few experiments were made with these compounds. Both produce large and embarrassing quantities of carbon in the flat diffusion flame so that acetylene was used diluted with hydrogen, and benzene was introduced into a methane flame by passing methane gas through a benzene saturator.

The absorption bands of acetylene were observed on the fuel side of the flame and reached the region of continuous absorption described above as pyrolysis absorption. Benzene, on the other hand, which absorbs strongly at wavelengths of the order of 2600 Å is not obscured by the pyrolysis absorption as the latter occurs at shorter wavelengths. There was a gap between the breakdown of the benzene as indicated by the disappearance of its absorption, and the onset of the continuous absorption of the carbon zone. It seems clear from these results that the hydrocarbon has ceased to exist shortly after the commencement of the pyrolysis continuum. The distance which the undecomposed benzene diffuses can be seen relative to the position of the carbon zone in the spectrogram of the flame (fig. 4(*e*)). The reactions of the hydrocarbon are thermal (since measurements already described indicate that free oxygen and OH radicals are not present in this part of the flame) and lead to hydrogen and solid carbon in the radiant zone at 2300° c. Not all the hydrocarbon is degraded into carbon however, otherwise methane would give about half the amount of carbon that comes from ethylene or acetylene; the observed ratio is more like 1 : 10.

It is possible that the stationary concentration of solid carbon is controlled by the water vapour present and that the decomposition of the hydrocarbon into solid carbon and hydrogen is complete in the carbon zone at 2000° c to 2300° c but the carbon reacts with the water vapour to form hydrogen and carbon monoxide which diffuse away and are burned in the main reaction zone further to the right. This process might be relatively more important in the case of methane than, say, acetylene because the water vapour concentration is obviously higher.

As soon as carbon particles have formed, their size prevents their transport horizontally by diffusion. The radiant carbon zone beginning near the burner top represents therefore a stream line in the flame and all other spectroscopic phenomena may conveniently be considered in relation to the position of the carbon zone.

A little to the right of the radiant carbon zone (i.e. on the oxygen side) rather weak C_2 bands occurred. These bands appear strongly in flames of pre-mixed hydrocarbon air or oxygen gases but their origin is not understood (Gaydon and Wolfhard 1950). It has been suggested that polymerization of the C_2 molecules is the source of carbon in the flame. Apart from energy considerations and other objections to this suggestion (Parker and Wolfhard 1950) the situation of these bands on the right of the carbon zone proves this suggestion is wrong. Both carbon and C_2 molecules need the same amount of energy for their excitation at the same wavelengths and we should expect the C_2 bands to appear inside the carbon zone or even a little to the left if C_2 molecules are formed before solid carbon. The different intensities of emission of C_2 in pre-mixed and diffusion flames is also worth noting. In pre-mixed flames the C_2 emission gets its strength from non-equilibrium conditions in the flame; in diffusion flames the bands are much weaker.

It seems to the authors that a more likely explanation at least of part of the C_2 bands is that C_2 molecules in the ground state are produced by vaporization of the carbon particles and that these molecules are thermally excited afterwards. It is known that C_2 radiation may be observed at corresponding temperatures in carbon furnaces (Brewer *et al.* 1948). The number of C_2 molecules does not therefore depend on the number of carbon particles but only on the presence of carbon and the temperature. C_2 will thus radiate most strongly at the right-hand side of the carbon cloud and the small shift of the C_2 bands to the right of the radiant carbon zone is readily explained on account of the temperature gradient. Two other observations are also accounted for. Firstly the C_2 bands were weaker in the methane flame than in the hotter ethylene or acetylene flames and secondly the introduction of small quantities of benzene into the methane flame did not affect the intensity of the C_2 bands. In the latter case the amount of carbon increased considerably but the temperature remained about the same.

It is still doubtful, however, whether all the C_2 radiation can be explained in this way in spite of its relatively feeble strength. Observations at different heights in the flame showed that the C_2 and CH radiations were stronger at the base of the flame than at the level normally investigated 1 cm above the burner. This was no surprise since some pre-mixing may be assumed in the 'dead space' at the burner mouth, and the characteristics of a pre-mixed flame in which C_2 and CH are fairly strong was to be expected. The reduction in strength of the C_2 and CH bands was rather gradual however in the vertical direction above the 'dead space'. It is therefore possible that more than one process of C_2 formation and excitation is involved. A distinction between the physical process of evaporation and thermal excitation of C_2 and the chemical process of C_2 formation similar to that in the pre-mixed flame might be attempted by examining the rotational temperature. It has been shown by Gaydon and Wolfhard (1950) that the rotational temperature of the C_2 is abnormally high in the pre-mixed gas flame. The application of this test would be difficult however since the C_2 radiation is very weak and close to the strongly radiant carbon zone.

The reason for the intensity of the CH radiation is also obscure. The absence of CH bands from the spectra of the interconal gases of pre-mixed gas flames indicates that the probable chemical equilibrium concentrations of this radical (Ward and Hussey 1949) are too small to produce any radiation. CH bands are observed in the inner cones of pre-mixed flames but they are not of thermal origin (Gaydon and Wolfhard 1948). The rotational temperature estimated from them is not abnormal and there is consequently no easy method of distinguishing between non-equilibrium and thermal radiation. In the diffusion flame the CH radiation was too weak for temperature measurements by the line reversal method and it was therefore impossible to obtain a value for comparison with the known temperature in that part of the flame. We suggest that the CH is formed chemically by a process such as $C_2 + OH \rightarrow CH + CO$. This reaction is probably very exothermic and may produce CH radicals which are chemiluminescent. On the other hand the CH radicals formed by this process may be thermally excited subsequently. More experimental evidence is required to support or refute the suggestion. In the present work we noticed that the strength of the CH radiation varied at different heights in the flame. It behaved in a similar manner to the C_2 radiation and was stronger at the base than it was higher up the flame.

4.3. *Additional Observations from the Spectra of other Flat Diffusion Flames*

(*a*) *Hydrocarbon–nitric oxide flames.* A hydrocarbon flat diffusion flame could be burnt with nitric oxide instead of oxygen. It seems that combustion occurred because the nitric oxide had time to dissociate extensively into nitrogen and oxygen, and combustion in the main reaction zone was essentially similar to that in the oxygen flame. This could be proved by the presence of lines of the oxygen bands in the main reaction zone. The end view of the flame was also similar to the oxygen flame and apparently divided into the main reaction zone (blue continuum) and a carbon zone (white light). Decomposition of nitric oxide requires a high activation energy and decomposition was not complete even in the main reaction zones. Nitric oxide in quantities greater than equilibrium persisted and diffused into the carbon zone. By using a methane–nitric oxide flame which had only a moderately intense carbon zone it was possible to measure the absorption bands of nitric oxide in the luminous carbon zone. Other bands were also observed and compared with similar bands in the oxygen flame. The CH emission bands had not changed but NH bands were of course stronger in the nitric oxide flame. In the oxygen flame these bands are due to a small amount of nitrogen from impurities. The strength of the carbon emission was perhaps a little greater in the NO flame and this point was carefully noted because nitric oxide is known to act as a chain-breaking molecule. Introduction of nitric oxide as diluent into the fuel of a methane–oxygen flame gave essentially the same result. If carbon formation is a chain reaction the nitric oxide might be expected to cause a reduction in carbon formation when oxygen is replaced by nitric oxide or when nitric oxide is introduced into the fuel. This effect was not observed.

(*b*) *Carbon monoxide–oxygen diffusion flame.* The flat diffusion flame of carbon monoxide gave principally radiation in the main reaction zone and this consisted of a strong continuum extending far into the ultra-violet region. At about 4 000 Å there were some bands superimposed on the continuum and these were identified as the so-called carbon monoxide flame spectrum. The bands are probably emitted by CO_2. Besides this system there were some OH bands due to moisture and these could be seen even in absorption. The Schumann–Runge oxygen bands were also present. The relative positions of these bands is of interest because Hornbeck has recently suggested that part of the reported CO_2 band structure is attributable to the O_2 bands (Hornbeck and Hopfield 1949). Fig. 6, which records the results obtained from the spectrogram of the carbon monoxide–oxygen flame, indicates that this suggestion is wrong because the two systems may be seen separated in space. The oxygen bands occur much more on the oxygen side than the CO_2 bands and their separation in this way is proof of their independence.

(*c*) *The hydrogen–oxygen diffusion flame.* This flame was considered in the previous paper and it was mentioned that the oxygen bands appeared strongly in emission and could be observed from 4 000 Å down to 2 400 Å and even lower. It has since been suggested that excitation of oxygen molecules in flames is not of thermal origin because the Schumann–Runge bands require a very high excitation energy. Thus in the carbon monoxide–oxygen pre-mixed gas flame Laidler (1949) proposed the following mechanism: $CO_2^* + O_2 \rightarrow O_2^* + CO_2$ in which an excited CO_2 molecule hands on its energy during collision to an oxygen molecule. The hydrogen flame provided an opportunity for deciding whether the O_2 radiation was thermal or due to chemiluminescence, because the oxygen bands stood out clearly on the spectrogram and were not partially obscured by a continuum as in the carbon monoxide flame. The method employed was to measure the excitation temperature by the line reversal technique and compare the result with the theoretical flame temperature. A hydrogen discharge lamp was used as the background light source and this was previously calibrated with

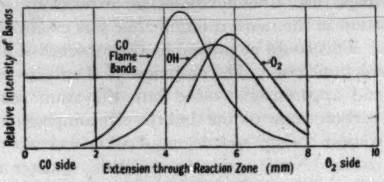

Fig. 6. Relative position of OH, O_2 and CO flame bands in the carbon monoxide–oxygen flat diffusion flame.

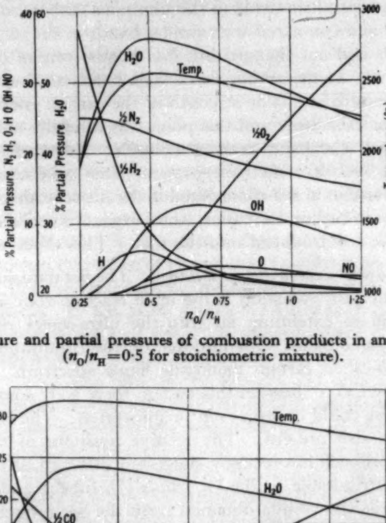

Fig. 7. Temperature and partial pressures of combustion products in ammonia–oxygen flames ($n_O/n_H=0{\cdot}5$ for stoichiometric mixture).

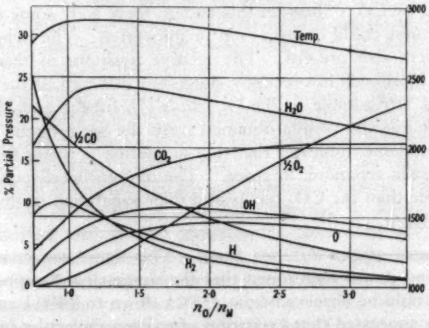

Fig. 8. Temperature and partial pressures of combustion products in ethylene–oxygen flames ($n_O/n_H=1{\cdot}5$ for stoichiometric mixture).

a carbon arc. The brightness of the carbon arc was assumed to be 3800° K independent of wavelength. The line reversal measurement was not easy because it required a long exposure time. The accuracy was probably not high but a reversal temperature of 2800° C ± 60° C was estimated and this agreed well with the temperature of the main reaction zone. The oxygen molecules like the OH molecules were therefore thermally excited in the flame, a result which was also suggested by the position of the O_2 emission bands in the ammonia, and ethylene–oxygen diffusion flames. The oxygen bands in the carbon monoxide–oxygen flame were weaker than those appearing in the hydrogen–oxygen flame. Hence there is no reason to suppose that the oxygen molecules are not in thermal equilibrium in the CO flame as well.

§ 5. A COMPARISON OF PRE-MIXED AND DIFFUSION FLAMES

The experimental results which have been obtained with oxygen diffusion flames illustrate some of the fundamental differences between these flames and those of the Bunsen type.

Firstly all pre-mixed gas flames start with a high chemical potential which breaks down in the reaction zone. Beyond that zone, i.e. above the inner cone of the Bunsen flame, the hot gases are essentially in chemical equilibrium. The diffusion flame on the other hand never develops large chemical potentials in the main reaction zone. Diffusion endeavours to change the gas composition but chemical reaction occurs at once and restores the equilibrium. This is probably only true in the main reaction zone and some chemical potential may develop during the decomposition of the fuel and oxidizer in the preheating zones on either side of the main reaction zone. Non-equilibrium conditions were observed in the decomposition of ammonia as it approached the main reaction zone and probably also in the decomposition of nitric oxide.

Secondly, there was no evidence of chemiluminescence in the main reaction zone of the diffusion flame, and no evidence of intermediate radicals such as HO_2 or HCO was found in either emission or absorption spectra. The absence of HCO bands in the main reaction zone of the hydrocarbon diffusion flame is understandable, since the principal reactions taking place there are between hydrogen, carbon monoxide and oxygen.

The reaction in the main reaction zone is a relatively slow process. If molecules such as OH, H_2O, CO_2 etc. are formed in an excited state by the reaction they are unlikely to be detected in that state because of the much stronger thermal radiation of the majority of the molecules which are already present in chemical equilibrium. The chemiluminescence of molecules such as CH, HO_2 etc., if formed as intermediates, should be discernible, however, because these molecules are never present in equilibrium. If the HO_2 radical is a comparatively long-lived intermediate of the combustion of hydrogen in oxygen it should be detected by thermal radiation or absorption in a flame of this kind where the long optical depth makes the test very sensitive. No absorption or emission which could be attributed to HO_2 was in fact found. It was characteristic of the diffusion flame that the C_2 and CH radiations were not observed in the main reaction zone, but occurred outside and in close proximity to the carbon zone.

Chemiluminescence is commonly observed in pre-mixed gas flames though it is not the only reason for enhanced radiation. Pre-mixed gas flames of hydrocarbons have a high excitation temperature which shows up particularly in the ultra-violet where the thermal radiation diminishes. This effect may be demonstrated by introducing iron atoms through the medium of iron pentacarbonyl (Gaydon and Wolfhard 1951). The intensity ratio between the iron lines in the far ultra-violet and those in the visible region is abnormal and is comparable with the corresponding ratio obtained in the spectrum of an iron arc. Some lines are more than a thousand times as strong as they should be. In diffusion flames at atmospheric pressure the results were very different. The iron behaved as though it was in thermal equilibrium and the iron lines in the far ultra-violet were very faint. This is an important difference between the two types of flames. It probably arises because in pre-mixed gas flames intermediates such as peroxides occur which cannot be formed in diffusion flames because the oxygen does not come in direct contact with the hydrocarbon molecule.

This fact may also explain the thermal behaviour of the OH radiation in diffusion flames, which again differs from that of pre-mixed gas flames. In the latter the OH radiation is chemiluminescent and possesses a high rotational temperature. It may originate in a reaction such as $CH + O_2 \rightarrow CO + OH^*$. This reaction is very improbable in a diffusion flame since the CH radiation is relatively weak and occurs at a position in the flame where the oxygen concentration is already very low. The OH radiation is thus confined to a region where the OH concentration and the temperature are high. These conditions exist more on the oxygen side of the flame.

Diffusion flames of hydrocarbons and oxygen showed certain changes at very low pressure. In contrast to the pre-mixed gas flame the thickness of the reaction zone did not alter with the pressure but the main reaction zone and the hydrocarbon decomposition zone appeared to merge slowly into one another. Carbon formation became weaker and ceased altogether at very low pressure. C_2, CH and OH radiations grew stronger. Iron pentacarbonyl was introduced and the iron lines again showed a high intensity in the far ultra-violet region indicating a high excitation temperature at low pressures. This change in behaviour of the diffusion flame at low pressure fits into our conception of the flame (§2 *et seq.*). At low pressure the reaction velocity decreases while the diffusion rate increases. The gases in the flame will begin to mix and allow a certain chemical potential to develop before the reaction can complete. The characteristics of the flame will change and some of the characteristics of the pre-mixed gas flame will appear. The increased strength of the C_2 and CH radiations, the high rotational temperature of the OH molecules, and the high excitation temperature of the iron atoms amply support this theory.

Lastly, a clear difference between diffusion and pre-mixed gas flames is shown by the influence of the oxides of sulphur on carbon formation. In pre-mixed gas flames sulphur trioxide promotes carbon formation whereas it has the reverse effect in diffusion flames (Wolfhard and Parker 1950).

§6. CONCLUSION

Visual observation of the flat flame immediately reveals two distinct zones. In the ammonia–oxygen flame there is broadly speaking a yellow zone on the fuel side and a blue zone on the oxygen side with a thin dark space between them. In the hydrocarbon–oxygen flame there is also a yellow zone on the fuel side which is easily recognized as the emission of incandescent carbon particles, and again there is a blue zone on the oxygen side with a dark space between. The similarity between the blue zones in the two flames is very marked and these zones resemble the single zone observed in the hydrogen–oxygen diffusion flame. Optical measurements revealed a great deal of more precise detail and it has now become necessary to label the different regions of the flame in order to avoid confusion. The blue zone is better identified as the main reaction zone because it is the hottest part of the flame. The emission from this zone is thermal and the constituent gases are essentially in chemical equilibrium. On either side of the main reaction zone a steep temperature gradient exists and these outer regions are broadly termed pre-heating zones. Fuels such as hydrocarbons and ammonia and oxidizers such as nitric oxide undergo considerable chemical change in these pre-heating zones. On the fuel side the change is principally a thermal decomposition because the main reaction zone presents a barrier to oxygen penetration.

ACKNOWLEDGMENT

Acknowledgment is made to the Chief Scientist, Ministry of Supply, for permission to publish this paper, which is reproduced with the permission of the Controller of H.M. Stationery Office.

REFERENCES

Brewer, L., Gilles, P. W., and Jenkins, F. A., 1948, *J. Chem. Phys.*, **16**, 797.

Frank, H. H., and Reichard, H., 1936, *Naturwissenschaften*, **24**, 171.

Füchtbauer, C., and Holm, E., 1925, *Phys. Z.*, **26**, 345.

Gaydon, A. G., and Wolfhard, H. G., 1948, *Proc. Roy. Soc.* A, **194**, 169; 1949, *Ibid.*, **199**, 89; 1950, *Ibid.*, **201**, 561, 570; 1951, *Ibid.*, A, **205**, 118.

Hornbeck, G. A., and Hopfield, H. S., 1949, *J. Chem. Phys.*, **17**, 982.

Laidler, K., 1949, *J. Chem. Phys.*, **17**, 221.

Parker, W. G., and Wolfhard, H. G., 1950, *J. Chem. Soc.*, 2038.

Van der Held, E. F. M., 1931, *Z. Phys.*, **70**, 508.

Ward, J. J., and Hussey, M. A., 1949, *3rd Symposium on Combustion, Wisconsin*, p. 601. (Baltimore: Williams and Wilkins).

Wolfhard, H. G., and Parker, W. G., 1949, *Proc. Phys. Soc.* A, **62**, 722; 1950, *Fuel*, **29**, 235.

The Spectrum-Line Reversal Method of Measuring Flame Temperature

By A. G. GAYDON and H. G. WOLFHARD
Chemical Engineering Department, Imperial College, London S.W.7

MS. received 26th *July* 1951

ABSTRACT. Processes of electronic excitation in flames are briefly discussed, and it is shown that if there is lack of equilibrium the reversal temperature may be closer to the effective vibrational temperature of the surrounding molecules than to the mean translational temperature. The lack of radiative equilibrium in all flames will cause measured temperatures to be too low; for a flame with air at 2 000° K using Na the error will be between 3·3° and 1·6° at 1 atm. and more at lower pressure. For hot flames, above 2 700° K, the OH band may be used for reversal measurements; it appears to give satisfactory results and has some advantages over the use of sodium.

§1. INTRODUCTION

THE spectrum-line reversal method of measuring flame temperature is experimentally quite simple and in fairly common use. The method depends on Kirchhoff's law that in equilibrium the emissivity and absorption coefficient at any wavelength must be equal. A method depending on this law was first used for luminous flames containing carbon particles by Kurlbaum (1902), and in 1903 Féry first used the resonance lines of sodium and other metals. The spectrum of a controllable continuous source, such as a strip-filament tungsten lamp, is viewed through the flame to which a little sodium or other metal has been added, and the brightness of the background source is adjusted so that the spectrum line of the added metal is seen neither in emission nor absorption by the flame against the background; the background source is then assumed to have the same brightness temperature as the flame, and hence the flame temperature can be determined by calibrating the background source against a black body. The experimental method has been fully described in a number of papers (Griffiths and Awbery 1929, Henning and Tingwaldt 1928, Loomis and Perrott 1928).

The method depends on the existence of equilibrium in the flame gases, and for flames with air numerous comparisons have been made between temperatures determined by the spectrum-line reversal method and those determined by other methods or calculated from thermochemical data. In the interconal gases of a premixed flame, well above the reaction zone, agreement is generally satisfactory and there is little reason to distrust the method. For the actual reaction zone of a flame, equilibrium is not to be expected, and it would not be surprising if the method gave results quite different from those expected for theoretical flame temperatures; indeed it is not easy to define temperature in the reaction zone of a flame. Our measurements (Gaydon and Wolfhard 1951) in the reaction zones of low-pressure flames have shown quantitatively the existence of abnormally high electronic excitation, and we have also shown more qualitatively that such effects also exist in the reaction zone at atmospheric pressure.

One of the most interesting regions of a flame is that just above the reaction zone or inner cone. Here disagreement between theoretically expected temperatures and those measured by spectrum-line reversal have been reported. Thus Lewis and von Elbe (1943) found that for flames with air the measured temperature was appreciably below the theoretical temperature in the region just above the visible reaction zone, and did not attain the theoretical value until some 6 to 10 mm above the inner cone. On the other hand, for flames of lean mixtures with oxygen, the temperature in this region appears too high. The reason for these discrepancies is not known, although Lewis and von Elbe suggest that it may be due to lag in vibrational excitation of the molecules.

With sodium, absorption in the cooler outer layers of the flame is always likely to give too low a temperature unless precautions are taken. Strong, Bundy and Larson (1949) have made an experimental study of this effect using an interferometer to examine the contours of the spectrum lines.

Experimental work on the sodium-line reversal method for flames with air indicates that provided we are well away from the reaction zone, the method gives reliable results; for very hot flames with oxygen not much work has been done to test it. The physical processes causing electronic excitation in flames do not seem to have been very fully considered. It is our purpose here to discuss these, and the effect that departure from true equilibrium might have on measured temperatures by the reversal method. We shall also discuss the magnitude of errors due to the flame gases not being in radiative equilibrium. For very hot flames there are some practical difficulties in using sodium, and we shall indicate the advantages we have found in using lines of the OH band for the reversal method.

§ 2. MECHANISM OF ELECTRONIC EXCITATION

In electric discharges and arcs the excitation to higher electronic states is caused by impact of free electrons accelerated in the electric field. In flame gases, however, the concentration of electrons is much lower and there is no field. The number of collisions with ordinary molecules is very much greater than with electrons (by a factor of at least 10^6), and since we shall see that excitation by molecules may be fairly efficient, that due to free electrons must be negligible in comparison.

Conversion of energy of electronic excitation into other forms can be studied by the quenching of fluorescence, and then, in equilibrium, we may apply the principle of microreversibility to learn about the reverse processes causing electronic excitation.

We should not expect that large amounts of translational energy could readily be converted into that of electronic excitation, and this is confirmed experimentally by the extreme weakness of quenching by monatomic gases. On the other hand, molecules, either diatomic or polyatomic, are frequently quite efficient in quenching fluorescence. The efficiency varies a great deal with the nature of both the quenching molecule and the excited species. The efficiency may be expressed by the value of the collision cross section σ_{AB}^2. The number of collisions a molecule of type A suffers per second with molecules of type B is

$$\sigma_{AB}^2 . n_B \left[\frac{8\pi \boldsymbol{R} T(M_A+M_B)}{M_A M_B}\right]^{1/2}$$

where n_B is the number of molecules of B per cm^3, $\boldsymbol{R}$ is the gas constant, T the absolute temperature and M_A and M_B the molecular weights of A and B.

Laidler and Shuler (1951) have collected some data (from Norrish and Smith and from Terenin and Prileshajewa) for quenching cross sections in various gases. For excited sodium Na(^{2}P) the following values are given, in (Ångströms)^2:

Inert gases	0	CH_4	0·11
H_2	7·4	C_2H_6	0·17
N_2	14·5	C_3H_8	0·2
CO	28·0	C_2H_4	44
I_2	40·0	C_3H_6	52
Br_2	100·0		

Cross sections for elastic collisions from viscosity data are of the order 10 Å^2, varying of course with the type of molecule. For an excited alkali atom they would be relatively large. Thus we see that the quenching efficiency may be of the order unity, or may be quite small. The general mechanism of energy transfer on collision has been reviewed by Laidler and Shuler (1951) and by Massey (1949). The results are best interpreted by considering the potential energy surfaces of the temporary collision complex. If there is an intersection of surfaces between which a radiationless transition is probable, then there is a chance that during the collision such a transition will occur, and as the complex breaks up it may then leave the products in different electronic states. This may lead in some cases to a dissociation of the colliding molecule, if the energy is sufficient, but more often the energy set free by the change from a high to a lower electronic state will be released mainly in the form of internal vibrational energy. We can see that the efficiency of such processes will depend on the form and position of intersection of the potential surfaces and may therefore vary widely with the nature of the colliding particles.

We may summarize this section by saying that electronic excitation in flames is unlikely to be due to collision with free electrons, or to conversion of translational energy into energy of electronic excitation. It may result from chemical processes, such as recombination of free atoms or radicals, and this type of process is likely to be especially important in the reaction zone, but the main process responsible for maintenance of equilibrium between excited and unexcited atoms in the interconal gases will be conversion between vibrational and electronic energy.

Thus if there are small departures from equilibrium, due perhaps to lag in vibrational excitation, then we should rather expect that the temperature given by the spectrum-line reversal method may be nearer to the mean effective vibrational temperature of the surrounding molecules than to their mean translational temperature. A measured temperature above the theoretical maximum value may therefore indicate that the molecules have some excess of vibrational energy and a deficit of translational energy.

§ 3. EFFECT OF DEPARTURE FROM RADIATIVE EQUILIBRIUM

Complete equilibrium is only attained in a constant temperature enclosure such as a black-body furnace. The majority of laboratory flames are optically thin, and depopulation of excited electronic states by emission of radiation is not compensated by absorption of radiation. The spectrum-line reversal method essentially determines the ratio of the populations of the excited and ground electronic states, and any reduction in the population of the excited state by radiation will cause the measured temperature to be lower than the mean temperature of the gas molecules.

Now we may assume that the main process responsible for maintaining equilibrium is the collision with gas molecules. In equilibrium the number of atoms excited and de-activated by collision must be equal. If we know the quenching cross section we can calculate the average time before de-activation by collision, and we can then compare this with the average time before de-activation by radiation if we know the radiative lifetime. To obtain an estimate of the magnitude of such effects, we shall consider sodium atoms in a flame with air at 2000° K, and assume that the majority of colliding molecules are nitrogen.

Taking the value of $14{\cdot}5 \times 10^{-16}$ cm^2 for the quenching cross section and using the formula for number of collisions, we find that the excited Na atom makes $3{\cdot}1 \times 10^9$ effective quenching collisions per second. For sodium the radiative lifetime (Stephenson 1951) is $1{\cdot}6 \times 10^{-8}$ sec. Thus the amount of depopulation by radiation, in the absence of any re-absorption, may amount to 2·0% of the depopulation by collision. Now from the Maxwell–Boltzmann law the proportion of atoms in the excited state should be $\exp(-E/\boldsymbol{k}T)$. If we put

$E = 16964$ cm^{-1} for Na(^{2}P), $\boldsymbol{k} = 0{\cdot}697$ cm^{-1} and $T = 2000$, we obtain a value for the population in the excited state. If we then assume the 2·0% reduction in population by loss of radiation and use the same expression to deduce the temperature, we find that it is 3·3° lower. A similar calculation for a flame at $\frac{1}{10}$ atm. pressure, when the number of quenching collisions will be smaller, gives an error through radiation loss of 27°, and at $\frac{1}{100}$ atm. of 160°.

These calculations have required a number of assumptions. First we assumed that the surrounding gas was nitrogen. It is possible that quenching by other molecules like H_2O and CO_2 might be rather different, but since that for N_2 is around unity, the effect would be small. We have also tacitly assumed that the quenching cross section in a hot gas is the same as for quenching experiments in cooler gas; again, since the efficiency is near unity, any change is likely to be small. We have also assumed no self-absorption; now for the reversal method to work, absorption must be appreciable, at least in the centre of the line. Even for a completely opaque flame, the outer layers of gas, which are the layers which would then be effective, would receive radiation from only a hemisphere while radiating to a whole sphere, so about half the calculated effect would occur. Also the wings of the line will not be self-absorbed to any extent, and will tend to show the whole effect. Thus the actual error will be between the calculated one (3·3° at 1 atm.) and a half of this value (1·6° at 1 atm.).

It is interesting to have some quantitative knowledge of this error. For flames of different composition, or for different spectrum lines, the error would be rather different; it seems that it is not likely to be very serious at atmospheric pressure, but would tend to become more important at low pressure.

§4. THE USE OF THE OH BAND FOR REVERSAL WORK

While sodium is the most convenient metal to add to a flame with air, for very hot flames, such as those of near stoichiometric mixtures with oxygen, it is not easy to introduce a controlled amount of sodium. For these powerful flames there is always a risk of the flame striking back violently; this complicates the use of spraying devices, and the flames are too hot to introduce the sodium directly on a wire. Also the sodium-line method always has the disadvantage that the sodium in the cooler outer layers of the flame tends to contribute to the result.

Now practically all flames contain OH radicals, and the OH band at 3064 Å can be reversed. Generally the concentration of OH tends to be highest in the hottest part of the flame, so that the effect of the cooler outer layers is less important than with sodium. Also by using lines of high rotational energy one can exercise a further selection in favour of the high temperature region of the flame, since levels of high rotational energy will only be highly populated in the hottest part of the flame.

For flames above 2700° K it is not possible to use a tungsten lamp as background source, and a carbon arc is the most suitable source yet developed. The positive crater has a brightness temperature at 6500 Å of about 3818° K (Henning and Tingwaldt 1928). Since the brightness of the arc itself cannot be varied, the effective brightness may be reduced with an adjustable rotating sector. Here again the OH reversal method is more sensitive than the Na method because at high temperatures a given change of brightness, say by 10%, corresponds in the yellow to a fairly large change in temperature, but in the ultra-violet around

3100 Å it corresponds to a much smaller change in temperature; thus if we can fix the reversal point to within an intensity of ±10%, the error in terms of temperature will be much smaller for OH than for Na.

The OH reversal method has the disadvantage that it has to be done photographically and with fairly large dispersion. We have found a quartz Littrow-type spectrograph, such as Hilger's commercial instruments, quite suitable. A medium quartz spectrograph can be used, but is less sensitive. With the Littrow-type instrument, exposure times for flames at around 3000° K are of the order 10 seconds. For flames below 2700° K exposure times would be very long, and the sector used in front of the arc would have to be set so finely that it would become difficult to read it accurately. The optical arrangements are of the usual type, except that more reliable results are obtained by using a quartz-fluorite achromat lens because the focus of the arc on the slit may be poor in the ultra-violet if it is adjusted visually and an achromat is not used.

We have used the OH reversal method on a number of flames, and for lines of high rotational quantum number have always obtained temperatures for the interconal gases which are in agreement with theoretical temperatures within the limits of experimental error. For lines arising from levels of low rotational quantum number we obtain fair agreement, but there is a tendency for the values to be somewhat low, by up to 30°; this is probably due to absorption in the cooler outer layers of the flame. In and very near the reaction zone the reversal temperatures are found to be too high.

The radiative life for excited OH is about 4×10^{-6} sec, which is much longer than that for Na. We might thus expect the lack of radiative equilibrium in flame gases to have a smaller effect on OH; however, we have obtained some evidence (Gaydon and Wolfhard 1948) that the quenching of excited OH by flame gases has, in terms of a normal gas-kinetic collision cross section, an efficiency of only about $\frac{1}{40}$, so that the longer effective collision life may cancel the good effect of the longer radiative life. The OH is likely to be more affected than Na by the abnormally high electronic excitation in the reaction zone; we have shown that this becomes more important at shorter wavelengths. However, this effect does not appear to extend more than about twice the thickness of the reaction zone, and should therefore not affect the main body of interconal gases. We may summarize by saying that provided a suitable spectrograph is available the OH reversal method is likely to be simpler and more accurate than the Na reversal method for very hot flames.

REFERENCES

GAYDON, A. G., and WOLFHARD, H. G., 1948, *Proc. Roy. Soc.* A, **194**, 169; 1951, *Ibid.*, **205**, 118.

GRIFFITHS, E., and AWBERY, J. H., 1929, *Proc. Roy. Soc.* A, **123**, 401.

HENNING, F., and TINGWALDT, C., 1928, *Z. Phys.*, **48**, 805.

KURLBAUM, F., 1902, *Phys. Z.*, **3**, 187 and 232.

LAIDLER, K. J., and SHULER, K. E., 1951, *Chem. Rev.*, **48**, 153.

LEWIS, B., and VON ELBE, G., 1943, *J. Chem. Phys.*, **11**, 75.

LOOMIS, A. G., and PERROTT, G. ST. J., 1928, *Industr. Engng. Chem.*, **20**, 1004.

MASSEY, H. S. W., 1949, *Rep. Prog. Phys.*, **12**, 248 (London: Physical Society).

STEPHENSON, G., 1951, *Nature, Lond.*, **167**, 112.

STRONG, H. M., BUNDY, F. P., and LARSON, D. A., 1949, *3rd Symposium on Combustion, Wisconsin*, 1948 (Baltimore: Williams and Wilkins).

The Structure of the Long Wave Absorption Edge of Insulating Crystals

By I. C. CHEESEMAN
Department of Mathematics, Imperial College, London

Communicated by H. Jones; *MS. received* 10*th July* 1951

ABSTRACT. A general process, by which light can be absorbed in insulators at frequencies less than the frequency corresponding to the energy gap, is considered. Using an Einstein model with a constant energy gap, calculation of such a process is made by means of the method of intermediate states. The results are tested for the case of cadmium sulphide, and agreement with experimental results is found to be good when allowance is made for mathematical approximations made in the calculations.

§1. INTRODUCTION

Two previous attempts have been made (Möglich and Rompe 1940, 1942) to explain the variation with temperature of the long-wave absorption edge of insulators. Neither method has given values, when tested, comparable with those obtained experimentally. In their first paper Möglich and Rompe proposed the method of multiple collisions, by means of which an electron interacts with several lattice waves and is lifted to the conduction band from the lowest band. Using the Debye model they made a calculation of the probability of such a transition. When this theory was applied to the shift of the long-wave absorption edge (Möglich, Riehl and Rompe 1940) a negligible shift, compared with experimental values, was obtained. In their second paper Möglich and Rompe suggested that the absorption edge would shift toward the red with increasing temperature, if allowance was made for the contraction of the energy gap between the first and second zones due to the expansion of the lattice. Calculation of this effect was made using the one-dimensional model of Kronig and Penney (1931), but the coefficient of linear thermal dilatation which was needed to produce the observed shift of 1 Å per degree K for the case of cadmium sulphide was 10^{-4}, which compares unfavourably with the experimental value of 4×10^{-6} obtained by Seiwert (1949). This theory is attractive, however, in that it may also be used to account similarly for the shift of the absorption edge to the blue with increasing pressure (Höhler 1949). In the particular case of cadmium sulphide, chosen because most experimental work has been done on it—by Seiwert (1949), Höhler (1949) and Kroger (1940) in particular—a simple consideration shows that, if the shift of 0·02 Å per atm. found by Höhler is completely accounted for by this process, it is impossible to obtain a thermal shift comparable with those obtained experimentally, namely 1 Å per degree K by Kroger and 1·4 Å per degree K by Seiwert. For, consider a unit cube of cadmium sulphide, then a volume change of $1{\cdot}5 \times 10^{-6}$ cm^3 due to the change in pressure of 1 atmosphere produces a shift of 0·02 Å. The same volume change, and hence the same change of energy gap under Möglich and Rompe's theory, is produced by varying the temperature by 0·88° K when the absorption edge shifts by only 0·124 Å. A further process must, therefore, be operating to produce the larger thermal shift.

In this paper we shall discuss possible transitions across the energy gap which are forbidden in the simple optical theory of solids. These transitions are permitted if the vibration of the lattice ions is taken into account. Considering the combined perturbation, we shall show that electrons from near the corners of the lowest zone can be raised to near the centre of the second zone, giving rise to an energy equation which permits light, of a lower frequency than allowed by the simple optical theory, to be absorbed. A linear shift with temperature of the absorption edge is also found.

§2. PERTURBATION CALCULATION OF THE INTERACTION OF LATTICE VIBRATIONS AND ELECTROMAGNETIC RADIATION ON ELECTRONS

In order to perform this perturbation calculation certain assumptions have to be made at the outset. It must be pointed out, however, that these approximations are only introduced to make the calculation manageable and do not alter the basic physical ideas. Firstly, we shall assume that the lattice is simple cubic, with two electrons per atom, and that the zones do not overlap. The first zone is then full and no conduction is possible. We assume also that the energy gap between the first two zones is independent of the temperature, thus ruling out in our model the process considered by Möglich and Rompe. For lattice vibrations we take an Einstein model. The wave function for the whole system is then the product of Bloch wave functions for the electrons and vibrational functions for the atoms. The quantum numbers are given by the wave vector $\mathbf{k}$ for the electrons, and $\mathbf{n}$ for the atoms, $\mathbf{n}$ having components in the x, y, z, directions. Both wave functions are normalized over an atomic cell.

Expanding the perturbed wave function in terms of the initial wave functions, we solve for any one coefficient $a(\mathbf{k}, \mathbf{n}, t)$ by the Dirac method of variation of constants. Fixing the initial state as $\mathbf{k}_0$, $\mathbf{n}_0$, the following equation is obtained for any perturbation H_1:

$$-i\hbar \frac{\partial a}{\partial t}(\mathbf{k}_f \mathbf{n}_f t) = (\mathbf{k}_f, \mathbf{n}_f | H_1 | \mathbf{k}_0, \mathbf{n}_0) \exp(E[\mathbf{k}_0 \mathbf{n}_0] - E[\mathbf{k}_f \mathbf{n}_f]) it/\hbar, \qquad \ldots\ldots(1)$$

where $(\mathbf{k}_f, \mathbf{n}_f | H_1 | \mathbf{k}_0, \mathbf{n}_0)$ is the matrix element between states $\mathbf{k}_0$, $\mathbf{n}_0$ and $\mathbf{k}_f$, $\mathbf{n}_f$, and $E[\mathbf{k}, \mathbf{n}]$ is the energy of the system in state $\mathbf{k}$, $\mathbf{n}$. In this problem the perturbation H_1 will contain two terms, caused by the light wave and the lattice vibrations respectively. It is given by

$$H_1 = (e\hbar/mci)\mathbf{A}\,\mathrm{grad} - \mathbf{R}\,.\,\mathrm{grad}\, V, \qquad \ldots\ldots(2)$$

where the vector potential of the light wave $\mathbf{A} = c\mathfrak{E}\,[\exp 2\pi i\nu t + \exp(-2\pi i \nu t)]/4\pi$, $\mathfrak{E}$ being the electric vector, ν the frequency of the light, $\mathbf{R}$ the displacement of the atom from its equilibrium position and V, which is a function of the electronic coordinate $\mathbf{r}$ only, the potential of the unperturbed lattice. In both cases grad implies differentiation with respect to the electronic coordinates only. The displacement $\mathbf{R}$ must be taken sufficiently small for this formula to be true, so that the change in V is negligible outside the atomic cell concerned (Mott and Jones 1936). Without loss of generality the electromagnetic vector can be taken in the x direction, when $\mathbf{A}$ has the components $(A_x, 0, 0)$. Substituting from eqn. (2) into eqn. (1), it is easily seen that the matrix element for the transition as a whole does not exist, since the selection rules make one or both terms in eqn. (2) negligible or identically zero. To solve the problem we must take a higher approximation in the solution by Dirac's method of variation of constants. This involves the use of intermediate states (Heitler 1944).

Consider any intermediate state $\mathbf{k}_\alpha$, $\mathbf{n}_\alpha$, chosen so that the matrix elements for the transitions between it and the initial, and between it and the final states are non-zero. Then, fixing $\mathbf{k}_0\mathbf{n}_0$ as the initial state, an equation similar to (1) is obtained with $\mathbf{k}_\alpha\mathbf{n}_\alpha$, replacing $\mathbf{k}_f\mathbf{n}_f$ throughout. This equation will only involve one term of H_1, the other giving a matrix element which is negligible or zero. Solving this differential equation for $a[\mathbf{k}_\alpha, \mathbf{n}_\alpha, t]$, the Dirac variation method is then repeated with these values as initial conditions for a transition from $\mathbf{k}_\alpha\mathbf{n}_\alpha$ to $\mathbf{k}_f\mathbf{n}_f$. This last calculation will involve the term in H_1 which was zero in the transition $\mathbf{k}_0\mathbf{n}_0$ to $\mathbf{k}_\alpha\mathbf{n}_\alpha$. The following equation for $a[\mathbf{k}_f, \mathbf{n}_f, t]$ is obtained:

$$a[\mathbf{k}_f, \mathbf{n}_f, t] = \sum_{\mathbf{k}_\alpha\mathbf{n}_\alpha} \frac{(\mathbf{k}_\alpha, \mathbf{n}_\alpha|H_1|\mathbf{k}_0, \mathbf{n}_0)(\mathbf{k}_f, \mathbf{n}_f|H_1|\mathbf{k}_\alpha, \mathbf{n}_\alpha)}{(E[\mathbf{k}_0\mathbf{n}_0]-E[\mathbf{k}_\alpha\mathbf{n}_\alpha])}$$

$$\times\left\{\frac{\exp\{(E[\mathbf{k}_0\mathbf{n}_0]-E[\mathbf{k}_f\mathbf{n}_f]+h\nu)it/\hbar\}-1}{(E[\mathbf{k}_0\mathbf{n}_0]-E[\mathbf{k}_f\mathbf{n}_f]+h\nu)} - \frac{\exp\{(E[\mathbf{k}_\alpha\mathbf{n}_\alpha]-E[\mathbf{k}_f\mathbf{n}_f]+h\nu)it/\hbar\}-1}{(E[\mathbf{k}_\alpha\mathbf{n}_\alpha]-E[\mathbf{k}_f\mathbf{n}_f]+h\nu)}\right\} \qquad \ldots\ldots(3)$$

in which the time-dependent part of H_1 has been integrated between the limits 0 and t, and we have neglected terms which lead to energy equations corresponding to the emission of light. Using the selection rules for the matrix elements only two distinct values of $\mathbf{k}_\alpha$ exist, and combining with each of these there are two values of $\mathbf{n}_\alpha$ for each of the three directions of vibration of the atom. The two values of $\mathbf{k}_\alpha$ are shown graphically in fig. 1, where $E[\mathbf{k}]$ is the energy of the state $\mathbf{k}$ which lies in the plane of energy discontinuity between the first and second zones and has its origin at the centre of the plane A where the energy is E_A.

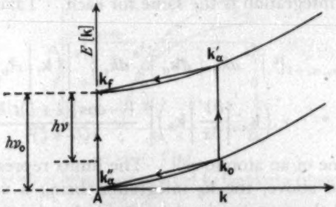

Fig. 1. Optical transitions across the energy gap from an initial state $\mathbf{k}_0$ to a final-state $\mathbf{k}_f$ through intermediate states $\mathbf{k}_\alpha'$ and $\mathbf{k}_\alpha''$.

From the figure it is obvious that an effective energy gap $h\nu$ is obtained which is considerably less than the true energy gap $h\nu_0$, with corresponding shift of the absorption edge to lower frequency.

The matrix element $(\mathbf{k}_\alpha'', \mathbf{n}_\alpha|\mathbf{R}\,\mathrm{grad}\,V|\mathbf{k}_0, \mathbf{n}_0)$ divides into three similar terms on expanding the scalar product. Since V is symmetrical in the electronic coordinates, this may be written separating the lattice and electronic terms as $3X_{n_0, n_0\pm1}(\mathbf{k}_\alpha''|\partial V/\partial x|\mathbf{k}_0)$, where the x component of $\mathbf{n}_\alpha$ must change from n_0 to $n_0 \pm 1$ to satisfy the selection rules of the harmonic oscillator. This reduces the number of terms in the summation of eqn. (3) from 12 to 4. Forming $|a[\mathbf{k}_f, \mathbf{n}_f, t]|^2$ we find that of the sixteen possible terms only four remain, the cross products of the terms in the sum disappearing because for large t they have no resonance values in the range of ν, $\nu<\nu_0$. We shall only consider one of these remaining terms in detail, obtaining the results for the others by symmetry. Taking the term corresponding to the transition through the intermediate state $\mathbf{k}_\alpha'', n_0+1$, and rearranging, we obtain the expression

$$6|X_{n_0,\,n_0+1}|^2 \left|\left(\mathbf{k}_f\left|A_0\frac{\partial}{\partial x}\right|\mathbf{k}_\alpha''\right)\cdot\left(\mathbf{k}_\alpha''\left|\frac{\partial V}{\partial x}\right|\mathbf{k}_0\right)\right|^2$$

$$\times\left\{\frac{1-\cos(\epsilon t/\hbar)}{(\epsilon+\zeta)\zeta\epsilon^2}+\frac{1-\cos(\zeta t/\hbar)}{(\epsilon+\zeta)\epsilon\zeta^2}-\frac{1-\cos[(\epsilon+\zeta)t/\hbar]}{\epsilon\zeta(\epsilon+\zeta)^2}\right\} \quad \ldots\ldots(4)$$

in which $\epsilon=E[\mathbf{k}_0]-E[\mathbf{k}_\alpha'']+W[n_0+1]-W[n_0]$, $\zeta=E[\mathbf{k}_\alpha'']-E[\mathbf{k}_f]+h\nu$ and $A_0=(e\hbar/mci\nu)(cI/2\pi)^{1/2}$, I being the intensity of the light wave which is defined as the energy crossing unit area per unit time. $W[n]$ is the energy of a linear harmonic oscillator in the state n.

§ 3. THE INTEGRATION OF EXPRESSION (4)

The expression numbered (4) is integrated over all occupied initial and all possible final states. For insulators the lowest zone is completely full and all other zones completely empty initially. The lowest zone for a simple cubic lattice is a cube, while the second zone is the volume between it and the dodecahedron surrounding it. Using reduced wave vectors the second zone is reflected into the first zone (Mott and Jones 1936), and thus the region of integration for both initial and final states is over this cube. The integrand (4) is symmetrical in $\mathbf{k}_f$ in any prism which is similar to one whose corners are given by $(0,0,0)$, $(\pi/a,0,0)$, $(\pi/a,0,\pi/a)$ and $(\pi/a,\pi/a,\pi/a)$, where a is the lattice constant, and the origin of coordinates is at the centre of the cube with the axes passing through the centres of the faces. We shall consider only the integration of one term in (4) since the method of integration is the same for each. Taking the third term we have

$$I=-\frac{288\Omega^2}{(2\pi)^6}|X_{n_0,\,n_0+1}|^2\int_0^{k_A}dk_x\int d\mathbf{k}_0\int_0^{k_x}dk_z\int_0^{k_z}\left|\left(\mathbf{k}_f\left|A_0\frac{\partial}{\partial x}\right|\mathbf{k}_\alpha''\right)\cdot\right.$$

$$\left.\times\left(\mathbf{k}_\alpha''\left|\frac{\partial V}{\partial x}\right|\mathbf{k}_0\right)\right|^2\frac{1-\cos[(\epsilon+\zeta)t/\hbar]}{\epsilon\zeta(\epsilon+\zeta)^2}\,dk_y, \quad \ldots\ldots(5)$$

where Ω is the volume of an atomic cell. The limits represent the prism whose coordinates are given above, the $\mathbf{k}_0$ integration being a volume integral. To evaluate this integral the two matrix elements under the sign of the integration must be estimated. Taking wave functions $\psi_{\mathbf{k}_f}=\exp(i\mathbf{k}\,.\,\mathbf{r})\sin\{2mE_A/\hbar^2\}^{1/2}x$, and $\psi_{\mathbf{k}_\alpha''}=\exp(i\mathbf{k}\,.\,\mathbf{r})\cos\{2mE_A/\hbar^2\}^{1/2}x$, where $\mathbf{k}$ is measured from the point A, we can evaluate the first matrix element. These wave functions are obtained from the nearly free electron wave functions (Wilson 1936) by neglecting a term which is small near the energy discontinuity. To this approximation the matrix element M_1 is given by

$$M_1{}^2=\left|\left(\mathbf{k}_f\left|A_0\frac{\partial}{\partial x}\right|\mathbf{k}_\alpha''\right)\right|^2=\frac{e^2IE_A}{\pi mc\nu^2}$$

which is constant when $\mathbf{k}_f$ and $\mathbf{k}_\alpha''$ refer to the same $\mathbf{k}$, otherwise it is identically zero.

Using the Schrödinger equation, the matrix element $(\mathbf{k}_\alpha''|\partial V/\partial x|\mathbf{k}_0)^2$ reduces to $|\mathbf{k}_0-\mathbf{k}_\alpha''|^2|V_0-E|^2$, where $|V_0-E|$ is the kinetic energy of the electron in its lowest state at the surface of the polyhedron (Mott and Jones 1936). In order to simplify the integration of eqn. (5), we take an average value of $|\mathbf{k}_0-\mathbf{k}_\alpha''|^2$, and then denote the matrix element by M_2. Assuming that the average has been taken, but leaving the actual calculation of values until later, since the integration imposes conditions on $\mathbf{k}_0$ and $\mathbf{k}_\alpha''$, eqn. (5) becomes

$$I = -\frac{288\Omega^2}{(2\pi)^6} |X_{n_0,\, n_0+1}|^2 M_1{}^2 M_2{}^2 \int_0^{k_A} dk_x \int d\mathbf{k}_0 \int_0^{k_x} dk_z \int_0^{k_z} \frac{1-\cos[(\epsilon+\zeta)t/\hbar]}{\epsilon\zeta(\epsilon+\zeta)^2}\, dk_y. \qquad \ldots\ldots(6)$$

Taking the electronic energies of the intermediate and final states to be $E[\mathbf{k}_\alpha''] = (x^2+y^2+z^2)$ and $E[\mathbf{k}_f] = E_B + \alpha(E_A{}^{1/2}-x)^2 + y^2 + z^2$, where E_B is the lowest energy in the second zone, $\alpha = 1 + 4E_B/\Delta E$, and where $x = k_x\hbar^2/2m$, $y = k_y\hbar^2/2m$, and $z = k_z\hbar^2/2m$. From this definition of $E[\mathbf{k}_\alpha'']$ and $E[\mathbf{k}_f]$ we see that ζ is a function of x only. Changing the variables from k_y, k_z, $\mathbf{k}_0$, k_x to $(\epsilon+\zeta)$, z, $\mathbf{k}_0$, x eqn. (6) becomes

$$I = -\frac{144\Omega^2}{(2\pi)^6} |X_{n_0,\, n_0+1}|^2 M_1{}^2 M_2{}^2 \left\{\frac{2m}{\hbar^2}\right\}^{3/2}$$

$$\times \int_0^{E_A{}^{1/2}} dx \int d\mathbf{k}_0 \int_0^{x} dz \int_a^b \frac{1-\cos[(\epsilon+\zeta)t/\hbar]\, d(\epsilon+\zeta)}{\epsilon\zeta(\epsilon+\zeta)^2(a+\epsilon+\zeta)^{1/2}}, \qquad \ldots\ldots(7)$$

where $a = E[\mathbf{k}_0] - \alpha(E_A{}^{1/2}-x)^2 - z^2 + h\nu + h\omega - E_B$,

$b = E[\mathbf{k}_0] - \alpha(E_A{}^{1/2}-x)^2 - 2z^2 + h\nu + h\omega - E_B$,

and $h\omega = W[n_0+1] - W[n_0]$.

For sufficiently large t the integrand can be regarded as a δ-function about $(\epsilon+\zeta)=0$, provided $\zeta=0$ does not come in the range of integration. $\zeta=0$ means that $\nu=\nu_0$ at least, and since we are only interested in values of $\nu<\nu_0$ this singularity does not occur. Similarly ϵ cannot be zero in this integration if ζ is not zero, since $\epsilon+\zeta=0$. Thus the limits may be taken as $+\infty$ and $-\infty$ respectively provided $a>0$ and $b<0$. Integrating eqn. (7) we have

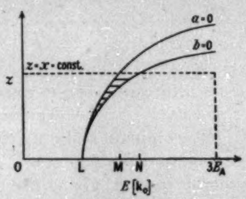

Fig. 2. Region of integration of z and $\mathbf{k}_0$ for fixed x (shown shaded).

$$I = \frac{144\Omega^2}{(2\pi)^6} |X_{n_0,\, n_0+1}|^2 M_1{}^2 M_2{}^2 \left\{\frac{2m}{\hbar^2}\right\}^{3/2} \frac{\pi t}{\hbar}$$

$$\times \int_0^{E_A{}^{1/2}} \frac{dx}{\zeta^2(x)} \int d\mathbf{k}_0 \int \frac{dz}{(E[\mathbf{k}_0] - \alpha(E_A{}^{1/2}-x)^2 - E_B + h\nu + h\omega - z^2)^{1/2}}, \qquad \ldots\ldots(8)$$

where the limits of $\mathbf{k}_0$ and z are determined by means of the original limits and the above inequalities. Putting $a=0$ and $b=0$, the inequalities define the region in a plane, $x=$ constant, between the two full curves in fig. 2. The dotted lines are the conditions imposed by the limits of integration in eqn. (7). The area over which the integration has to be taken is shown shaded.

Performing the integration over z in two parts corresponding to the ranges LM and MN of $E[\mathbf{k}_0]$ respectively we find that eqn. (8) becomes

$$I=\frac{144\Omega^2}{(2\pi)^6}\left\{\frac{2m}{\hbar^2}\right\}^{3/2}|X_{n_0,\,n_0+1}|^2 M_1{}^2 M_2{}^2 \frac{\pi t}{\hbar}\int_0^{E_A{}^{1/2}}\frac{dx}{\zeta^2(x)}$$
$$\times\left[\int\frac{\pi}{4}\,d\mathbf{k}_0+\int\left\{\sin^{-1}\left(\frac{x}{[E[\mathbf{k}_0]-\alpha(E_A{}^{1/2}-x)^2-E_B+h\nu+h\omega]^{1/2}}\right)-\frac{\pi}{4}\right\}d\mathbf{k}\right]. \qquad \ldots\ldots(9)$$

The volume integration over $\mathbf{k}_0$ is, for convenience, taken between surfaces of constant energy. If dS is an element of such a surface, the volume $d\mathbf{k}_0$ becomes $d\mathbf{k}_0=dE\,dS/|\mathrm{grad}\,E|$. Since the integrands are functions of $E[\mathbf{k}_0]$ only, the integration over dS can be expressed in terms of the density of states $N(E)$. Integrating over dS eqn. (9) becomes

$$I=\frac{144\Omega}{(2\pi)^3}\left\{\frac{2m}{\hbar^2}\right\}^{3/2}|X_{n_0,\,n_0+1}|^2 M_1{}^2 M_2{}^2 \frac{\pi t}{\hbar}\int_0^{E_A{}^{1/2}}\frac{dx}{\zeta^2(x)}\left[\int_\beta^{\beta+x^2}N(E)\frac{\pi}{4}\,dE\right.$$
$$\left.+\int_{\beta+x^2}^{\beta+2x^2}N(E)\left\{\sin^{-1}\left(\frac{x}{[E[\mathbf{k}_0]-\alpha(E_A{}^{1/2}-x)^2-E_B+h\nu+h\omega]^{1/2}}\right)-\frac{\pi}{4}\right\}dE\right], \qquad \ldots\ldots(10)$$

where $\beta=\alpha(E_A{}^{1/2}-x)^2+E_B-h\nu-h\omega$. Since the range of integration of E is small and $N(E)$ is a slowly varying function with no singularities, we may take $N(E)$ constant over the integration. The value of $N(E)$ is adjusted to the average value of $N(E[\mathbf{k}_0])$ for the whole range of $E[\mathbf{k}_0]$. Performing the integration over E, eqn. (10) simplifies to

$$I=\frac{144\Omega}{(2\pi)^3}N(E)\left\{\frac{2m}{\hbar^2}\right\}^{3/2}|X_{n_0,\,n_0+1}|^2 M_1{}^2 M_2{}^2 \frac{\pi t}{\hbar}\int_0^{E_A{}^{1/2}}\frac{x^2}{\zeta^2(x)}\,dx, \qquad \ldots\ldots(11)$$

where $\zeta(x)=x^2-\alpha(E_A{}^{1/2}-x)^2+h\nu-E_B$.

The other two terms in the expression (4), if treated similarly, give contributions for $\zeta=0$ and $\epsilon=0$ respectively. Since we are only interested in $h\nu$ less than ΔE, the term for which $\zeta=0$ is omitted, and since the process we are considering requires $\epsilon+\zeta=0$, we cannot have $\epsilon=0$ unless $\zeta=0$, which implies $\nu=\nu_0$. Hence we can exclude the other term in (4) giving rise to the condition $\epsilon=0$.

In evaluating integral (5) it will be noticed that it is immaterial whether we take $\epsilon=E[\mathbf{k}_0]-E[\mathbf{k}_\alpha{}'']+h\omega$ or $\epsilon=E[\mathbf{k}_0]-E[\mathbf{k}_\alpha{}'']-h\omega$. We now assume that the matrix elements satisfy the following conditions, $(\mathbf{k}_f|A_0\partial/\partial x|\mathbf{k}_\alpha{}'')=(\mathbf{k}_\alpha{}'|A_0\partial/\partial x|\mathbf{k}_0)$, $(\mathbf{k}_\alpha{}''|\partial V/\partial x|\mathbf{k}_0)=(\mathbf{k}_f|\partial V/\partial x|\mathbf{k}_\alpha{}')$, and $X_{n_0,\,n_0+1}=X_{n_0,\,n_0-1}$ approximately. Defining the integral of $a(\mathbf{k}_f,\mathbf{n}_f)$ over all initial and final states to be $P(\mathbf{k}_0,\mathbf{k}_f)t$, where P is the probability of a transition from state $\mathbf{k}_0$ to state $\mathbf{k}_f$ in unit time, we find that

$$P(\mathbf{k}_0,\mathbf{k}_f)=\frac{576\Omega}{(2\pi)^3}N(E)\left\{\frac{2m}{\hbar^2}\right\}^{3/2}|X_{n_0,\,n_0+1}|^2 M_1{}^2 M_2{}^2 \frac{\pi}{\hbar}\int_0^{E_A{}^{1/2}}\frac{x^2}{\zeta(x)}\,dx. \qquad \ldots\ldots(12)$$

The last integral is readily evaluated.

§ 4. EVALUATION AND COMPARISON WITH EXPERIMENTAL VALUES OF THE ABSORPTION COEFFICIENT K

Seiwert has determined the true absorption coefficient K for cadmium sulphide from measurements of the intensities of the incident and transmitted beams through a crystal of known thickness, reflection at the surface being taken into account. The relation between K in cm^{-1} and the probability P of the absorption of a light quantum of frequency ν by an atom in time t is given by $K = NPh\nu/I$, when N is the number of atoms per cm^3 in a crystal, and I is the intensity of the light at the point in the crystal to which P refers.

In order to calculate P the matrix elements $|X_{n_0,\, n_0+1}|$ and M_2 have to be estimated. $|X_{n_0,\, n_0+1}|^2$ is evaluated in the usual manner by averaging the squares of the amplitudes of the oscillations of the atoms over all initial states. $|X_{n_0,\, n_0+1}|^2$ is then given by

$$|X_{n_0,\, n_0+1}|^2 = \frac{T\hbar^2}{M\Theta^2\boldsymbol{k}}, \qquad \ldots\ldots(13)$$

where M is the mass of the atom, Θ the Einstein temperature, T the absolute temperature, and $\boldsymbol{k}$ Boltzmann's constant.

M_2^2 was defined in § 3 as the average value of $|\mathbf{k}_0 - \mathbf{k}_\alpha''|^2\,|V_0 - E|^2$ taken over all permissible values of $\mathbf{k}_0$ and $\mathbf{k}_\alpha''$, which we now know are those satisfying $\epsilon + \zeta = 0$. Since $|\mathbf{k}_0 - \mathbf{k}_\alpha''|^2 = k_0^2 + k_\alpha''^2 - 2k_0k_\alpha'' \cos\alpha$, where α is the angle between the vectors $\mathbf{k}_0$ and $\mathbf{k}_\alpha''$, the average over all possible values of α makes the third term vanish. The average of $k_0^2 + k_\alpha''^2$ over all k_f after substituting from $\epsilon + \zeta = 0$ for k_0 is $(m/\hbar^2)[(14+\alpha)E_A/5 + 2(E_B - h\nu - h\omega)]$. Thus assuming a value of $|V_0 - E|$ we determine M_2^2.

So far this calculation is quite general. In order to test its value, we shall compare the results obtained from it with the experimental values of Seiwert; a copy of his values are given in fig. 3 (*b*). From his graphs we see that the total absorption at absolute zero would take place approximately at $\nu_0 = 5{\cdot}906 \times 10^{14}$ c/s, that is an energy gap of 2·43 ev. This limits the value of E_A since we have taken the lattice to be simple cubic, because the highest energy in the lowest zone ($3E_A$) must be less than $E_A + h\nu_0$ in order to make the substance insulating. We have taken $E_A = 1{\cdot}12$ ev and E_B as 3·55 ev. In addition, in an attempt to see if a Debye model would make any significant difference to the result, we allowed $h\omega$ to take the value of the maximum of the Debye spectrum at the temperature considered. Taking $|V_0 - E|$ to be 5 ev we give in the table the values of M_2^2 at various frequencies and temperatures.

Values of $M_2^2 \times 10^8$ at Various Temperatures and Frequencies

	$h\nu$ (ev)			
	2·1	2·2	2·3	2·4
T (° K) = 288 $h\omega$ (ev) = 0·045	38·85	38·21	37·57	36·96
T (° K) = 654 $h\omega$ (ev) = 0·103	38·43	37·83	37·21	36·61
T (° K) = 858 $h\omega$ (ev) = 0·135	38·23	37·63	37·03	36·41

The error in taking the values of M_2^2 to be the same as those obtained by replacing $h\omega$ by $-h\omega$ in $\epsilon + \zeta = 0$ is negligible. The values of K calculated from the values of the parameters given above are shown in fig. 3 (*a*).

From these graphs the long wave absorption limit is seen to shift to the red by 0·63 Å per degree K. This compares favourably with the experimental value of 1·4 Å per degree K when allowance is made for all the approximations included in the calculation. Comparison of the two graphs, however, shows a discrepancy in the rate with which the curves become asymptotic to the line $\nu = \nu_0$. If this line were to shift to lower values of ν with increasing temperature, agreement would be considerably improved. This could be effected by a process such as that suggested by Möglich and Rompe in their second paper. We must conclude, however, that the process considered here is the most important since it gives good approximations to both the shape and shift of the long-wave absorption edge.

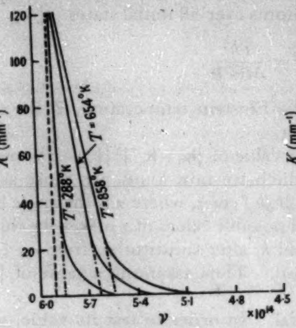

Fig. 3 (*a*). Theoretical values of *K*.

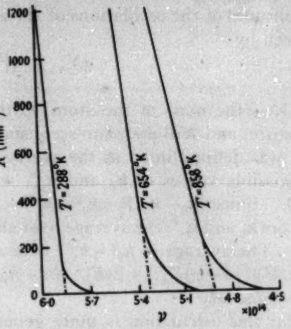

Fig. 3 (*b*). Experimental values of *K*.

ACKNOWLEDGMENTS

I am glad to have this opportunity of expressing my thanks to Professor H. Jones for introducing the subject of this paper to me and for many valuable suggestions and discussions, and to the Department of Scientific and Industrial Research for a maintenance allowance which made this work possible.

REFERENCES

Heitler, W., 1944, *The Quantum Theory of Radiation*, 2nd edition (Oxford: University Press).
Höhler, G., 1949, *Ann. Phys., Lpz.*, **4**, 371.
Kroger, F. A., 1940, *Physica*, **7**, 1.
Kronig, R. de L., and Penney, W. G., 1931, *Proc. Roy. Soc.* A, **130**, 499.
Möglich, F., Riehl, N., and Rompe, R., 1940, *Z. tech. Phys.*, **21**, 128.
Möglich, F., and Rompe, R., 1940, *Z. Phys.*, **115**, 707; 1942, *Ibid.*, **119**, 472.
Mott, N. F., and Jones, H., 1936, *The Theory and Properties of Metals and Alloys* (Oxford: University Press).
Seiwert, R., 1949, *Ann. Phys., Lpz.*, **6**, 241.
Wilson, A. H., 1936, *The Theory of Metals* (Cambridge: University Press).

Oriented Deposits on Crystalline Substrates

By D. W. PASHLEY
Physics Department, Imperial College, London

Communicated by G. P. Thomson; MS. received 27th July 1951

ABSTRACT. Layers of silver and thallium halides have been evaporated, *in vacuo*, on to cleavage surfaces of rocksalt, potassium bromide, magnesium oxide and mica, at various substrate temperatures. These layers have been studied by means of electron diffraction. Examples of both high and low inter-atomic misfits between the substrate and the oriented overgrowth are found. In the case of silver chloride on potassium bromide, a chemical reaction occurred between the substrate and the deposit. Thallium chloride crystallized in an abnormal rocksalt type structure on potassium bromide, but had its normal caesium chloride type structure on the other substrates used.

§ 1. INTRODUCTION

During the course of preparing specimens of various substances for certain electron diffraction studies, some results concerning crystal orientation on various crystalline substrates have been obtained. Since such results are of current theoretical interest (see van der Merwe 1949, Smollett and Blackman 1951), it is considered desirable that these data should be added to the existing information. This paper therefore presents some results obtained from an electron diffraction study (reflection technique) of evaporated deposits of silver and thallium halides on freshly cleaved surfaces of single crystals of rocksalt, potassium bromide, magnesium oxide and mica.

§ 2. SPECIMEN PREPARATION

The specimens were prepared by evaporating the halide (*in vacuo*) on to the various crystalline substrates, the halide being heated in a small tungsten spiral. The distance between the tungsten spiral and the substrate was about 12 cm, and the residual gas pressure lower than 10^{-4} mm Hg. The substrate crystals were contained in holes in a brass block, during the deposition, and this brass block was heated by means of a coil placed below it. In this way the substrate temperature could be varied from 15° c to 250° c. The thickness of the halide layers was usually of the order of 100 Å, as determined from the amount of halide evaporated from the tungsten spiral.

§ 3. RESULTS

In most cases the evaporated layers gave rise to diffraction patterns which consisted of one or more simple cross-grating patterns. These allowed the orientation of the halide to be determined. The orientation of the substrate relative to the electron beam direction was given by its Kikuchi line patterns, which were still present, although rather diffuse. No Laue spots were obtained from the substrate, except when part of the surface was free from the deposit. The results of the interpretations are given in the table, and two of the more interesting of these interpretations are given below.

Deposit	Structure of deposit	Substrate surface	Structure of substrate	Substrate temp. (° c)	Orientation Results Parallel planes		Parallel axes		% Misfit	Remarks
					Sub.	Dep.	Sub.	Dep.		
AgCl	A	NaCl (100)	A	15–150	(100)	(100)	[001]	[001]	−1·4	—
		NaCl (110)	A	150	(110)	(110)	[001]	[001]	−1·4	(110) NaCl surface prepared by H_2O etching
		Mica (001)	E	15–150	(001)	(111)	[100]	$[1\bar{1}0]$ or $[\bar{1}10]$	−24	—
		MgO (100)	A	15–120	(100)	(100)	‘ Fibrous ’		—	Also much randomly oriented AgCl
				120–150	(100)	(100)	‘ Fibrous ’		—	Almost entirely fibrous, with slight parallel growth
				150–250	—	—	—	—	—	Mainly random, with slight preference for parallel growth
		KBr (100)	A	15	(100)	(100)	[001]	[001]	−16	Reacts with substrate
				150	(100)	(100)	[001]	[001]	−12	Only AgBr on diffraction pattern. Misfits quoted are for AgBr on KBr
					(100)	(111)	[001]	$[1\bar{1}0]$ or $[\bar{1}10]$	+8 & −38	
					(100)	(111)	[011]	$[1\bar{1}0]$ or $[\bar{1}10]$	−12 & +53	
AgBr	A	NaCl (100)	A	15–150	(100)	(100)	[001]	[001]	+2·3	No chemical reaction
		Mica (001)	E	15–150	(001)	(111)	[100]	$[1\bar{1}0]$ or $[\bar{1}10]$	−21	—
		KBr (100)	A	15	(100)	(100)	[001]	[001]	−12	—
				200	(100)	(100)	[001]	[001]	−12	Relative proportions of each orientation vary from specimen to specimen
					(100)	(111)	[001]	$[1\bar{1}0]$ or $[\bar{1}10]$	+8 & −38	
					(100)	(111)	[011]	$[1\bar{1}0]$ or $[\bar{1}10]$	−12 & +53	
		MgO (100)	A	150	(100)	(100)	‘ Fibrous ’		—	Spots appreciably arced
AgI	C	Mica (001)	E	15	(001)	(111)	[100]	$[1\bar{1}0]$ or $[\bar{1}10]$	−12	Two modifications occur together in varying proportions
	D	Mica (001)	E	15	(001)	(001)	[100]	[100]	−12	
TlCl	B	NaCl (100)	A	120	(100)	(110)	[011]	[001] or $[1\bar{1}0]$	−3·5 & +37	Also other weak orientations
		Mica (001)	E	120	(001)	(111)	[100]	$[1\bar{1}0]$ or $[\bar{1}10]$	+6	Second orientation very weak
					(001)	(100)	[100]	[001] or [011]	−25 & −57	
		KBr (100)	A	120	(100)	(110)	[011]	[001] or $[1\bar{1}0]$	−17 & +17	Mostly crystallizes in structure A
TlCl	A	KBr (100)	A	120	(100)	(100)	[001]	[001]	−6	

A=rocksalt type structure; B=caesium chloride type structure; C=zinc blende type cubic structure; D=zincite type hexagonal structure; E=monoclinic structure.

(i) *Silver Chloride on Potassium Bromide*

It was found, when silver chloride was deposited on to potassium bromide, that a chemical reaction between the deposit and the substrate occurred, so that silver bromide and potassium chloride were both formed. Fig. 1 (Plate) shows the pattern obtained from such a layer, which was prepared with the substrate at room temperature. The Kikuchi lines arise from the substrate, and the analysis of the spot patterns is indicated in fig. 2. Parallel orientations of potassium bromide, potassium chloride, silver bromide, and silver chloride occur simultaneously. The Laue spots from the substrate are observed in this case, because part of the surface was shielded from the silver chloride during the deposition. There is also parallel oriented metallic silver present; this formed during the electron bombardment of the silver halide (Pashley 1950).

When the substrate was maintained at a higher temperature (150° c) during the deposition of the silver chloride, the diffraction patterns indicated only silver bromide, and no silver chloride or potassium chloride. The silver bromide pattern could then be identified both from its spacings and from the alternations in spot intensity which occurred due to structure factor. Such alternations are less marked with silver chloride. Under these conditions the silver bromide was either in the parallel orientation, or in a (111) orientation (see table). The two orientations occurred in very varying proportions from specimen to specimen, even when the two specimens were prepared simultaneously.

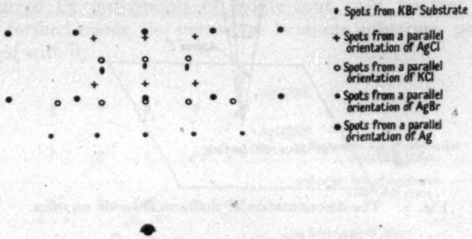
• Spots from KBr Substrate
+ Spots from a parallel orientation of AgCl
○ Spots from a parallel orientation of KCl
• Spots from a parallel orientation of AgBr
• Spots from a parallel orientation of Ag

Fig. 2. The analysis of fig. 1.

(ii) *Thallium Chloride Deposits*

When thallium chloride was deposited on rocksalt or mica, the normal bulk structure of thallium chloride (cubic, CsCl type) was observed. On potassium bromide, however, the thallium chloride was found to crystallize with a rocksalt type structure having a cube edge of 6·17 ± 0·06 Å. Fig. 3 shows the pattern from such a layer, with the electron beam set along the potassium bromide [001] azimuth, the strong cubic cross-grating pattern indicating that the new structure is in parallel orientation on the substrate. This abnormal structure was usually accompanied by a small amount of thallium chloride with the normal structure, some of which was in the same orientation as observed on rocksalt substrates.

Two further features are of interest. Firstly, the diffraction spots from the thallium chloride layers on rocksalt were often split up into pairs of subsidiary spots. This splitting was consistent with the presence of (111) type facets perpendicular to the surface, causing extensions of the reciprocal lattice points perpendicular to these facets. The identification of the facets cannot be considered conclusive, however, because the magnitude of the splitting did not allow sufficiently accurate measurements to be made.

Secondly, the diffraction spots from the thallium chloride layers on mica were also split up into pairs of subsidiary spots, on two of the specimens examined. This splitting is illustrated in fig. 4, which shows the pattern obtained at the thallium chloride $[2\bar{1}\bar{1}]$ azimuth. In this instance, the paired spots are due to a disorientation effect, and indicate that the thallium chloride (111) planes are rotated by approximately two degrees from being parallel to the mica (001) planes. Since the splitting occurred at all azimuthal settings of the specimens, it follows that the rotations occurred about all axes lying in the halide (111) plane. The [111] axis of any given thallium chloride crystallite thus lies on a cone of semi-apical angle 2° (see fig. 5), the distribution of [111] axes around this conical surface being uniform. The diffraction patterns from these specimens are obtained by considering each reciprocal lattice point to be replaced by a circular loop. No explanation of this effect has so far been found, but the effect might have some relation to the 'spiral growth' described by Frank (1949). The diffraction effects to be expected from crystals containing spiral dislocations have been discussed by Wilson (1948) and Frank (1948), and these effects bear some resemblance to the observed circular loops. This point will be discussed in more detail in a future publication.

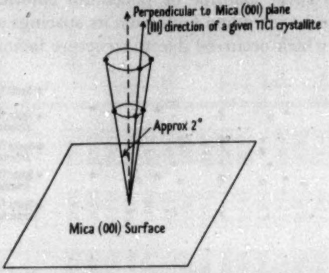
Perpendicular to Mica (001) plane
[111] direction of a given TlCl crystallite
Approx 2°
Mica (001) Surface

Fig. 5. The disorientation of thallium chloride on mica.

Fig. 4 also shows a diffuse streak pattern in the background. These streaks arise from continuous rods of intensity through all of the reciprocal lattice points, and along all of the [100] type directions. Similar diffuse patterns also occurred with the silver halides. These effects will be considered in detail in a later report.

§ 4. DISCUSSION

The inter-atomic misfits between the substrate and overgrowth lattices is indicated in the table for all of the observed orientations. Although there are several examples of small misfits, there are also cases of fairly high misfits. In particular it is noted that silver chloride orients on mica, with a misfit of −24%. Royer (1928) has grown many substances with a rocksalt type structure on mica, by crystallization from solution. He found that substances for which the misfit was less than about 15% were oriented (with the same orientations as now observed for silver chloride), but that for larger misfits no orientation occurred The fact that the silver chloride orients, despite the −24% misfit, therefore suggests that the method of growth of oriented deposits is an important factor to be taken into account by any theory of the process; an upper limit of percentage misfit observed for one method of growth does not necessarily apply to other methods of growing the same series of substances. Thus although the percentage misfit does appear to have some significance in connection with the appearance of oriented overgrowths, a small percentage misfit is certainly not an essential condition. The orientation of the silver halides on magnesium oxide presents an interesting case. A good numerical fit (misfit of approximately 6%) could be obtained if the orientation indicated in fig. 6 were to occur. This orientation would require ions of similar sign to be adjacent (e.g. at P, fig. 6), however, and this probably explains why it does not occur.

When silver chloride was deposited on potassium bromide at 150° c, diffraction patterns due to silver bromide only were observed, so that all of the silver chloride had presumably reacted with the potassium bromide. In such cases no patterns due to potassium chloride were obtained (potassium chloride was only observed with depositions at the lower substrate temperatures). This might mean that the reaction occurred by movements of halide ions only, so that the potassium chloride was formed inside the potassium bromide substrate, possibly forming a mixed crystal with it.

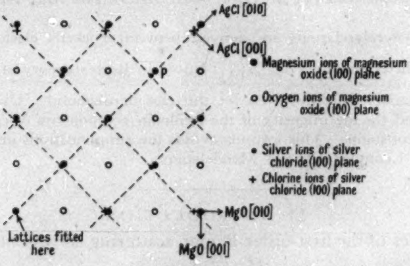
AgCl [010]
AgCl [001]
● Magnesium ions of magnesium oxide (100) plane
○ Oxygen ions of magnesium oxide (100) plane
• Silver ions of silver chloride (100) plane
+ Chlorine ions of silver chloride (100) plane
P
MgO [010]
MgO [001]
Lattices fitted here

Fig. 6. A non-observed orientation of AgCl on MgO.

The final point worthy of note is the change of structure of thallium chloride from its normal caesium chloride type structure to a rocksalt type structure. Caesium chloride itself is known to switch to a rocksalt type structure above 445° c, and the ammonium halides also undergo similar transitions. Recently Schultz (1950) has reported a case of caesium bromide (normally caesium chloride type structure) crystallizing with a rocksalt type structure when evaporated on to a lithium fluoride substrate. Such transitions must be influenced by the substrate, since the thallium chloride had its normal structure when grown on mica and rocksalt, but had the rocksalt type structure when deposited on potassium bromide under identical experimental conditions. The fit of the abnormal thallium chloride structure on potassium bromide is only 6% compared with 17% for the normal structure. On mica and rocksalt substrates, however, the best possible fits which could occur for the abnormal structure are larger than those which actually occur for the normal structure.

ACKNOWLEDGMENTS

The author wishes to thank Sir George Thomson and Dr. M. Blackman for their interest in the work and for valuable discussion. He also wishes to thank Messrs. Hilger and Watts (Hilger Division) for supplying the rocksalt and potassium bromide used.

REFERENCES

Frank, F. C., 1948, *Research*, **2**, 542; 1949, *Discussions of the Faraday Society*, No. 5, 48.
van der Merwe, J. H., 1949, *Discussions of the Faraday Society*, No. 5, 201.
Pashley, D. W., 1950, *Acta Crystallogr.*, **3**, 163.
Royer, L., 1928, *Bull. Soc. Franç. Min.*, **51**, 7.
Schultz, L. G., 1950, *J. Appl. Phys.*, **21**, 942.
Smollett, M., and Blackman, M., 1951, *Proc. Phys. Soc.* A, **64**, 683.
Wilson, A. J. C., 1948, *Research*, **2**, 541.

On the Relations between the Photo-Elastic Properties and the Raman Effect in Crystals

By O. THEIMER*

Department of Mathematical Physics, University of Edinburgh

Communicated by M. Born; MS. received 24th May 1951

ABSTRACT. General relations are derived between Pockel's elasto-optical constants and the polarizability derivatives $\alpha_{\varrho\sigma,\mu}\begin{pmatrix} l \\ kk' \end{pmatrix}$ used in Born's theory of the Raman effect in crystals. Numerical data are given for the case of diamond. Using these relations a formula is derived for the intensity of the Brillouin components of crystals in terms of the elasto-optical constants. This formula avoids the simplifications implied in an earlier expression due to Leontowitsch and Mandelstamm.

§1. INTRODUCTION

All properties of the first-order Raman scattering are essentially determined by the derivatives $\alpha_{\varrho\sigma,\mu}\begin{pmatrix} l-l' \\ kk' \end{pmatrix}$ (ρ, σ, $\mu = 1, 2, 3$) of the polarizability tensor, which describe the changes of the polarizability of the atom $\begin{pmatrix} l \\ k \end{pmatrix}$ (l denotes cell index, k denotes the different atoms in the elementary cell of a compound lattice), when any other atom $\begin{pmatrix} l' \\ k' \end{pmatrix}$ is slightly displaced in the direction μ from the equilibrium position.

The numerical values of these characteristic constants are so far unknown; their calculation presents in most cases considerable difficulties. There are three possibilities of determining these constants: theoretical calculation with the help of quantum mechanics, determination of the intensity ratio between Rayleigh and Raman scattering, and calculations based on photo-elastic measurements.

The theoretical calculation is confined to very simple systems, because of mathematical difficulties. It appears that in no case has it so far been carried out; a possible exception is the hydrogen molecule, which, according to a remark of Burstein and Smith (1948) (without quotation), has been treated by Wang.

---

* Now at Physics Department, Technische Hochschule, Graz, Austria.

The intensities of the Rayleigh and Raman scattering are simply related only in the case of gases. Here, however, the experimental difficulties of obtaining accurate values for the intensity ratio are considerable, because of the extremely weak intensity of the Raman scattering. The situation with regard to liquids, on the other hand, is confused from the theoretical point of view. In liquids, the scattering with unchanged or nearly unchanged frequency is a mixture of Rayleigh and Raman or Brillouin scattering, to which the polarizability $\alpha_{\varrho\sigma}$ and the polarizability derivatives $\alpha_{\varrho\sigma,\mu}$ contribute unknown shares. But even when this fact is not taken into account there remain other difficulties, such as the size of the region within which the scattered light is coherent, which are not known.

Similar difficulties arise in crystals. In an ideal crystal there is no Rayleigh scattering if the wavelength of the incident light is longer than twice the lattice constant.* All real Rayleigh scattering, which again in most cases can hardly be separated from the Brillouin components, results from lattice imperfections. For this kind of scattering no reliable theory exists.

Most of these difficulties disappear if one tries to derive the polarizability derivatives from the elasto-optical constants p_{ik}, which are closely connected with them. The only fundamental limitation of this method arises from the fact that the elasto-optical constants are essentially macroscopic constants and that their number is usually smaller than the number of independent $\alpha_{\varrho\sigma,\mu}\begin{pmatrix} l-l' \\ kk' \end{pmatrix}$, which are atomistic quantities. Only if the symmetry of a crystal is high enough can some of the $\alpha_{\varrho\sigma,\mu}\begin{pmatrix} l-l' \\ kk' \end{pmatrix}$ at least be determined separately. This is, for instance, the case with diamond.

In this paper general relations between the photo-elastic constants and the polarizability derivatives will be given. The resulting formulae will be used to calculate the polarizability and the polarizability derivatives of diamond from photo-elastic measurements of Ramachandran (1950).

Further, a formula for the intensity of the Brillouin components of crystals in terms of the elasto-optical constants will be derived. This formula avoids the numerous simplifications made in the derivation of the formula of Leontowitsch and Mandelstamm (1931) which have been discussed in a previous paper (Theimer 1951).

§2. GENERAL THEORY OF THE DIELECTRIC PROPERTIES OF CRYSTALS

A well-known and remarkable feature of the atomistic theory of the dielectric properties of crystals is the existence of the two different formulae of Lorentz–Lorenz and Drude, which describe the relation between the polarizabilities of the single atoms and the macroscopic index of refraction. In the present paper a similar relation will be investigated, namely the relation between the polarizability derivatives $\alpha_{\varrho\sigma,\mu}\begin{pmatrix} l-l' \\ kk' \end{pmatrix}$ of the single atoms and the macroscopic changes of the dielectric properties, which are described by the elasto-optical constants p_{ik}. It is, therefore, necessary to discuss shortly the problems connected with the existence of two different formulae for the index of refraction, in order to avoid ambiguity.

---

* This statement is only approximately true, since there is always a Rayleigh scattering resulting from the mechanical and electrical inharmonicity of the crystals. This second-order Rayleigh scattering can, however, be neglected in most crystals, compared with the first-order effects.

For the purpose of this paper the difference between the two formulae can be considered to be purely formal, i.e. depending on the definition. In both cases the total polarization $\mathbf{P}$ of the crystal is represented as the sum of the electric moments $\mathbf{p}\binom{l}{k}$ induced in the single atoms

$$\mathbf{P}=\sum_{u}\mathbf{p}\binom{l}{k}. \qquad \ldots\ldots(2.1)$$

The $\mathbf{p}\binom{l}{k}$, however, are expressed in a different way:

$$\mathbf{p}\binom{l}{k}=\kappa\binom{l}{k}\mathbf{E}\ldots(a), \quad \text{and} \quad \mathbf{p}\binom{l}{k}=\alpha\binom{l}{k}\mathbf{F}\ldots(b). \qquad \ldots\ldots(2.2)$$

Here the $\kappa\binom{l}{k}$ and the $\alpha\binom{l}{k}$ are the atomic susceptibilities* and polarizabilities of the single atoms, $\mathbf{E}$ the average macroscopic electric field in the crystal and $\mathbf{F}$ the effective microscopic field polarizing the single atoms. Definition (*a*) corresponds to Drude's formula, (*b*) to the formula of Lorentz–Lorenz.

This formal aspect of the problem is, of course, of little importance compared with the numerous questions of real physical interest which are connected with the determination of $\mathbf{F}$. But it is just this formal aspect which is important for the present paper, as it allows the unambiguous definition of the physical entities used in the following sections. Since in all existing papers on the Raman effect in crystals the dipole moments $\mathbf{p}\binom{l}{k}$ induced in the single atoms are represented as functions of $\mathbf{E}$ and not of $\mathbf{F}$, the definition (2.2 *a*) will be used which justifies the application of equation (3.7). It is, however, convenient to change the notation and to write $\alpha\binom{l}{k}$ for the atomic susceptibility, since this is the common usage in all papers on the Raman effect.

§ 3. THE RELATIONS BETWEEN THE ELASTO-OPTICAL CONSTANTS p_{ik} AND THE POLARIZABILITY DERIVATIVES $\alpha_{\varrho\sigma,\mu}\binom{l-l'}{kk'}$

Let ϵ^{-1} be the reciprocal tensor of the dielectric constant, which determines the index ellipsoid and S an homogeneous strain defined by† $S_{\varrho\varrho}=\partial u_\varrho/\partial r_\varrho$, $S_{\varrho\sigma}=\partial u_\varrho/\partial r_\sigma+\partial u_\sigma/\partial r_\varrho$, where $\mathbf{r}$ = position vector, $\mathbf{u}$ = displacement vector of a lattice point, $\rho, \sigma=1, 2, 3$.

---

* The macroscopic susceptibility κ is defined as the polarization per unit field and unit volume. The atomic susceptibility $\kappa\binom{l}{k}$, introduced here, is however not related to the unit volume. The notation has been chosen to indicate that the summation of $\kappa\binom{l}{k}$ over all atoms in 1 cm^3 gives immediately the susceptibility.

† Usually $S_{\varrho\sigma}$ is defined as $S_{\varrho\sigma}=\frac{1}{2}(\partial u_\varrho/\partial r_\sigma+\partial u_\sigma/\partial r_\varrho)$. Here, according to Pockel, the factor $\frac{1}{2}$ is omitted; thus terms with mixed indices can then be treated in the same manner as terms with equal indices.

The homogeneous strain S produces a change in ϵ^{-1}, which in first approximation may be considered as a linear function of the deformation:

$$\Delta\epsilon^{-1}_{\varrho\sigma} = \epsilon^{-1}_{\varrho\sigma} - \epsilon^{(0)-1}_{\varrho\sigma} = \sum_{\mu\nu} p_{\varrho\sigma,\mu\nu} S_{\mu\nu}. \qquad \ldots\ldots(3.1)$$

The $p_{\varrho\sigma,\mu\nu}$ are Pockel's elasto-optical constants.

For such small changes in ϵ^{-1} and the dielectric tensor ϵ, we obtain, by differentiating the identity

$$\sum_{\mu} \epsilon^{-1}_{\varrho\mu}\epsilon_{\mu\sigma} = \delta_{\varrho\sigma}, \qquad \ldots\ldots(3.2)$$

the first-order relation:

$$\sum_{\mu} \{\Delta\epsilon^{-1}_{\varrho\mu}\epsilon^{(0)}_{\mu\sigma} + \epsilon^{(0)-1}_{\varrho\mu}\Delta\epsilon_{\mu\sigma}\} = 0. \qquad \ldots\ldots(3.3)$$

For cubic crystals for which

$$\epsilon^{(0)}_{\mu\sigma} = \delta_{\mu\sigma}\epsilon, \quad \epsilon^{(0)-1}_{\varrho\mu} = \delta_{\varrho\mu}\epsilon^{-1} \qquad \ldots\ldots(3.4)$$

the above relation reduces to

$$\Delta\epsilon^{-1}_{\varrho\sigma} = -\frac{\Delta\epsilon_{\varrho\sigma}}{\epsilon^2} = \sum_{\mu\nu} p_{\varrho\sigma,\mu\nu} S_{\mu\nu}. \qquad \ldots\ldots(3.5)$$

The corresponding changes of susceptibility $\Delta\alpha_{\varrho\sigma}$ can be found in the following way: put ($\mathbf{D}$ = dielectric displacement vector)

$$\mathbf{D} = \epsilon\mathbf{E} = \mathbf{E} + 4\pi\mathbf{P} \quad \text{and} \quad \mathbf{P} = \alpha\mathbf{E}, \qquad \ldots\ldots(3.6)$$

then

$$\alpha = (\epsilon - 1)/4\pi. \qquad \ldots\ldots(3.7)$$

Hence

$$\Delta\alpha_{\varrho\sigma} = \Delta\epsilon_{\varrho\sigma}/4\pi = \sum_{\mu\nu} \alpha_{\varrho\sigma,\mu\nu} S_{\mu\nu}, \qquad \ldots\ldots(3.8)$$

where

$$\alpha_{\varrho\sigma,\mu\nu} = -(\epsilon^2/4\pi) p_{\varrho\sigma,\mu\nu}. \qquad \ldots\ldots(3.9)$$

We now derive expressions for the $\alpha_{\varrho\sigma,\mu\nu}$ in terms of the $\alpha_{\varrho\sigma,\mu}\binom{l}{kk'}$ which are used in the theory of the Raman effect.

Consider first arbitrary displacements $\mathbf{u}\binom{l}{k}$ of the atoms $\binom{l}{k}$ and denote with $\Delta\alpha_{\varrho\sigma}\binom{l}{k}$ the changes of the susceptibility of the atom $\binom{l}{k}$, caused by the displacements $\mathbf{u}\binom{l'}{k'}$ of the other atoms. Then

$$\Delta\alpha_{\varrho\sigma}\binom{l}{k} = \sum_{\mu}\sum_{l'k'} \alpha_{\varrho\sigma,\mu}\binom{l-l'}{kk'} u_{\mu}\binom{l'}{k'}. \qquad \ldots\ldots(3.10)$$

The total change of the susceptibility of the whole crystal is

$$\Delta\alpha_{\varrho\sigma} = \sum_{lk} \Delta\alpha_{\varrho\sigma}\binom{l}{k} = \sum_{\mu}\sum_{lk}\sum_{l'k'} \alpha_{\varrho\sigma,\mu}\binom{l-l'}{kk'} u_{\mu}\binom{l'}{k'}. \qquad \ldots\ldots(3.11)$$

In the case of a homogeneous strain $S_{\mu\nu} = \partial u_\mu/\partial r_\nu + \partial u_\nu/\partial r_\mu$ the displacements are linear functions of $S_{\mu\nu}$. These functions, however, are different in the classical continua theory and in the correct atomistic theory of Born. In the classical continua theory they are

$$u_{\mu}\binom{l'}{k'} = \sum_{\nu} \frac{\partial u_\mu}{\partial r_\nu} r_\nu\binom{l'}{k'}. \qquad \ldots\ldots(3.12)$$

In lattice dynamics (3.12) is a zero order approximation which holds only for the centres of gravity of the single elementary cells. The actual displacements $u_\mu \binom{l'}{k'}$ of the different atoms in the elementary cell of a compound lattice differ from (3.12) by a term independent of l' of the form

$$u_\mu^{(1)} \binom{l'}{k'} = \sum_{\nu\eta} \Gamma_{\mu\nu\eta}(k') \frac{\partial u_\nu}{\partial r_\eta}. \qquad \ldots\ldots(3.13)$$

In the general case $\Gamma_{\mu\nu\eta}(k')$ is a somewhat complicated function of the dynamical matrix of the lattice, which has been given by Begbie and Born (1947).[*]

The total displacement $u \binom{l'}{k'}$ connected with a homogeneous strain is from (3.12) and (3.13):

$$u_\mu \binom{l'}{k'} = u_\mu^{(0)} \binom{l'}{k'} + u_\mu^{(1)}(k') = \sum_\nu \left[\frac{\partial u_\mu}{\partial r_\nu} r_\nu \binom{l'}{k'} + \sum_\eta \Gamma_{\mu\nu\eta}(k') \frac{\partial u_\nu}{\partial r_\eta} \right]. \qquad \ldots\ldots(3.14)$$

The susceptibility changes of the single atoms k depend, of course, mainly on the displacements of the other atoms $\binom{l'}{k'}$, which are not too distant from them, i.e. the first, second, third . . . neighbours. To express this (3.11) applied to a homogeneous strain has to be written in a different form. Write

$$\mathbf{u} \binom{l'}{k'} = \mathbf{u} \binom{l}{k} - \mathbf{u} \binom{l-l'}{kk'}, \qquad \ldots\ldots(3.15)$$

where

$$\mathbf{u} \binom{l-l'}{kk'} = \mathbf{u}(l) - \mathbf{u}(l') + \mathbf{u}(k) - \mathbf{u}(k'). \qquad \ldots\ldots(3.16)$$

Then (3.11) becomes

$$\Delta\alpha_{\varrho\sigma} = \sum_\mu \sum_{lk} \sum_{l'k'} \alpha_{\varrho\sigma,\mu} \binom{l-l'}{kk'} \left[u_\mu \binom{l}{k} - u_\mu \binom{l-l'}{kk'} \right]. \qquad \ldots\ldots(3.17)$$

Put $l-l'=l$ and use the relation $\sum_{lk'} \alpha_{\varrho\sigma,\mu} \binom{l}{kk'} = 0$, which follows from the invariance of $\alpha_{\varrho\sigma}$ against rigid translations of the whole lattice: then (N = number of elementary cells per cm^3)

$$\Delta\alpha_{\varrho\sigma} = -N \sum_\mu \sum_k \sum_{lk'} \alpha_{\varrho\sigma,\mu} \binom{l}{kk'} u_\mu \binom{l}{kk'}. \qquad \ldots\ldots(3.18)$$

Introduce (3.14) in (3.18), then

$$\Delta\alpha_{\varrho\sigma} = -N \sum_{\mu\nu} \sum_k \sum_{lk'} \alpha_{\varrho\sigma,\mu} \binom{l}{kk'} \left[\frac{\partial u_\mu}{\partial r_\nu} r_\nu \binom{l}{kk'} + \sum_\eta \Gamma_{\mu\nu\eta}(kk') \frac{\partial u_\nu}{\partial r_\eta} \right]. \qquad \ldots\ldots(3.19)$$

Rearrange with respect to the $\partial u_\mu / \partial r_\nu$, then

$$\Delta\alpha_{\varrho\sigma} = \sum_{\mu\nu} \alpha_{\varrho\sigma,\mu\nu} \frac{\partial u_\mu}{\partial r_\nu}, \qquad \ldots\ldots(3.20)$$

where

$$\alpha_{\varrho\sigma,\mu\nu} = -N \sum_k \sum_{lk'} \left[\alpha_{\varrho\sigma,\mu} \binom{l}{kk'} r_\nu \binom{l}{kk'} + \sum_\eta \alpha_{\varrho\sigma,\eta} \binom{l}{kk'} \Gamma_{\eta\mu\nu}(kk') \right].$$

$(\partial u_\mu / \partial r_\nu)\alpha_{\varrho\sigma,\mu\nu}$ represents the changes of the susceptibility $\alpha_{\varrho\sigma}$ of the crystal connected with a shear $\partial u_\mu / \partial r_\nu$ of the angle between the μ- and ν-axes of the undeformed crystal. The same shear and the same susceptibility change results from a homogeneous deformation $\partial u_\nu / \partial r_\mu$, if $\partial u_\mu / \partial r_\nu = \partial u_\nu / \partial r_\mu$. Hence

$$(\partial u_\mu / \partial r_\nu)\alpha_{\varrho\sigma,\mu\nu} = (\partial u_\mu / \partial r_\nu)\alpha_{\varrho\sigma,\nu\mu} \qquad \ldots\ldots(3.21)$$

or

$$\alpha_{\varrho\sigma,\mu\nu} = \alpha_{\varrho\sigma,\nu\mu}. \qquad \ldots\ldots(3.22)$$

---

[*] (3.13) can be derived from eqns. (2.5) and (2.22) of Begbie and Born if one replaces q_γ by $(1/u_\beta)\, \partial u_\beta / \partial r_\gamma$. This substitution is allowed for long elastic waves as can be seen from differentiating $u_\beta = U_\beta \exp(i\mathbf{q} \cdot \mathbf{r})$.

With the help of the invariance condition (3.22) and taking into account that the factor $\frac{1}{2}$ has been omitted in the symmetrized strain components $S_{\mu\nu}=\partial u_\mu/\partial r_\nu+\partial u_\nu/\partial r_\mu$, (3.20) reads

$$\Delta\alpha_{\varrho\sigma}=\sum_{\mu\nu}\alpha_{\varrho\sigma,\mu\nu}S_{\mu\nu}. \qquad \ldots\ldots(3.23)$$

A comparison between (3.23) and (3.8), (3.9) yields

$$N\sum_k\sum_{lk'}\left[\alpha_{\varrho\sigma,\mu}\binom{l}{kk'}r_\nu\binom{l}{kk'}+\sum_\eta\alpha_{\varrho\sigma,\eta}\binom{l}{kk'}\Gamma_{\eta\mu\nu}(kk')\right]=\frac{\epsilon^2}{4\pi}p_{\varrho\sigma,\mu\nu}. \qquad \ldots\ldots(3.24)$$

This is the general relation between the susceptibility derivatives $\alpha_{\varrho\sigma,\mu}\binom{l}{kk'}$ and the elasto-optical constants $p_{\varrho\sigma,\mu\nu}$ in cubic crystals.

§4. NUMERICAL VALUES OF THE $\alpha_{\varrho\sigma,\mu}\binom{l}{kk'}$ IN DIAMOND

The photo-elastic constants of diamond have been determined by Ramachandran (1950). There are only three independent $p_{\varrho\sigma,\mu\nu}$ in cubic crystals. They are given (in the notation of Pockel) in table 1.

Table 1

$$p_{11}=p_{\varrho\varrho,\varrho\varrho}=p_{\sigma\sigma,\sigma\sigma}=p_{\mu\mu,\mu\mu}=-0{\cdot}31$$

$$p_{12}=p_{\varrho\varrho,\sigma\sigma}=p_{\varrho\varrho,\mu\mu}=p_{\sigma\sigma,\varrho\varrho}=p_{\sigma\sigma,\mu\mu}=p_{\mu\mu,\varrho\varrho}=p_{\mu\mu,\sigma\sigma}=0{\cdot}09$$

$$p_{44}=p_{\varrho\sigma,\varrho\sigma}=p_{\sigma\mu,\sigma\mu}=p_{\mu\varrho,\mu\varrho}=p_{\sigma\varrho,\sigma\varrho}=p_{\mu\sigma,\mu\sigma}=p_{\varrho\mu,\varrho\mu}=-0{\cdot}12$$

All the other $p_{\varrho\sigma,\eta\nu}$ are zero

The great number of $\alpha_{\varrho\sigma,\mu}\binom{l}{kk'}$ is reduced by the particularly high symmetry of diamond to four independent constants, if the simplifying assumption is made that the susceptibility of the atom k depends only on the displacements of the first neighbours and of the atom k itself ($l=0, 1, 2, 3, 4$). This assumption is quite admissible in atomic lattices with homopolar binding.

The symmetry relations between the $\alpha_{\varrho\sigma,\mu}\binom{l}{kk'}$ of diamond have been derived in a previous paper (Theimer 1951) and are presented in table 2.

Table 2

$\alpha_{\varrho\sigma,\mu}\binom{l}{kk'}\diagdown l$	0	1	2	3	4	$\alpha_{\varrho\sigma,\mu}\binom{l}{kk'}\diagdown l$	0	1	2	3	4
$\alpha_{11,1}$	0	A	$-A$	$-A$	A	$\alpha_{12,1}=\alpha_{23,3}=\alpha_{21,1}=\alpha_{32,3}$	0	E	$-E$	E	$-E$
$\alpha_{22,2}$	0	A	$-A$	A	$-A$	$\alpha_{23,2}=\alpha_{31,1}=\alpha_{32,2}=\alpha_{13,1}$	0	E	E	$-E$	$-E$
$\alpha_{33,3}$	0	A	A	$-A$	$-A$	$\alpha_{31,3}=\alpha_{12,2}=\alpha_{13,3}=\alpha_{21,2}$	0	E	$-E$	$-E$	E
$\alpha_{11,2}=\alpha_{33,2}$	0	B	$-B$	B	$-B$	$\alpha_{12,3}=\alpha_{21,3}$	$-4D$	D	D	D	D
$\alpha_{22,3}=\alpha_{11,3}$	0	B	B	$-B$	$-B$	$\alpha_{23,1}=\alpha_{32,1}$	$-4D$	D	D	D	D
$\alpha_{33,1}=\alpha_{22,1}$	0	B	$-B$	$-B$	B	$\alpha_{31,2}=\alpha_{13,2}$	$-4D$	D	D	D	D

The $\alpha_{\varrho\sigma,\mu}\binom{\bar{l}}{k'k}$ ($\bar{l}$ denotes the neighbours of the atom k') are found with the help of the relation $\alpha_{\varrho\sigma,\mu}\binom{l}{kk'}=-\alpha_{\varrho\sigma,\mu}\binom{\bar{l}}{k'k}$.

The values of $r_\varrho\binom{l}{kk'}$ for diamond have been given by Smith (1948); they are contained in table 3.

The values of $\Gamma_{\mu\nu\eta}$ are (Theimer 1951)

$$\Gamma_{\mu\nu\eta}(kk')=\Gamma_{\mu\nu\eta}(k)-\Gamma_{\mu\nu\eta}(k')=\begin{cases}0{\cdot}66\ a/2 \text{ for } \mu\neq\nu\neq\eta,\\ 0 \text{ for all other cases.}\end{cases} \qquad \ldots\ldots(4.1)$$

Using tables 1, 2, 3 and eqns. (3.24) and (4.1) the susceptibility derivatives A, B, D, E are $(R=\epsilon^2/16\pi Na=5{\cdot}88\times10^{-16}$, $\epsilon=n^2=6{\cdot}81$, $n=2{\cdot}61=$ index of refraction)

$$A=p_{11}R=-1{\cdot}82\times10^{-16}\,\text{cm}^2,\quad B=p_{12}R=0{\cdot}53\times10^{-16}\,\text{cm}^2,$$
$$(E+0{\cdot}66D)=p_{44}R=-0{\cdot}71\times10^{-16}\,\text{cm}^2. \qquad \ldots\ldots(4.2)$$

For the susceptibility $\alpha(k)$ of the carbon atom in diamond one gets from the definition (3.7):

$$\alpha=\sum_{lk}\alpha\binom{l}{k}=2N\alpha(k)=\frac{\epsilon-1}{4\pi}, \qquad \ldots\ldots(4.3)$$

$$\alpha(k)=\frac{\epsilon-1}{8\pi N}=2{\cdot}62\times10^{-24}\ \text{cm}^3. \qquad \ldots\ldots(4.4)$$

These values for A, B $(E+0{\cdot}66D)$ and $\alpha(k)$ give calculations of the relative intensities of the Brillouin components of diamond in good agreement with experiment (Theimer 1951). The numerical values given in (4.2) and (4.4) are valid for radiation with wavelength $\lambda=2536$ Å.

Table 3

$\mathbf{r}\backslash l$	1	2	3	4	$\mathbf{r}\backslash\bar{l}$	$\bar{1}$	$\bar{2}$	$\bar{3}$	$\bar{4}$
x_1	$\frac{1}{2}a$	$-\frac{1}{2}a$	$-\frac{1}{2}a$	$\frac{1}{2}a$	x_1	$-\frac{1}{2}a$	$\frac{1}{2}a$	$\frac{1}{2}a$	$-\frac{1}{2}a$
x_2	$\frac{1}{2}a$	$-\frac{1}{2}a$	$\frac{1}{2}a$	$-\frac{1}{2}a$	x_2	$-\frac{1}{2}a$	$\frac{1}{2}a$	$-\frac{1}{2}a$	$\frac{1}{2}a$
x_3	$\frac{1}{2}a$	$\frac{1}{2}a$	$-\frac{1}{2}a$	$-\frac{1}{2}a$	x_3	$-\frac{1}{2}a$	$-\frac{1}{2}a$	$\frac{1}{2}a$	$\frac{1}{2}a$

$a=$lattice constant$=1{\cdot}78\times10^{-8}$ cm.

§ 5. THE BRILLOUIN EFFECT IN CRYSTALS

The intensity of the Brillouin components of crystals can be calculated from the following formula (Theimer 1951):

$$I=\frac{h}{N\pi\nu\binom{Q}{j_e}}\,\frac{1}{1-\exp\left\{-h\nu\binom{Q}{j_e}\Big/\boldsymbol{k}T\right\}}\,\alpha_{\varrho\sigma}\binom{Q}{j_e}\alpha^*_{\mu\nu}\binom{Q}{j_e}A_\sigma A^*_\nu s_\varrho s_\mu, \qquad \ldots\ldots(5.1)$$

where $\mathbf{A}$, $\mathbf{A}^*$ are the complex amplitudes of the incident light wave, $\mathbf{s}=$unit vector normal to the direction of observation, $\nu\binom{Q}{j_e}$ is the frequency of the lattice normal vibration j_e with wave vector $\mathbf{Q}$, which fulfils the condition $\mathbf{Q}=\mathbf{Q}''-\mathbf{Q}'$. ($\mathbf{Q}'$, $\mathbf{Q}''$ are the wave vectors of the incident and the scattered light.)

$$\alpha_{\varrho\sigma}\binom{Q}{j_e}=iN\sum_\mu\sum_k\left\{\alpha^{(0)}_{\varrho\sigma}(k)Q_\mu+\sum_\nu\sum_{lk'}\left[\alpha_{\varrho\sigma,\mu}\binom{l}{kk'}Q_\nu r_\nu\binom{l}{kk'}\right.\right.$$
$$\left.\left.+\sum_\eta\alpha_{\varrho\sigma,\eta}\binom{l}{kk'}\Gamma_{\eta\mu\nu}(kk')Q_\nu\right]\right\}u_\mu\left(k\,\middle|\,\begin{matrix}Q\\ j_e\end{matrix}\right)^{-}. \qquad \ldots\ldots(5.2)$$

Here $u_\mu\left(k\,\middle|\,\begin{matrix}Q\\ j_e\end{matrix}\right)$ is the displacement of the atom k if the lattice performs the vibration $\binom{Q}{j_e}$. The index $j_e=1, 2, 3$ denotes three elastic vibrations, which can roughly be interpreted as one longitudinal and two transverse waves. Eqn. (5.2) can be expressed in terms of the photo-elastic constants.

Multiply (3.24) by $iQ_\nu u_\mu \begin{pmatrix} Q \\ \cdot \\ j_e \end{pmatrix}$ and sum over all μ, ν, then

$$iN\sum_{\mu\nu}\sum_{k}\sum_{lk'}\left[\alpha_{\varrho\sigma,\mu}\begin{pmatrix} l \\ kk' \end{pmatrix}Q_\nu r_\nu\begin{pmatrix} l \\ kk' \end{pmatrix}+\sum_{\eta}\alpha_{\varrho\sigma,\eta}\begin{pmatrix} l \\ kk' \end{pmatrix}\Gamma_{\eta\mu\nu}(kk')Q_\nu\right]u_\mu\left(k\middle|\begin{matrix} Q \\ \cdot \\ j_e \end{matrix}\right)$$
$$=\frac{i\epsilon^2}{4\pi}\sum_{\mu\nu}p_{\varrho\sigma,\mu\nu}Q_\nu u_\mu\left(k\middle|\begin{matrix} Q \\ \cdot \\ j_e \end{matrix}\right). \qquad \ldots\ldots(5.3)$$

(5.3) is identical with the second term of (5.2). The first term of (5.2) is, according to (4.3),

$$iN\sum_{\mu}\sum_{k}\alpha_{\varrho\sigma}(k)Q_\mu u_\mu\begin{pmatrix} Q \\ \cdot \\ j_e \end{pmatrix}=i\sum_{\mu}\frac{\epsilon_{\varrho\sigma}-1}{4\pi}Q_\mu u_\mu\begin{pmatrix} Q \\ \cdot \\ j_e \end{pmatrix}. \qquad \ldots\ldots(5.4)$$

(5.3) and (5.4) combined give

$$\alpha_{\varrho\sigma}\begin{pmatrix} Q \\ \cdot \\ j_e \end{pmatrix}=\frac{i}{4\pi}\sum_{\mu}\left\{(\epsilon_{\varrho\sigma}-1)Q_\mu+\epsilon^2\sum_{\nu}p_{\varrho\sigma,\mu\nu}Q_\nu\right\}u_\mu\begin{pmatrix} Q \\ \cdot \\ j_e \end{pmatrix}. \qquad \ldots\ldots(5.5)$$

There are still the eigenfrequencies $\nu\begin{pmatrix} Q \\ \cdot \\ j_e \end{pmatrix}$ in the intensity formula (5.1), which can be replaced by macroscopic constants. In the region $a|Q|\ll 1$ (a = lattice constant) there is a velocity of sound $\mathbf{v}\begin{pmatrix} s \\ \cdot \\ j_e \end{pmatrix}$ for each elastic branch j_e, which does not depend on $|Q|$ but only on the direction $\mathbf{Q}/|Q|=\mathbf{s}$; hence the frequency is $2\pi\nu\begin{pmatrix} s \\ \cdot \\ j_e \end{pmatrix}=\left|v\begin{pmatrix} s \\ \cdot \\ j_e \end{pmatrix}\right||Q|$.

The velocity of sound $\mathbf{v}\begin{pmatrix} s \\ \cdot \\ j_e \end{pmatrix}$ is completely determined by the elastic constants c_{ik} and the density ρ of the crystal. Hence the intensities of the Brillouin components can be represented as functions of the macroscopic constants c_{ik}, p_{ik}, and ρ. The simple form of (5.5) only holds in the case of cubic crystals. For crystals with lower symmetry the relation between the $\alpha_{\varrho\sigma}\begin{pmatrix} Q \\ \cdot \\ j_e \end{pmatrix}$ and the $p_{\varrho\sigma,\mu\nu}$ is, according to the general formula (3.4), much more complicated. Further, the macroscopic formula does not allow the calculation of the intensity ratio between the Brillouin components and the optical Raman lines. This ratio can be obtained only with the help of (5.1) and (5.2) and the corresponding formula for the Raman effect with optical vibrations (Theimer 1951).

ACKNOWLEDGMENTS

It is a pleasure to thank Professor Max Born for much encouragement and advice during the course of this work and the British Council for the award of a scholarship.

REFERENCES

Begbie, G. H., and Born, M., 1947, *Proc. Roy. Soc.* A, **188**, 179.
Burstein, E., and Smith, P. L., 1948, *Proc. Indian Acad. Sci.* A, **28**, 377.
Leontowitsch, M., and Mandelstamm, S., Jr., 1931, *Phys. Z. Sowjet*, **1**, 317.
Ramachandran, G. N., 1950, *Proc. Indian Acad. Sci.* A, **32**, 171.
Smith, H. J. M., 1948, *Phil. Trans. Roy. Soc.* A, **241**, 105.
Theimer, O., 1951, *Proc. Phys. Soc.* A, **64**, 1012.

The Effect of Dissolved Gases on the Tensile Strength of Liquids

BY C. G. KUPER AND D. H. TREVENA
Royal Society Mond Laboratory, Cambridge

Communicated by H. N. V. Temperley; MS. received 16*th May* 1951, *and in amended form* 24*th July* 1951

ABSTRACT. A theoretical investigation is made of the amount by which a dissolved gas should reduce the tensile strength of a liquid. The tensile strength is assumed proportional to the surface energy of a vapour nucleus, which is further assumed to have the form of a product of a function of its radius and a function of the dissolved gas concentration. The surface tension of a one-component system is expressed in terms of the van der Waals constants (developing Fowler's theory) and the treatment is extended to a two-component system on the basis of Wall and Stent's theory of van der Waals binary mixtures. The conclusion is reached that the reduction in the tensile strength of water caused by saturating it with air at a pressure of one atmosphere is less than $\frac{1}{2}\%$.

§ 1. INTRODUCTION

THE present theories of the tensile strength of liquids all appear to give values very much higher than experiment. Most of the experiments, such as those of the Berthelot tube type, give values for the tensile strength of water less than 60 atmospheres (Temperley 1947). That this discrepancy is, at any rate partially, due to the experimental conditions is suggested by the recent experimental work of Trevena (1950), which gives values for water of up to 300 atmospheres. Similar values were also obtained by Briggs (1950), Ursprung (1915) and Renner (1915). The lowest theoretical value, due to Temperley (1947), is about 500 atmospheres.

Many authors attempt to explain this discrepancy between theory and experiment by arguing that the ability of a liquid to withstand tension is reduced by the presence in it of *dissolved* gases; others believe that small bubbles of gas, in the liquid or in Griffiths cracks in the containing walls, are mainly responsible for the lowering of the tensile strength. The present theory attempts to decide between these possibilities by estimating the amount by which the tensile strength of a liquid is reduced by dissolved gas.

Temperley's theory is based on the use of a van der Waals equation of state,

$$(p+a/V^2)(V-b)=\boldsymbol{R}T. \qquad \ldots\ldots(1)$$

For suitable temperatures (less than some value T_m) it is possible to obtain metastable regions of negative pressure, i.e. tension.

On the other hand, theories such as that of Döring (1939), Fürth (1941), Frenkel (1946) and Fisher (1948), which attempt to calculate the rate of growth of a gas bubble, predict values for the tensile strength of water greater than 1000 atmospheres. Consideration of the stability of a microscopic bubble clearly necessitates a knowledge of the surface tension of the liquid. It is usually assumed that the surface tension at the boundary of such a bubble is the same as that over a plane surface, but, as the bubble must be of the order of molecular size (if its probable time of formation is to be less than 1 sec, say), this assumption appears unwarranted. Since the energy needed to create a small bubble and the van der Waals constant a are both measurements of the intermolecular attraction, we shall assume a value for the effective surface tension of a small bubble that will give a predicted tensile strength in agreement with that given by Temperley's theory.

We will write $\sigma=\sigma(r)$, the surface tension of a bubble of radius r and $\sigma^0=\sigma(\infty)$, the surface tension of a plane surface. Then for the bubble to exist in (unstable) equilibrium,

$$r=2\sigma/(p-p') \qquad \ldots\ldots(2)$$

where p and p' are the pressures in the bubble and liquid respectively. If the tension $t=-p'$ is greater than the value from (2), the bubble will expand indefinitely, and the liquid will rupture, while if it is less than $-p'$, the bubble will collapse. Hence the tensile strength is $t=2\sigma/r$ (neglecting p which is small compared with t).

If σ_w, σ_w^0 are the corresponding quantities for the pure liquid, we assume

$$\sigma/\sigma^0=\sigma_w/\sigma_w^0. \qquad \ldots\ldots(3)$$

We shall also denote the tensile strength of the pure liquid by t_w. r, in the 'hole' theory, is the radius of the largest bubble which can be formed by fluctuations, in a reasonable time, and is of the order of d, the intermolecular spacing. We assume r unaltered by the dissolved gas. Then $t_w=2\sigma_w/r$, and therefore

$$t/t_w=\sigma/\sigma_w=\sigma^0/\sigma_w^0. \qquad \ldots\ldots(4)$$

Hence the problem of finding the effect of dissolved gas on the tensile strength reduces, on our assumptions, to that of finding the effect of the solute on the surface tension. The assumptions seem justified if the arrangement of molecules in the liquid is not greatly altered by the dissolved gas, which is probably correct until the concentration reaches several per cent. We now proceed to discuss the surface tension in some detail.

§2. SURFACE TENSION AND THE PARACHOR

For a liquid in equilibrium with its own vapour the surface tension σ is given by

$$\sigma^{1/4}=(\rho_c-\rho_v)P/M^* \qquad \ldots\ldots(5)$$

where ρ_c, ρ_v are the densities of the liquid and vapour respectively, M^* the (chemical) molecular weight and P the so-called parachor. This equation is due to Sugden (1930) and is discussed further in the Appendix. Let us write $\sigma^{1/4}=\tau$, $(P/M^*)_c\rho_c=\tau_c$, $(P/M^*)_v\rho_v=\tau_v$. Then in virtue of eqn. (5) we have

$$\tau=\tau_c-\tau_v. \qquad \ldots\ldots(6)$$

Thus if τ_c and τ_v can be determined then τ, and hence σ, is known.

The determination of τ_c and τ_v for the liquid and vapour phase respectively demands a knowledge of the density, molecular weight and the parachor for that particular phase. The first two quantities can be readily found but the determination of the parachor is not so easy. Using the results of a paper by Fowler (1937) it has, however, been found possible to express the parachor of a substance in terms of known quantities if one assumes that the substance obeys a van der Waals equation of state; this extension of Fowler's theory is given in the Appendix, where it is shown that the parachor P is given by

$$P=\varpi a^{1/4}b^{7/12} \qquad \ldots\ldots(7)$$

where $\varpi = [3(3\alpha' + 1)/64\pi \boldsymbol{N}^{1/3}]^{1/4}$, $\alpha' = 1{\cdot}91$, $\boldsymbol{N}$ = Avogadro's number and a, b are the van der Waals constants for the substance.

Thus, for a van der Waals liquid and vapour, it should be possible to determine τ_c and τ_v respectively and hence σ. We shall now proceed to do this.

§ 3. THE SURFACE TENSION OF A VAN DER WAALS TWO-COMPONENT SYSTEM

We have seen that if the equation of state obeyed by a liquid is that of van der Waals then we can determine the parachor and hence the surface tension σ in terms of the van der Waals constants.

Let us therefore consider a gas whose van der Waals constants are a_1, b_1 which is dissolved in a liquid whose van der Waals constants are a_2, b_2; we shall treat this mixture as a van der Waals binary mixture. Such mixtures have been discussed by several workers.

If x_1 and x_2 are the molecular concentrations of the two components, then van der Waals assumed that the constants a, b for the mixture are given by

$$a = x_1{}^2 a_1 + 2x_1 x_2 a_{12} + x_2{}^2 a_2, \qquad b = x_1 b_1 + x_2 b_2, \qquad \ldots\ldots(8)$$

where a_{12} is a constant depending on the inter-species interaction. In our case component 1 is the gas and component 2 the liquid. Let x be the concentration of gas in the condensed phase. Then $x_1 = x$, $x_2 = (1 - x)$, and the two constants for the mixture in the condensed phase are given by

$$a_c = a_2 + 2x(a_{12} - a_2), \qquad b_c = b_2 + x(b_1 - b_2), \qquad \ldots\ldots(9)$$

where we have neglected x^2, which is justifiable for concentrations of gas up to 10%.

Let y be the concentration of gas in the vapour phase. Then, in a similar way, we find that the constants for the mixture in the vapour phase are given by

$$a_v = a_2 + 2y(a_{12} - a_2), \qquad b_v = b_2 + y(b_1 - b_2), \qquad \ldots\ldots(10)$$

where y^2 has been neglected on the ground that y^2 is small when x^2 is small. We justify this below.

We must now proceed to determine τ_c and then τ_v.

(i) *The Condensed Phase*

In this phase, since $\boldsymbol{RT} \ll a_c b_c$, then for one mole the volume $V = b_c$ approximately. (This amounts to taking the point C instead of A in fig. 1.)

The units of V are cm³ mole⁻¹; hence if ρ_c is expressed in g/cm³ we have $\rho_c = M^*/b_c$. Now for the condensed phase, the parachor P_c is $\varpi a_c{}^{1/4} b_c{}^{7/12}$. Thus $\tau_c = P_c/b_c = \varpi a_c{}^{1/4} b_c{}^{-5/12}$ or

$$\tau_c = \varpi a_2{}^{1/4} b_2{}^{-5/12} \{1 + x(a_{12}/2a_2 - 5b_1/12b_2 - 1/12)\} \qquad \ldots\ldots(11)$$

in virtue of eqns. (9). Thus τ_c has been expressed in terms of the van der Waals constants of the two components of our mixture.

(ii) *The Vapour Phase*

Wall and Stent (1949) give the following equations for the partial pressures of a two-component van der Waals mixture

$$\log p_1 = \log x_1 + \log(a_c/b_c{}^2) + 2\left\{\frac{x_1 a_1 + x_2 a_{12}}{a_c} - \frac{b_1}{b}\right\} + \frac{1}{\boldsymbol{RT}}\left\{\frac{a_c b_1}{b_c{}^2} - \frac{2x_1 a_1 + 2x_2 a_{12}}{b_c}\right\}, \qquad \ldots\ldots(12)$$

$$\log p_2 = \log x_2 + \log(a_c/b_c{}^2) + 2\left\{\frac{x_2 a_2 + x_1 a_{12}}{a_c} - \frac{b_2}{b_c}\right\} + \frac{1}{\boldsymbol{RT}}\left\{\frac{a_c b_2}{b_c{}^2} - \frac{2x_2 a_2 + 2x_1 a_{12}}{b_c}\right\},$$

where x_1, x_2 are the concentrations in the condensed phase. From eqn. (12) we have, after some reduction and substituting for x_1, x_2 and a_c, b_c,

$$\log(p_1/p_2) = \log x + \left\{2\left(\frac{a_{12}}{a_2} - \frac{b_1}{b_2}\right) + \frac{1}{b_2\boldsymbol{R}T}\left(\frac{a_2 b_1}{b_2} - 2a_{12} + a_2\right)\right\} + \mathrm{O}(x)$$

$$= \log x + \{\alpha + \beta/T + a_2/b_2\boldsymbol{R}T\} + \mathrm{O}(x) \qquad \text{(say).} \qquad \ldots\ldots(13)$$

If we put $C = \alpha + \beta/T + a_2/b_2\boldsymbol{R}T$ then we have

$$p_1/p_2 = x \exp\{C + \mathrm{O}(x)\}. \qquad \ldots\ldots(14)$$

Since y is the molecular concentration in the vapour phase, then, provided the vapour pressure is small, we may apply Dalton's law of partial pressures, i.e.

$$y = \frac{p_1}{p_1 + p_2} = \frac{p_1/p_2}{1 + p_1/p_2}. \qquad \ldots\ldots(15)$$

Thus, in virtue of equation (14) we have $y = xe^C$ to the first order in x. Hence y is approximately proportional to x; in other words, if the concentration of the gas component in the condensed phase is small, so also is its concentration in the vapour phase.

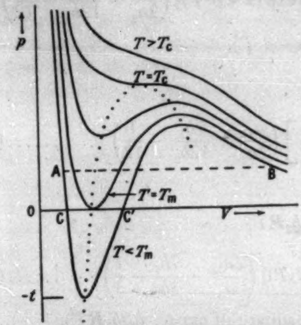

Fig. 1. Van der Waals isotherms. Provided $T < T_m$ the liquid exhibits a tensile strength t. The broken line AB is the equilibrium curve.

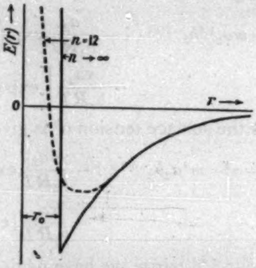

Fig. 2. Molecular interaction potentials of the form $E(r) = -\mu/r^6 + \lambda/r^n$. Dotted curve $n = 12$ full curve $n \to \infty$. The latter form has been used in the text.

From eqn. (9) we have $(a_c/b_c^2) = (a_2/b_2^2)(1 + \alpha x)$. Also, from eqn. (12) we have

$$p_1 = x\frac{a_c}{b_c^2}\left\{\exp\left(\alpha + \frac{\beta}{T}\right)\right\}\{1 + \mathrm{O}(x)\}, \qquad p_2 = (1 - x)\frac{a_c}{b_c^2}\left\{1 - \frac{a_2}{b_2\boldsymbol{R}T} - \alpha x + \mathrm{O}(x^2)\right\},$$

the definitions of α and β being given in eqn. (13). Thus the total pressure p in the vapour phase is given by

$$p = p_1 + p_2 = (a_2/b_2^2)\{x \exp(\alpha + \beta/T) + (1 - x)\exp(-a_2/b_2\boldsymbol{R}T)\},$$

neglecting $\mathrm{O}(x^2)$. Since $a_2/b_2 \ll \boldsymbol{R}T$, $\exp(-a_2/b_2\boldsymbol{R}T)$ may be neglected in comparison with $\exp(\alpha + \beta/T)$. Thus

$$p = \frac{a_2}{b_2^2}\{\exp(-a_2/b_2\boldsymbol{R}T)\}\{1 + x\exp(\alpha + \beta/T + a_2/b_2\boldsymbol{R}T)\}. \qquad \ldots\ldots(16)$$

As we are at the point B (fig. 1), we may apply the perfect gas equation with sufficient accuracy. We then have $1/V = p/\boldsymbol{R}T$ or

$$\frac{\rho_v}{M^*} = \frac{p}{\boldsymbol{R}T} = \frac{a_2}{b_2^2\boldsymbol{R}T}\{\exp(-a_2/b_2\boldsymbol{R}T)\}\{1 + x\exp(\alpha + \beta/T + a_2/b_2\boldsymbol{R}T)\}.$$

Then τ_v is given by $\tau_v = \varpi a_v^{1/4} b_v^{7/12} \rho_v / M^*$. ......(17)

Now

$$a_v^{1/4} b_v^{7/12} = a_2^{1/4} b_2^{7/12} \left\{ 1 + y\left(\frac{a_{12} - a_2}{2a_2} + \frac{7}{12}\frac{b_1 - b_2}{b_2} \right) \right\} \qquad \text{from eqns. (10)}$$

$$= a_2^{1/4} b_2^{7/12} \{1 + x(a_{12}/2a_2 + 7b_1/12b_2 - 13/12) \exp(\alpha + \beta/T + a_2/b_2\boldsymbol{RT})\},$$

since $y = xe^C$. So, after some reduction, we have, on substituting in eqn. (17)

$$\tau_v = \frac{\varpi a_2^{5/4} b_2^{-17/12}}{\boldsymbol{RT}} \left\{ \exp\left(\frac{-a^2}{b^2\boldsymbol{RT}} \right) \right\} \left\{ 1 + x\left(\frac{a_{12}}{2a_2} + \frac{7b_1}{12b_2} - \frac{1}{12} \right) \exp\left(\alpha + \frac{\beta}{T} + \frac{a_2}{b_2\boldsymbol{RT}} \right) \right\}. \qquad \text{......(18)}$$

Thus τ_v is determined in terms of the van der Waals constants. Hence, from eqns. (11) and (18), we have

$$\begin{aligned} \tau &= \tau_c - \tau_v \\ &= \varpi a_2^{1/4} b_2^{-5/12} \left\{ 1 + x\left(\frac{a_{12}}{2a_2} - \frac{5b_1}{12b_2} - \frac{1}{12} \right) - \frac{a_2}{b_2\boldsymbol{RT}} \exp\left(\frac{-a_2}{b_2\boldsymbol{RT}} \right) \right. \\ &\qquad \left. - \frac{a_2}{b_2\boldsymbol{RT}} x[\exp(\alpha + \beta/T)] \left(\frac{a_{12}}{2a_2} + \frac{7b_1}{12b_2} - \frac{1}{12} \right) \right\} \end{aligned}$$

or, neglecting unity compared with $\exp(\alpha + \beta/T)$,

$$\begin{aligned} \tau = \varpi a_2^{1/4} b_2^{-5/12} &\left\{ 1 - \frac{a_2}{b_2\boldsymbol{RT}} \exp\left(\frac{-a_2}{b_2\boldsymbol{RT}} \right) \right. \\ &\left. - \frac{xa_2}{b_2\boldsymbol{RT}} \left[\exp\left(\alpha + \frac{\beta}{T} \right) \right] \left(\frac{a_{12}}{2a_2} + \frac{7b_1}{12b_2} - \frac{1}{12} \right) \right\}. \qquad \text{......(19)} \end{aligned}$$

Thus the surface tension σ^0 is given by

$$\begin{aligned} \sigma^0 = \tau^4 = \varpi^4 a_2 b_2^{-5/3} &\left\{ 1 - \frac{4a_2}{b_2\boldsymbol{RT}} \exp(-a_2/b_2\boldsymbol{RT}) \right. \\ &\left. - \frac{xa_2}{b_2\boldsymbol{RT}} [\exp(\alpha + \beta/T)] \left(\frac{2a_{12}}{a_2} + \frac{7b_1}{3b_2} - \frac{1}{3} \right) \right\} \qquad \text{......(20)} \end{aligned}$$

to about 5%, since we have neglected the square of $\exp(-a_2/b_2\boldsymbol{RT})$.

§4. REDUCTION IN TENSILE STRENGTH OF A LIQUID OWING TO DISSOLVED GAS

We can now find the effect of dissolved gas on the surface tension, and hence on the tensile strength, of a liquid. For a pure liquid $x = 0$, and so from eqn. (20), we have

$$\sigma_w^0 = \varpi^4 a_2 b_2^{-5/3} \{1 - (4a_2/b_2\boldsymbol{RT}) \exp(-a_2/b_2\boldsymbol{RT})\}. \qquad \text{......(21)}$$

Remembering that $t/t_w = \sigma^0/\sigma_w^0$ we have the following relation between the tensile strength of the liquid with dissolved gas and that of the pure liquid

$$t/t_w = 1 - (xa_2/b_2\boldsymbol{RT})[\exp(\alpha + \beta/T)] \left(\frac{2a_{12}}{a_2} + \frac{7b_1}{3b_2} - \frac{1}{3} \right). \qquad \text{......(22)}$$

For small concentrations of gas we have already seen that

$$p_1 = (xa_2/b_2^2) \exp(\alpha + \beta/T)$$

and so we have

$$\frac{\Delta t}{t_w} = -\frac{p_1 b_2}{\boldsymbol{RT}} \left(\frac{2a_{12}}{a_2} + \frac{7b_1}{3b_2} - \frac{1}{3} \right). \qquad \text{......(23)}$$

This equation gives the relative *decrease* $\Delta t/t_w$ in the value of the tensile strength which is to be expected due to the presence of the dissolved gas.

§5. NUMERICAL VALUES

Let us now take as an example the case of water containing dissolved air. If we assume that $a_{12} = \sqrt{(a_1 a_2)}$ we can compute the weakening caused by each of the component gases of air by means of eqn. (23). The data are listed in table 1. We then find, if the water is saturated with air at one atmosphere pressure, $\Delta t/t_w = 7 \times 10^{-4}$ for oxygen, $\Delta t/t_w = 31 \times 10^{-4}$ for nitrogen, $\Delta t/t_w = 0{\cdot}3 \times 10^{-4}$ for argon. ($p_1 = 0{\cdot}8$ atmosphere for nitrogen, 0·2 atmosphere for oxygen and 0·01 atmosphere for argon.)

Table 1

Substance	H_2O	O_2	N_2	A
Critical density (g/cm³)	0·329	0·430	0·311	0·531
Critical pressure (atmospheres)	218	49·7	33·5	48·0
a (atm. lit²)	0·490	0·0203	0·0202	0·0200
b (litres)	0·0274	0·0372	0·0451	0·0376

Thus we see that the maximum weakening caused by air dissolved at a pressure of one atmosphere is about $\frac{1}{2}\%$ and that the amount of weakening is independent of the solubility of the gas, provided only that this is small enough for the approximations to apply. The smallness of the decrease in tensile strength is rather unexpected. It should be emphasized that this theory gives the order of magnitude of the effect only, but it is unlikely to be changed significantly by the use of different van der Waals constants.

§6. DISCUSSION

The conclusion that the presence of dissolved gas only causes a negligible diminution in the intrinsic strength of liquids seems surprising, yet it does not seem to be in disagreement with the experimental evidence. For example, the high values obtained by Ursprung (1915) and Renner (1915) were for the tensile strength of cell sap, which cannot possibly have been air-free, and was, in all probability, nearly saturated. Again, Scott *et al.* (1948) introduced a very elaborate technique for preparing Berthelot tubes containing water with a very small gas content, yet they did not find any significant increase in the observed tensile strength over that found, for example, by Meyer (1911), Worthington (1892) or Temperley (1947) in glass apparatus. Thus, in accordance with the speculations of Vincent (1943), the discrepancy between theoretical and experimental values of t appears not to be explicable in terms of dissolved gas, but must presumably be sought in the small bubbles of air trapped in Griffiths cracks in the wall of the container.

On the other hand, there does seem to be definite evidence that the observed tensile strength, as measured by ultrasonic methods, does increase as the gas is removed (see, for example, Blake 1949). This increase may be, at any rate partially, due to the removal of *undissolved* gas nuclei, and further the mechanism of rupture may involve the process termed by Blake ‘rectified diffusion’, that is a progressive diffusion of gas into microscopic bubbles in forced oscillation in the ultrasonic field. Such a mechanism is absent when the stress is purely hydrostatic.

ACKNOWLEDGMENTS

We wish to express our thanks to Mr. H. N. V. Temperley for suggesting this problem and for many helpful discussions. One of us (C. G. K.) is indebted to Cambridge University for a Research Maintenance Grant and the other (D. H. T.) to the University of Wales for a University Fellowship.

APPENDIX

THE SURFACE TENSION OF A DIETERICI LIQUID

The assumptions made in deriving either van der Waals'

$$(p+a/V^2)(V-b)=\boldsymbol{R}T \qquad \ldots\ldots(1)$$

or Dieterici's equation of state

$$p(V-b)=\boldsymbol{R}T\exp(-a/\boldsymbol{R}TV) \qquad \ldots\ldots(\mathrm{A}\,1)$$

are of rigid, perfectly elastic molecules, which are subject to a short-range attractive interaction. These are just the assumptions on which any simple qualitative explanation of surface tension is based, and it should therefore be possible to express the surface tension of a liquid which obeys such an equation of state in terms of the constants a and b of the above equations. The two equations are identical, provided we neglect $O(1/V^2)$.

Macleod (1923) found empirically that $\sigma \propto (\rho_{\mathrm{liq}}-\rho_{\mathrm{vap}})^4$ over a wide range of temperatures, where σ is the surface tension, and the ρ's are the densities in g/cm^3. Sugden (1930) defined the parachor P by the equation

$$P=M^*\sigma^{1/4}/(\rho_{\mathrm{liq}}-\rho_{\mathrm{vap}}) \qquad \ldots\ldots(\mathrm{A}\,2)$$

where M^* is the (chemical) molecular weight of the substance. He suggested that the parachor might be a useful parameter for studying the structure of complex molecules.

Fowler (1937), in a statistical theory of the surface tension of liquids, showed that Macleod's formula should hold near the critical point. In this region, eqn. (A 1) rather than (1) should hold, and we therefore follow Fowler in treating a Dieterici rather than a van der Waals liquid. But having found the surface tension in terms of the constants a and b, we revert to van der Waals' equation in the text of the paper, where the conditions are far from critical. (A Dieterici liquid has no tensile strength, on Temperley's theory.) Fowler derives the following expression for the parachor:

$$P^4=-\frac{\pi \boldsymbol{N}^2 M^{*2}}{192\rho_{\mathrm{cr}}^{\,2}}\int_d^\infty r^3[3g_0(r)+1]E(r)\,dr \qquad \ldots\ldots(\mathrm{A}\,3)$$

where ρ_{cr} = critical density of the substance, and $g_0(r)$ is the radial distribution function for a liquid at fairly low temperatures.

This equation is derived from a rather more general model than the simple Dieterici liquid, and as it stands it does not lend itself readily either to numerical computation or to use in the main body of the present paper. By expressing the quantities in it in terms of the a and b of eqn. (A 1) we shall derive a formula which, while of more restricted applicability, is more readily useful for those liquids for which (A 1) is adequate.

The constant b is four times the effective volume of the molecules, whence

$$b=4\boldsymbol{N}(4\pi/3)(r_0/2)^3 \quad \text{or} \quad r_0=(3b/2\pi\boldsymbol{N})^{1/3} \qquad \ldots\ldots(\mathrm{A}\,4)$$

where r_0 is the effective diameter of a molecule.

It can easily be shown (see, for example, Slater 1939) that

$$a=\tfrac{1}{2}\boldsymbol{N}^2\int_{r_0}^\infty 4\pi r^2 E(r)\,dr$$

where $E(r)$ is the interaction potential energy. Following Lennard-Jones and Devonshire (1937) we take $E(r)$ of the form

$$E(r) = -\mu/r^6 + \lambda/r^n.$$

(We take the limit $n \rightarrow \infty$, instead of $n = 12$, i.e. we assume perfectly rigid molecules of finite size. Fig. 2 shows that the two assumptions differ little.) With this expression for $E(r)$ we deduce

$$a = 2\pi\mu \mathbf{N}^2/3r_0^{\,2} \qquad \ldots\ldots\text{(A 5)}$$

and thus μ is given by

$$\mu = 3r_0 a/2\pi \mathbf{N}^2 = 9ab/4\pi^2 \mathbf{N}^3. \qquad \ldots\ldots\text{(A 6)}$$

Fowler introduces a quantity α', defined by

$$\int_d^\infty r^3 E(r) g_0(r)\, dr = \alpha' \int_d^\infty r^3 E(r)\, dr. \qquad \ldots\ldots\text{(A 7)}$$

He shows that for a solid close-packed lattice $\alpha' = 1{\cdot}91$. In any case $\alpha' \geqslant 1$ and as the final expression for P will be proportional to $(3\alpha' + 1)^{1/4}$, the extreme values $\alpha' = 1$ and $\alpha' = 1{\cdot}91$ give values for P differing by only 16%. In fact Fowler's assumption of close-packing is probably not far from the truth, and therefore α' is taken to be $1{\cdot}91$. Then eqn. (A 3) reduces to

Table 2†

Substance	ρ_{cr}	M^*	V_{cr}	b	p_{cr}	a	$a^{1/4}$	$b^{7/12}$	$P_{\text{theor.}}$	$P_{\text{surf.tens.}}$
Argon A	0·531	39·9	75·2	37·6	48·6	2·03	1·20	8·29	54·5	52·5
Nitrogen N_2	0·311	28·0	90·2	45·1	33·9	2·05	1·21	9·22	65·5	60·4
Methane CH_4	0·162	16·0	98·8	49·4	46·4	3·32	1·36	9·73	78·3	(73·2)
Ammonia NH_3	0·235	17·0	72·3	36·1	113·0	4·39	1·45	8·11	68·8	60·7
Hydrogen chloride HCl	0·42	36·5	86·9	43·4	82·7	4·64	1·46	9·02	72·6	67·8
Water H_2O	0·329	18·0	54·7	27·4	221	49·8	2·66	6·90	108	52·6
Ethyl ether $(C_2H_5)_2O$	0·263	74·0	271	135	36·0	19·5	2·10	17·5	216	212
Carbon tetrachloride CCl_4	0·558	154	303	151	45·6	31·1	2·36	18·7	259	220
Benzene C_6H_6	0·304	78·0	257	128	48·3	23·6	2·19	17·0	218	206
Chlorobenzene C_6H_5Cl	0·365	112·5	308	154	45·2	30·8	2·36	18·9	261	245

† Units are as follows: ρ_{cr}, g/cm^3; V_{cr}, cm^3/mole; b, cm^3/mole; p_{cr}, dyn/cm$^2 \times 10^6$; a, dyn cm^4/mole$^2 \times 10^{12}$; $a^{1/4}$, dyn$^{1/4}$ cm/mole$^{1/2} \times 10^5$.

$$P^4 = \frac{\pi \mathbf{N}^2 M^{*2}}{192\rho_{cr}^{\,2}} \, \frac{(3\alpha' + 1)}{2d^2}. \qquad \ldots\ldots\text{(A 8)}$$

For a cubic close-packed lattice $d = (b/2\sqrt{2}\mathbf{N})^{1/3}$ ……(A 9)

and for a Dieterici liquid $\rho_{cr} = M^*/V_{cr} = M^*/2b$. ……(A 10)

Substituting (A 9) and (A 10) in (A 8) we obtain

$$P = \varpi a^{1/4} b^{7/12}, \qquad \ldots\ldots\text{(A 11)}$$

where $\varpi = [3(3\alpha' + 1)/64\pi \mathbf{N}^{1/3}]^{1/4}$. Thus, provided we take a suitable value of α' ($\alpha' = 1{\cdot}9$, see above), P is now expressed wholly in terms of known quantities. a and b are found from the critical constants, by means of the well-known relations for a Dieterici fluid: $b = \frac{1}{2}V_{cr} = \frac{1}{2}M^*/\rho_{cr}$ (where ρ_{cr} is in g/cm^3 and b in cm^3/mole^1), $a = 4e^2b^2p_{cr} = 29{\cdot}55b^2p_{cr}$ (where p_{cr} is in dyn/cm^2 and a in dyn cm^4/mole^2) and $\varpi = 5{\cdot}87 \times 10^{-3}$. Table 2 shows values of the various relevant quantities for a number of substances and we see that, with the exception of water, the values of P deduced from (A 11) are in moderate agreement with those deduced from the surface tension by the definition (A 2).

REFERENCES

Blake, F. G., 1949, *J. Acoust. Soc. Amer.*, **21**, 464.
Briggs, L. W., 1950, *J. Appl. Phys.*, **21**, 721.
Döring, W., 1939, *Z. Phys. Chem.* B, **38**, 292.
Fisher, J. C., 1948, *J. Appl. Phys.*, **19**, 1062.
Fowler, R. H., 1937, *Proc. Roy. Soc.* A, **159**, 229.
Frenkel, J., 1946, *Kinetic Theory of Liquids* (Oxford : University Press).
Fürth, R., 1941, *Proc. Camb. Phil. Soc.*, **37**, 252.
Lennard-Jones, J. E., and Devonshire, A. F., 1937, *Proc. Roy. Soc.* A, **163**, 53.
Macleod, D. B., 1923, *Trans. Faraday Soc.*, **19**, 38.
Meyer, J., 1911, *Abh. Dtsch. Bunsen-Gesell.*, No. 6.
Renner, M., 1915, *Jb. wiss. Bot.*, **56**, 617.
Scott, A. F., *et al.*, 1948, *J. Chem. Phys.*, **16**, 495.
Slater, J. C., 1939, *Introduction to Chemical Physics* (New York : McGraw-Hill).
Sugden, S., 1930, *The Parachor and Valency* (London : Routledge).
Temperley, H. N. V., 1947, *Proc. Phys. Soc.*, **59**, 199.
Trevena, D. H., 1950, *Ph.D. Thesis*, University of Wales.
Ursprung, G., 1915, *Ber. dtsch. Bot. Ges.*, **33**, 153.
Vincent, R. S., 1943, *Proc. Phys. Soc.*, **55**, 41.
Wall, F. T., and Stent, G. S., 1949, *J. Chem. Phys.*, **17**, 1112.
Worthington, A. M., 1892, *Phil. Trans. Roy. Soc.*, A **183**, 355.

Classical Theory of Compressibility

By P. J. PRICE*
Royal Society Mond Laboratory, Cambridge

MS. received 28th September 1951

ABSTRACT. By extending Green's treatment of the classical virial theorem, a formula for the bulk modulus of an assembly of atoms, when classical physics applies, is derived. This formula involves the binary and ternary distribution functions.

In the appendix to the second paper (Green 1947) of Born and Green's series on the theory of liquids, a simple derivation is given of the virial theorem for an assembly of atoms to whose interaction classical mechanics applies. In this paper the same technique is used to derive a formula, evidently new, for the compressibility (or, rather, for the bulk modulus $-V(\partial p/\partial V)_T$). To establish the notation and method to be used we begin by recapitulating Green's treatment of the pressure. The coordinates of the N atoms are combined in a single $3N$-vector $\mathbf{x}$, and their interaction potential denoted by $\Phi(\mathbf{x})$. Let them be confined in an enclosure (which we shall vary without changing its shape) of volume V. Consider now the integral

$$I(f) \equiv \int d^{3N}\mathbf{x} f(\mathbf{x}) \qquad \ldots\ldots(1)$$

---

* Now at Department of Chemistry, Duke University, Durham, North Carolina.

taken over the enclosure N times. To 'differentiate with respect to V', we replace $\mathbf{x}$ by $\lambda\mathbf{x}$ and carry out $[d/d\lambda \ldots .]_{\lambda=1}$: this is the operation $3V\,d/dV$. Then we have

$$3V dI(f)/dV = \Big[\lambda d/d\lambda \Big\{ \lambda^{3N} \int d^{3N}\mathbf{x} f(\lambda\mathbf{x}) \Big\}\Big]_{\lambda=1} = 3NI(f) + I(\mathbf{x}\,.\,\nabla f). \quad \ldots\ldots(2)$$

The Helmholtz potential A is given by the phase integral

$$\mathrm{e}^{-A/kT} = Q \equiv a(kT)^{3N/2} I(\mathrm{e}^{-\Phi/kT}), \quad \ldots\ldots(3)$$

where a is a constant of no interest here. Differentiating (3) with respect to volume, by (2):

$$-3V(\partial A/\partial V)_T\, \mathrm{e}^{-A/kT} = a(kT)^{3N/2}[3NkTI(\mathrm{e}^{-\Phi/kT}) - I(\mathbf{x}.\,\nabla\Phi \mathrm{e}^{-\Phi/kT})]. \quad \ldots\ldots(4)$$

Now the thermal average of a function $f(\mathbf{x})$ is

$$\langle f \rangle = I(f(\mathbf{x})\mathrm{e}^{-\Phi/kT})/I(\mathrm{e}^{-\Phi/kT}). \quad \ldots\ldots(5)$$

Then, from the definition of the pressure $p \equiv -(\partial A/\partial V)_T$, eqn. (4) reduces to the classical virial theorem

$$3pV = 3NkT - \langle \mathbf{x}\,.\,\nabla\Phi \rangle. \quad \ldots\ldots(6)$$

Eqn. (6) takes a more usual form if we assume that

$$\Phi = \Sigma_2 \phi(r_{ij}), \quad \ldots\ldots(7)$$

where the $\mathbf{r}_i$ are the particle coordinates (projections of $\mathbf{x}$), $\mathbf{r}_{ij} = \mathbf{r}_i - \mathbf{r}_j$, and $\Sigma_2 \equiv \frac{1}{2}\Sigma\Sigma_{i \neq j}$ is the sum over pairs of (i, j). If (7) holds, then

$$(\mathbf{x}\,.\,\nabla)^n \Phi = \Sigma_2 \phi_n(r_{ij}), \text{ where } \phi_n(r) \equiv (r\,d/dr)^n \phi(r). \quad \ldots\ldots(8)$$

It is then convenient to introduce the multiple probability densities in coordinate space, $n_q(\mathbf{r}_1, \mathbf{r}_2, \ldots \mathbf{r}_q)$, which we normalize so that $I(n_N) = 1$ and $n_{q-1} = \int^{(q)} n_q$, where $\int^{(q)}$ stands for $\int^V d^3\mathbf{r}_q$, and for convenience we suppose n_N made symmetrical in the particle coordinates. Then, using (8), eqn. (6) reduces to

$$3pV = 3NkT - \tfrac{1}{2}N(N-1)\int^{(1,2)} n_2(\mathbf{r}_1, \mathbf{r}_2)\phi_1(r_{12}). \quad \ldots\ldots(9)$$

Passing to the derivation of the compressibility formula, we write (6) in the form

$$(3pV - 3NkT)I(\mathrm{e}^{-\Phi/kT}) = -I(\mathbf{x}\,.\,\nabla\Phi\ \mathrm{e}^{-\Phi/kT})$$

and apply $3V\partial/\partial V$ again, obtaining

$$3V[\partial(3pV)/\partial V]_T I(\mathrm{e}^{-\Phi/kT}) + (3pV - 3NkT)\{3NI(\mathrm{e}^{-\Phi/kT}) - (kT)^{-1}I(\mathbf{x}\,.\,\nabla\Phi\mathrm{e}^{-\Phi/kT})\}$$
$$= -\{3NI(\mathbf{x}\,.\,\nabla\Phi\mathrm{e}^{-\Phi/kT}) + I[\{(\mathbf{x}\,.\,\nabla)^2\Phi - (\mathbf{x}\,.\,\nabla\Phi)^2/kT\}\mathrm{e}^{-\Phi/kT}]\}.$$

That is, by using (6),

$$9V[\partial(pV)/\partial V]_T + \langle(\mathbf{x}\,.\,\nabla)^2\Phi\rangle = (kT)^{-1}[\langle(\mathbf{x}\,.\,\nabla\Phi)^2\rangle - \langle\mathbf{x}\,.\,\nabla\Phi\rangle^2] \quad \ldots\ldots(10)$$
$$= (kT)^{-1}D, \text{ say.}$$

The implications of (10) may be seen by applying (7) and (8). Then

$$\langle(\mathbf{x}\,.\,\nabla)^2\Phi\rangle = \tfrac{1}{2}N(N-1)\int^{(1,2)} n_2(1, 2)\phi_2(12), \quad \ldots\ldots(11)$$

with the obvious abbreviations. To reduce the 'fluctuation' term D of (10) we have, by (8),

$$\langle(\mathbf{x}\,.\,\nabla\Phi)^2\rangle = \tfrac{1}{2}N(N-1)\Big\{\int^{(1,2)} n_2(1, 2)\phi_1^{\,2}(12)$$
$$+ 2(N-2)\int^{(1,2,3)} n_3(1, 2, 3)\phi_1(12)\phi_1(23)$$
$$+ \tfrac{1}{2}(N-2)(N-3)\Big[\int^{(1,2)} n_2(1, 2)\phi_1(12)\Big]^2\Big\}. \quad \ldots\ldots(12)$$

Combining the square of the final term of (9) with (10), (11) and (12), we obtain, finally,

$$9V[\partial(pV)/\partial V]_T = \tfrac{1}{2}N(N-1)\Big\{ -\int^{(1,2)} n_2(1,2)\phi_2(12) + (kT)^{-1}\Big[\int^{(1,2)} n_2(1,2)\phi_1{}^2(12) + 2(N-2)\int^{(1,2,3)} n_3(1,2,3)\phi_1(12)\,\phi_1(23) - (2N-3)\Big(\int^{(1,2)} n_2(1,2)\phi_1(12)\Big)^2\Big]\Big\}. \qquad \ldots\ldots(13)$$

Thus, subject to approximation (7), the compressibility depends on n_1, n_2 and n_3, but not on the higher n_q; whereas the pressure depends on n_1 and n_2 only. By dropping the essentially positive coefficient of $(kT)^{-1}$ in (13) we obtain, for a fluid, the inequality

$$9[\partial(pV)/\partial V]_T + \tfrac{1}{2}\nu^2\int^{\infty} g(r)\phi_2(r)d^3\mathbf{r} > 0.$$

Here we have set $n_2(1,2) = n_1(1)n_1(2)[g(r_{12}) + O(1/N)]$, $\nu = N/V$, and assumed N very large. On the other hand, (13) itself simplifies, if we substitute the Kirkwood approximation

$$n_3(1,2,3) = n_2(1,2)n_2(2,3)n_2(3,1)/n_1(1)n_1(2)n_1(3)$$

to

$$9[\partial(pV)/\partial V]_T + \tfrac{1}{2}\nu^2\int^{\infty} g(r)\phi_2(r)\,d^3\mathbf{r} = (kT)^{-1}\Big\{\tfrac{1}{2}\nu^2\int^{\infty} g(r)\phi_1{}^2(r)d^3\mathbf{r} + \nu^3\iint^{\infty} g(r_1)g(r_2)[g(r_{12})-1]\phi_1(r_1)\phi_1(r_2)d^3\mathbf{r}_1\,d^3\mathbf{r}_2\Big\}. \qquad \ldots\ldots(14)$$

If the radial distribution $g(r)$ and the interaction $\phi(r)$ are sufficiently well known in a particular case, (14) could provide a test of the accuracy of the Kirkwood approximation. When used to derive expressions for the virial coefficients, eqn. (14) would also provide a test of Green's (1947) integral equation for $g(r)$ independent of that given by the virial eqn. (9), which was recently put to this use by Rushbrooke and Scoins (1951). More general expressions, analogous to (13), could clearly be derived for the elastic constants, in the case of a crystal.

Returning to the general and (for classical physics) exact result (10), the 'fluctuation' expression D clearly must vanish at least as fast as T, when $T \to 0$, for the formula to be applicable. For a classical crystal $D \to 0$ as the temperature goes to absolute zero, because the atoms are finally in fixed positions, at low temperatures the r.m.s. deviations of the normal coordinates, and hence of the distances between atoms, vary as $T^{1/2}$. Hence D may be expected to vary as T, and the right-hand side of (10) to tend to a finite value (calculable in terms of the normal lattice vibrations) at absolute zero. In reality, the presence of the term in D shows that *the formal identity of the classical and quantal formulae for thermodynamic pressure* (Price 1950) cannot hold for compressibility as, owing to the zero-point motion, D/kT must tend to infinity at absolute zero. It is hoped to publish later the quantum treatment corresponding to the classical theory of the present paper.

ACKNOWLEDGMENT

This work was supported by an award from the Department of Scientific and Industrial Research, which is gratefully acknowledged.

REFERENCES

GREEN, H. S., 1947, *Proc. Roy. Soc.* A, **189**, 103.
PRICE, P. J., 1950, *Phil. Mag.*, **41**, 948.
RUSHBROOKE, G. S., and SCOINS, H. I., 1951, *Phil. Mag.*, **42**, 582.

The Experimental Determination of the Spectrum of a Betatron

By K. PHILLIPS
Research Department, Metropolitan–Vickers Electrical Co. Ltd., Trafford Park, Manchester

MS. received 12*th July* 1951

ABSTRACT. By measuring the energy of photo-protons from deuterium the x-ray spectrum of a betatron, of maximum energy 20 Mev, has been deduced. A small difference between the experimental determination and the theoretical curve in the 10 Mev region is found.

Several previous attempts (Lasich and Riddiford (1947), Bosley *et al.* (1948), Koch and Carter (1950), Wang and Wiener (1950)) have been made to determine the x-ray intensity spectrum of betatrons. The simplest and most elegant method seems to be due to Wang and Wiener, who used a plate soaked in heavy water for a 10 Mev machine. For higher x-ray energies there is the added complication due to photo-protons produced in the emulsion from (γ, p) reactions in silver, oxygen and bromine. This difficulty has been resolved by using heavy wax film targets. The heavy wax has a chemical formula C_nD_{n+2} ($n \simeq 30$) and contains about 25% of deuterium by weight. The film, 5 microns thick, was supported on a thin backing of 'Cellophane' which was in turn fastened to a substantial metal frame, the latter being made so that the wax fitted closely to the surface of a quarter-plate C2 Ilford emulsion 200 microns thick.

The emulsion and film were exposed perpendicularly to the axis of the collimated x-ray beam at a distance of about 150 cm from the 0·010-in. thick tungsten target for a period of two minutes, the x-ray output from the machine being about 10 röntgens per minute at one metre, as measured on a thick-walled ionization chamber, with a maximum energy of 18·5 Mev. In order to estimate any possible background effect an ordinary paraffin wax film was used as a target and exposed under similar conditions. The plates were developed in a solution of Azol and 1% potassium bromide.

Several square centimetres of emulsion were scanned and only photo-protons with angles of dip between 5° and 45° were accepted. Over 1,000 photo-protons were measured in the heavy wax plates, whilst in the control plates only about 40 tracks entering from outside the emulsion were found. The majority of the latter protons had energies less than 2 Mev. The number of photo-protons produced by x-rays at different energies from 4 to 18·5 Mev is shown in the histogram (fig. 1). The smooth curve is the theoretical distribution of the number of protons expected from the Bethe–Peierls theory of the photo-disintegration of the deuteron and from the Bethe–Heitler theory of bremsstrahlung. The intensity spectrum is given in fig. 2, and it can be seen to differ slightly from the theoretical curve. It exhibits similar characteristics to the spectrum found by Koch and Carter using pair production, in a cloud chamber, to measure the number of quanta. For instance, the increase in the number of quanta in the 10 Mev region and the rapid fall towards the high energy tip are illustrated. These two factors are obviously dependent upon the point of normalization of the theoretical curve and the experimental histogram. If, however, the theoretical proton–energy curve is transformed, by adjusting the width of the energy intervals into a rectangular distribution, the conclusions will be independent of normalization. This transformation has been carried out in fig. 3, and the experimental results again illustrate an increase in the medium energy regions and a more rapid fall off towards 18 Mev. The causes of these two effects may be inherent in the betatron since it is unlikely that the theory of bremsstrahlung is at fault. The increase may be tentatively explained by assuming that the electrons, after acceleration, strike the tungsten target and are scattered back into the doughnut. After further revolutions the scattered electrons hit the target again. The process may occur more than once, and the measured spectrum would be the summation of more than one bremsstrahlung curve, one due to the primary beam and the other due to lower energy scattered electrons. It would be of considerable interest to carry out a spectral analysis of some non-cyclic accelerator, as this would rule out the possibility of the electrons striking the target more than once.

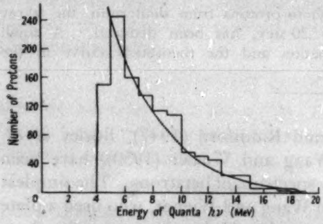

Fig. 1. Histogram of number of protons plotted against energy of incident quanta.

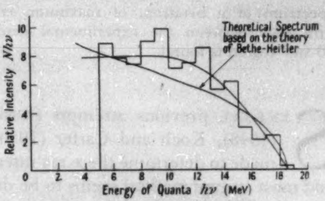

Fig. 2. Theoretical and experimental intensity spectra.

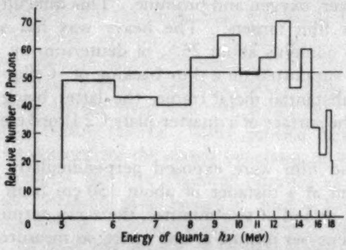

Fig. 3. Histogram of relative number of protons plotted against energy of incident quanta transformed into a rectangular distribution.

ACKNOWLEDGMENTS

I wish to acknowledge the assistance given to me by all the members of the betatron team and to thank Drs. E. H. S. Burhop and C. T. Griffiths, of University College, London, for providing the wax film. I also wish to thank

Mr. F. R. Perry for his encouragement and advice, and Sir A. P. M. Fleming, Director of Research and Education, and Mr. B. G. Churcher, Manager of Research Department, Metropolitan–Vickers Electrical Co. Ltd., for permission to carry out this work.

REFERENCES

Bosley, W., Craggs, J. D., Nash, F., and Payne, R. M., 1948, *Nature, Lond.*, **161**, 1022.
Koch, H. W., and Carter, R. K., 1950, *Phys. Rev.*, **77**, 165.
Lasich, W. B., and Riddiford, L., 1947, *J. Sci. Instrum.*, **24**, 177.
Wang, P. K. S., and Wiener, M., 1950, *Phys. Rev.*, **78**, 1724.

The Angular Distribution of Synchrotron Target Radiation

By E. G. MUIRHEAD, B. M. SPICER and H. LICHTBLAU
Physics Department, University of Melbourne

Communicated by L. H. Martin; MS. received 22nd May 1951

ABSTRACT. Some measurements on the angular distribution of thin target radiation produced in a synchrotron are reported using ionization chambers to measure the x-ray intensity. Quantitative agreement has been obtained with the bremsstrahlung–multiple scattering theories of Schiff and Lawson for the case of a platinum target in the range of electron energies of 10–14 MeV.

§ 1. INTRODUCTION

The theoretical angular distribution of thin target radiation was first formulated by Schiff (1946), who attributed the angular spread to multiple elastic scattering of the electrons and their subsequent radiative collisions with the target nuclei. More recently, an essentially equivalent theory has been presented by Lawson (1950), in which the simplification lies in the form taken for the polar diagram of a single radiative transition. The common features of the two theories are: (i) the prediction of symmetry about the line of maximum intensity, which lies in the direction of the incident electron beam, and (ii) the inverse proportionality of the angular width and the incident electron energy. In practice, Lawson's formula is more directly useful since it avoids the divergence of Schiff's formula for small values of the angle θ. Because of this divergence, Schiff's formula is applicable only to angles somewhat greater than μ/E, where μ is the rest energy of the electron, and E the total electron energy. We have found it possible to remove this limitation by a simple modification of the Schiff formula which makes it applicable for all angles. This was achieved by using the asymptotic property of the exponential integral, namely $\mathrm{Ei}(-y_1)-\mathrm{Ei}(-y_2)\to\ln(y_1/y_2)$ as y_1, $y_2\to 0$. The second exponential integral term is determined from the condition $I(\theta)/I(0)\to 1$ as $\theta\to 0$. This modification then allows for the finite width of the radiation polar diagram, which plays an important role at small angles. The expression thus obtained is analogous to that of Lawson. Calculations made for a tungsten target, using the modified formula, differ by less than one per cent from the

.A
5
2

published curves of Schiff. The following are the expressions of the radiative polar diagrams for the three cases:

$$\frac{I(\theta)}{I(0)} = \frac{-\mathrm{Ei}\{-(E\theta)^2 \ln(183Z^{-1/3})/1510{\cdot}8t\}}{\ln\{1510{\cdot}8t/\mu^2 \ln(183Z^{-1/3})\} - 0{\cdot}5772} \quad \text{(Schiff),} \qquad \ldots\ldots(1)$$

$$\frac{I(\theta)}{I(0)} = \frac{-\mathrm{Ei}\{-(E\theta)^2 \ln(183Z^{-1/3})/1510{\cdot}8t\} + \mathrm{Ei}\{-(E\theta)^2/1{\cdot}787\mu^2\}}{\ln\{1510{\cdot}8t/\mu^2 \ln(183Z^{-1/3})\} - 0{\cdot}5772} \quad \text{(Modified Schiff),} \qquad \ldots\ldots(2)$$

$$\frac{I(\theta)}{I(0)} = \frac{-\mathrm{Ei}\{-(E\theta)^2/(440t + 2\mu^2)\} + \mathrm{Ei}\{-(E\theta)^2/2\mu^2\}}{\ln(1 + 220t/\mu^2)} \quad \text{(Lawson),} \qquad \ldots\ldots(3)$$

where $I(\theta)$ is the intensity, for a given target distance, at an angle θ with respect to the direction of incidence of the electrons, E the electron energy in MeV, μ the rest energy of the electron in the same units, and t the target thickness expressed in radiation lengths (Rossi and Griesen 1941). These formulae are applicable to target thicknesses in the range from 10^{-3} to 10^{-1} radiation lengths.

Comparison with theory of the experimental results obtained with a betatron or synchrotron is complicated by a lack of knowledge of the exact conditions under which the electrons strike the target. Radial oscillations of the electrons contribute the main uncertainty in the knowledge of their angle of incidence, so that the effective thickness of the target may be slightly different from its geometrical thickness. However, this factor is usually of secondary importance since the intensity at an angle θ is relatively insensitive to small changes in the target thickness.

Approximate agreement with theory has been reported in several experiments (Lawson 1950, Lees and Metcalfe 1950, Allen-Williams and Appleyard 1949 a, b) but in most cases, the target conditions have made a quantitative comparison impossible. Preliminary reports (Baldwin, Boley and Pollock 1950, Lanzl and Hanson 1950) confirm, with reservations, Schiff's theory, although deviations from theory in the case of heavy elements were found by Baldwin *et al.* It is the purpose of this paper to present data on the angular distribution obtained with a 14 MeV synchrotron using air-ionization chambers for the intensity measurements.

§ 2. EXPERIMENTAL ARRANGEMENT

(i) *Production of the X-ray Beam*

The accelerated electrons were made to spiral slowly out from the equilibrium orbit at the end of the acceleration time and the X-ray beam was produced in a platinum target, 0·005 in. (0·045 radiation length) thick, which was mounted out from the back of the injector anode perpendicular to the electron orbit. The target was a flag three millimetres square, which ensured that the X-ray beam was produced well clear of the injector anode. The azimuthal position of the target was chosen in order to reduce scattering from the magnet poles and energizing coils to a minimum. The peak electron energy was obtained from the experimentally determined magnetic field characteristics. Using this magnetic calibration the gamma–neutron threshold in silver has been determined and the value obtained is in good agreement with the value given by Baldwin and Koch (1945).

(ii) *Detection and Monitoring*

The X-ray intensity was measured by a cylindrical aluminium ionization chamber of one centimetre wall thickness. This instrument, which is direct reading, was shown to be linear for the intensities encountered during the experiment. Good resolution was obtained by using the chamber in the end-on position at a distance of 3½ metres from the target; under these conditions, the chamber subtended an angle at the target of about one degree. A thin-walled integrating chamber, used for monitoring the x-ray output was placed in a standard position and in such a way as not to interfere with the beam proper. To allow for fluctuations, the intensity at each angular position of the ionization chamber was read regularly during a suitable period and the integrated intensity estimated. The latter was normalized to a standard irradiation using the corresponding monitor readings. For some runs, the two chambers were interchanged and no significant difference was found for the results of these runs.

(iii) *Scattered Radiation*

The effect of scattered radiation was estimated by placing a lead absorber, seven inches thick, directly in front of the ionization chamber, which was mounted on a light frame to minimize the effect of scattering. The measured intensity under these conditions was entirely due to scattered radiation and was comparable with the scattered intensity present in the absence of the lead absorber. The residual intensity thus measured was found to be distributed isotropically in the region of the beam, and never exceeded one-half of one per cent of the x-ray intensity at the beam centre. The contribution of scattered radiation is therefore negligible for the present experiments.

§ 3. RESULTS

Using the inverse square law, a small correction was applied in order to reduce all readings to the same target–chamber distance. Each set of readings was given a preliminary examination by plotting the intensity as a function of the arbitrary angular position of the ionization chamber. In every case the distribution was found to be completely symmetrical. This procedure is necessary since the centre of the beam was observed to alter in the case of distributions measured in the horizontal plane through the target as the electron energy was altered, as predicted by Allen-Williams and Appleyard (1949 a). From these curves the characteristic angular width α subtended at the target between the lines of maximum and half-maximum intensity are obtained; the results are tabulated in table 1. It can be seen that the product of angular width by the peak electron energy is, within experimental error, a constant characteristic of the target, as predicted. The value of this product as given by Schiff's formula for a target of thickness 0·045 radiation length is 76·7, as compared with our experimental mean value of 77·8. Lawson's theory gives 80·9. From this it follows that there is no significant difference between the effective and the geometrical thickness of the target.

Table 1. Characteristic Angular Width α as a Function of the Electron Energy E

E (MEV)	α (deg.)	$E\alpha$ (MEV. deg.)	Plane of angular distribution
10·2	7·9	80·6	Horizontal
12·3	6·2	76·3	,,
12·7	5·9	75·0	,,
13·1	6·0	78·6	,,
13·8	5·5	75·9	,,
11·6	6·7	77·7	Vertical
12·1	6·3	75·8	,,
12·3	6·1	81·8	,,
		Mean 77·8	

An overall test of the theory is possible by compounding the various runs first by converting the independent variable θ, measured with respect to the beam centre, to the product of angle and peak energy $E\theta$. The results are given in table 2 and are displayed in the figure for ease of comparison with theory. The errors shown are the probable errors obtained from table 2 assuming the spread of values to be entirely due to experimental errors. Comparison is made with (i) the Schiff curve, (ii) the Lawson curve, and (iii) the modified Schiff curve, each being calculated under the conditions mentioned above. Although the precision of the experiments is not sufficient for a decision to be made between the forms of the distribution, there is slightly better overall agreement with the modified Schiff curve than with the other two. The deviation at small angles for the Schiff law is due to the breakdown of the theoretical assumptions for angles less than $1/2E$ radians.

Table 2. Experimental Values of $100I(\theta)/I(0)$ as a Function of $E\theta$ for a Series of Electron Energies E (MEV)

E \ $E\theta$	10·2 H (1)	12·3 H (2)	12·7 H (3)	13·1 H (4)	13·8 H (5)	11·6 V (1)	12·1 V (2)	12·$\bar{3}$ V (3)	Mean
10	97·0	98·5	96·3	94·7	96·0	98·0	97·0	97·0	96·8±0·3
20	90·7	95·8	90·3	87·0	87·8	94·0	91·7	94·2	91·4±0·7
30	82·3	90·6	83·0	79·7	80·7	88·0	85·0	89·5	84·8±1·0
40	74·0	83·2	75·0	72·7	73·6	79·5	77·7	83·0	77·3±1·1
50	67·0	75·3	67·8	65·6	66·5	70·8	69·6	76·0	69·8±0·9
60	60·8	65·1	60·2	59·6	59·3	62·3	62·0	68·0	62·2±0·7
70	55·5	56·0	53·1	54·3	53·0	55·0	54·3	60·0	55·1±0·5
80	50·4	49·1	47·3	49·1	48·0	48·2	47·6	51·5	48·9±0·4
90	43·8	44·0	42·7	44·3	43·5	41·3	41·8	44·0	43·2±0·3

H (1)–H (5) distributions in horizontal plane through target.
V (1)–V (3) distributions in vertical plane through target.

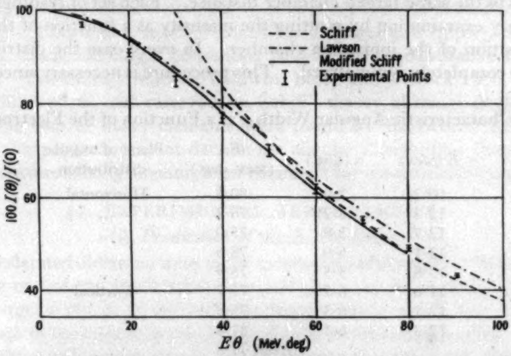

Radiation polar diagrams for target thickness of 0·045 radiation length.

In some sets of measurements, two peaks were observed in the angular distribution curves. This phenomenon, which has been found for several different electron energies, was due to two separate beams as shown by the existence of two sets of Geiger–Müller counter pulses separated by about one millisecond. There were found to be two different acceptance times for electron injection, one of which gave rise to two beams and the other to a single beam. Consequently care was exercised in choosing the appropriate injection conditions during the course of the experiment. Double beam distributions were excluded from the data presented above.

§4. CONCLUSION

As noted above, all distributions were found to be completely symmetrical, in contrast with the results of Lees and Metcalfe (1950) and Allen-Williams and Appleyard (1949 b). In our case asymmetrical distributions were not observed after precautions were taken to eliminate scattering from dense bodies near the synchrotron. Also the use of an external target removes more completely the effect of scattering from the magnet poles and the small yet complicating effect of the residual betatron beam.

The formulae of Lawson and Schiff (modified form), as applied to a target of platinum of 0·045 radiation length, are in agreement, within the statistical error, with the experimental results given above. Brief details of a similar experiment by Lanzl and Hanson (1950) have recently appeared, in which angles of half intensity for 17 Mev electrons impinging on gold targets of various thicknesses were slightly less than predicted by Schiff's theory. On the other hand, Baldwin, Boley and Pollock (1950) found good agreement for targets of low atomic number but deviations from theory, which increased with atomic number of the target material, for thicknesses of the order of 10^{-2} radiation length. The only known difference in experimental conditions was the use of electrons of energy 70 Mev, and therefore a possible explanation of the deviation found in this case lies in the increasing importance of the bremsstrahlung process in determining the angular distribution at an energy as high as 70 Mev. From the figure it is possible to suggest that even in the 10–14 Mev range, the bremsstrahlung distribution, which plays a major part at small values of θ, is somewhat narrower than assumed by either Schiff or Lawson. For lower or higher energies, deviations may be expected, in the former case on theoretical grounds (Schiff 1946), and in the latter in the light of the experimental work discussed above.

Further work seems to be called for in order to decide at what energies the assumptions of the Schiff and Lawson theories regarding the bremsstrahlung polar diagram become inadequate.

ACKNOWLEDGMENTS

The authors wish to express their appreciation to Professor L. H. Martin for his encouragement during the course of this work.

The cost of the synchrotron was met from a grant made by the Commonwealth Scientific and Industrial Research Organization (Australia).

REFERENCES

Allen-Williams, D. J., and Appleyard R. K., 1949 a, *Proc. Camb. Phil. Soc.*, **45**, 305; 1949 b, *Brit. J. Radiol.*, **22**, 106.

Baldwin G. C., and Koch, H. W., 1945, *Phys. Rev.*, **67**, 1.

Baldwin, G. C., Boley, F. I., and Pollock, H. C., 1950, *Phys. Rev.*, **79**, 210 (A).

Lanzl, L. H., and Hanson, A. O., 1950, *Bull. Amer. Phys. Soc.*, **25**, No. 5, 21.

Lawson, J. D., 1950, *Proc. Phys. Soc.* A, **63**, 653.

Lees, D. J., and Metcalfe, L. H., 1950, *Proc. Phys. Soc.* A, **63**, 661.

Rossi, B., and Griesen, K., 1941, *Rev. Mod. Phys.*, **13**, 240.

Schiff, L. I., 1946, *Phys. Rev.*, **70**, 87.

Angular Distribution of Elastically Scattered Deuterons and Disintegration Protons from the Bombardment of Beryllium by 7·7 Mev Deuterons

By F. A. EL-BEDEWI
Nuclear Physics Laboratory, University of Liverpool

Communicated by H. W. B. Skinner; MS. received 12th July 1951

ABSTRACT. The deuteron beam from the Liverpool 37 in. cyclotron was used to bombard a thin beryllium foil in a vacuum chamber. The photographic plate method was employed in detecting the charged particles emitted from the reaction. The angular distribution of the elastically scattered deuterons shows a secondary maximum at 65°. Angular distributions of the two longest range proton groups are compared with the recent theories of the angular distributions of the (d, p) and (d, n) reactions. The results indicate that both the ground state and first excited state of the residual nucleus ^{10}Be have even parity and spin either 0, 1, 2 or 3.

§ 1. INTRODUCTION

Attention has been recently given to the study of the distribution of particles emitted in nuclear reactions with respect to their angle of emission. The investigation of such distributions for protons resulting from the bombardment by deuterons of about 8 Mev indicates interesting characteristics at small angles of emission. Pronounced maxima are observed in the cases of oxygen (Burrows, Gibson and Rotblat 1950) and aluminium (Holt and Young 1950, Gove 1951) and are attributed to the possibility of the stripping of the deuteron in its passage past the target nucleus. In the light of the recent theories proposed by Butler (1950) and Bhatia and Huang (unpublished) such observation can give information regarding the spin and parity of the appropriate state of the final nucleus.

In the present work the angular distributions of the two longest range proton groups from the (d, p) reaction with beryllium are investigated. Also the angular distribution of the elastically scattered deuterons from this mono-isotopic light element is found to show features similar to those observed by Guggenheimer, Heitler and Powell (1947) in the scattering of 6·5 Mev deuterons by oxygen and nitrogen and in the scattering of 8 Mev deuterons by neon (Middleton and Tai 1951).

§ 2. METHOD

A thin beryllium foil 0·325 Mg/cm^2 thick was bombarded in a vacuum chamber by a beam of deuterons of 7·70 Mev mean energy provided by the Liverpool 37 in. cyclotron. The cross section of the beam had a diameter of 1·5 mm and its angular divergence was about one-third of a degree. The emitted particles were detected in Ilford C2 emulsion 200 μ thick and examined with a binocular microscope with magnification of about 900. A detailed description of the apparatus used in the present experiment, as well as the method of measurement, was reported by Rotblat, Burrows and Powell (1951) and El-Bedewi (1951).

The experiment was carried out with two different exposures to allow for the expected sharp rise of the emitted particles near the forward direction.

A normalization was obtained by measuring the intensities of different groups of particles at an angle of 30° in both exposures. The mean ratio of the intensities of the forward to the backward exposures was found to be $0{\cdot}51 \pm 0{\cdot}01$. Also, for the investigation of particles emitted within a continuous angular range the foil was tilted to the direction of the incident deuterons by either 45° or 135° to suit the forward or backward exposures respectively.

In examining the plates, a certain area of the emulsion surface was carefully explored and all the tracks belonging to the elastically scattered deuterons and the two longest range proton groups from the reaction $^{9}\mathrm{Be(d, p)}^{10}\mathrm{Be}$ were recorded. The position of measurement was chosen such that the angles of approach of the particles entering into the emulsion were between 6° and 10°. The loss of tracks through scattering out of the top surface of the emulsion was then found to be less than 2% everywhere. Throughout the whole series of measurements only three tracks were observed to run into the glass backing of the emulsion, as might be expected from a comparison of the ranges of tracks under consideration with the thickness of the emulsion used. Since the percentage of tracks scattered out of the emulsion was small, the variation of this loss at various angles of observation should be even smaller. Therefore, in the results presented below, no correction of this loss was made. The errors shown in the figs. 2, 3 and 4 are those of a statistical nature only.

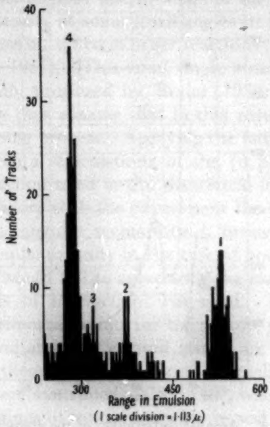

Fig. 1. Histogram of disintegration products of beryllium bombarded by 7·7 MeV deuterons at 70°.

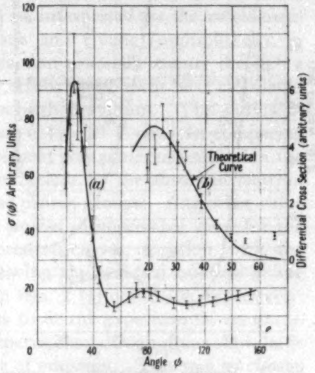

Fig. 2. Angular distribution of proton group 1 in the centre-of-mass system.

§ 3. ANGULAR DISTRIBUTION OF THE PROTON GROUPS

A representative histogram for the upper end of the particle spectrum at an angle of observation of 70° is shown in fig. 1. Groups 1 and 4 are identified, using known *Q*-values, as being due to protons leading to the ground state and to a level at 3·375 MeV of the residual nucleus $^{10}\mathrm{Be}$. Groups 2 and 3 are due to oxygen contamination in the target. The angular distributions of groups 1 and 4 have been measured by a method similar to that described by Chadwick, May, Pickavance and Powell (1944). The number of tracks belonging to group 1 is known directly from the plotted histograms since it is well separated from all other groups. In the case of group 4 great care has been taken to discriminate that group from the neighbouring tracks resulting from the foil contamination. By fitting Gaussian curves, reliable counting was achieved at all angles of observation except for those between 30° and 60°, where there was an overlapping with group 3. Fortunately, the angular distributions for protons from the reaction $^{16}O(d, p)^{17}O$ have been worked out in this laboratory (Burrows *et al.* 1950) under the same conditions, and one can calculate the ratio of the numbers of protons belonging to the ground state to those belonging to the first excited state of ^{17}O at a certain angle of emission. Since the ground state group 2 was well separated in the spectrum from the beryllium target, it was possible, by making use of this known ratio, to estimate the number of protons due to contamination in group 4. This procedure was repeated for each angle where the two groups overlapped.

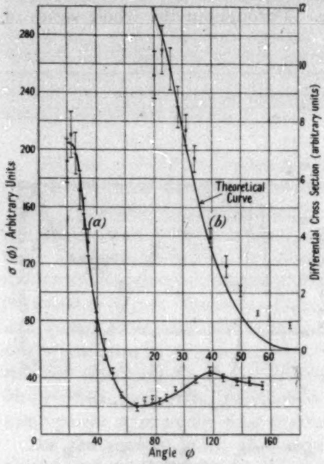

Fig. 3. Angular distribution of proton group 4 in the centre-of-mass system.

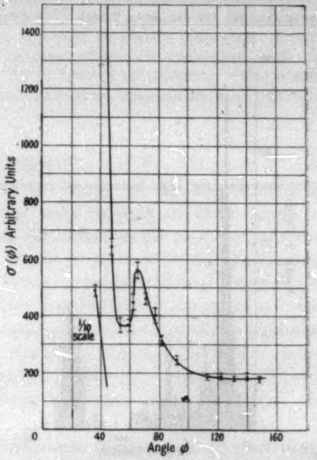

Fig. 4. Angular distribution of the elastically scattered deuteron group in the centre-of-mass system.

After calculating the relative intensities of each group at the various angles of observation, they were normalized, transformed to the centre-of-mass system of coordinates and then represented as shown in figs. 2 (*a*) and 3 (*a*). These results are based on the measurements of a total of 1664 tracks for the group 1 and over 22 different angles and 3 846 tracks for the group 4 over 23 angles. The distribution for the former group shows a forward maximum at 25° with a smaller one at 75° and a slight rise at the backward angles. The other group appears to show a forward maximum at about 20°, but the statistics are not good enough to establish this definitely.

§ 4. ANGULAR DISTRIBUTION OF THE ELASTICALLY SCATTERED DEUTERON GROUP

In order to count the number of particles belonging to the elastically scattered deuterons from beryllium only, histograms for the accepted tracks in the neighbourhood of its range are plotted for each angle of measurement and then fitted with Gaussian curves. The angular distribution was then calculated as previously described and represented as shown in fig. 4, where the scale of the coordinates is chosen to be the same as for the proton groups. These results are based on the measurements of a total of 6075 tracks over 16 different angles at intervals of 2½° at the secondary maximum appearing about 60°, and 10° for the rest of the distribution.

§ 5. DISCUSSION

The angular distributions of the proton groups show a pronounced increase in intensity at some small angles or in the forward direction of emission similar to those observed in other reactions (Holt and Young 1950, Burrows *et al.* 1950, Gove 1951). This small angle structure can be interpreted by the mechanism recently proposed by Butler (1950) and Bhatia and Huang (unpublished), in which they assume that in this region the reaction proceeds mainly through a stripping process. Applying the latter theory, Huby and Newns have calculated theoretical calculations of the (d, p) reaction with beryllium. The radius of interaction used in the theoretical formula was $5 \cdot 41 \times 10^{-13}$ cm. In comparing the theory with the experiment the best agreement was achieved only when the orbital angular momentum l_n brought to the nucleus by the absorbed neutron was equal to unity in the case of both of these proton groups. Any other value of l_n would fail to agree with the experiment unless an impossible value for the radius of interaction was used. The theoretical curves, together with the experimental points for the proton groups leaving the residual nucleus in the ground and first excited states, are shown in figs. 2 (*b*) and 3 (*b*) respectively. The theoretical curves were normalized so as to fit the experimental results in the neighbourhood of 25° to 40°, where the experimental distributions show large variations of intensities with respect to angles of emission. This was so chosen because the theoretical distributions for different values of l_n show marked differences in the steepest slopes along the distribution curves. Similar results can also be obtained by applying Butler's theory and assuming the radius of interaction to be $4 \cdot 8 \times 10^{-13}$ cm. In all the measured angular distributions the points corresponding to the two smallest angles (17½° and 20°) were found to be lower than would be expected from the theoretical curves. This may be due to loss of particles in the apparatus, since these angles are near to the geometrical cut-off of the apparatus, which was known to be at approximately 16°.

Information about the spins and parities of the appropriate states of the final nucleus can be thus obtained if these properties are known for the ground state of the initial nucleus. Recent work reported by Schuster and Pake (1951) gives the spin of the ground state of ^{9}Be to be 3/2. The parity of this state is known to be odd. The fact that $l_n = 1$ for both the ground and the first excited states of ^{10}Be indicates that these have even parity and spin either 0, 1, 2 or 3. Hornyak *et al.* (1950) give spin zero and even parity for the ground state of ^{10}Be. Also a gamma transition from that excited state to the ground state is reported by Rasmussen, Hornyak and Lauritsen (1949). If the assignment of spin zero, even parity to the ground state is correct, this would exclude spin zero for the excited state, but the other possibilities for the spin remain.

With regard to the secondary maximum appearing in the distribution of the elastically scattered deuterons, a theoretical estimate of the angle at which this secondary peak ought to appear has been worked out by Huby (private communication), on the assumption that at this angle the coulomb scattering is negligible compared with the nuclear scattering. Using the Born approximation with a spherically symmetric nuclear potential effective at a radius of $5{\cdot}41 \times 10^{-13}$ cm, the angle found is 64°, which is in good agreement with the observed angle.

ACKNOWLEDGMENTS

The author is greatly indebted to Dr. J. R. Holt for suggesting the problem and for his constant interest and encouragement. Thanks are also due to Dr. R. Huby and Mr. H. Newns for the theoretical calculations, and to the Egyptian Government for a maintenance grant.

REFERENCES

Burrows, H. B., Gibson, W. M., and Rotblat, J., 1950, *Phys. Rev.*, **80**, 1095.

Butler, S. T., 1950, *Phys. Rev.*, **80**, 1095.

Chadwick, J., May, A. N., Pickavance, T. G., and Powell, C. F., 1944, *Proc. Roy. Soc.* A, **183**, 1.

El-Bedewi, F. A., 1951, *Proc. Phys. Soc.* A, **64**, 947.

Gove, H. E., 1951, *Phys. Rev.*, **81**, 364.

Guggenheimer, K. M., Heitler, H., and Powell, C. F., 1947, *Proc. Roy. Soc.* A, **190**, 196.

Holt, J. R., and Young, C. T., 1950, *Proc. Phys. Soc.* A, **63**, 833.

Hornyak, W. F., Lauristen, T., Morrison, P., and Fowler, W. A., 1950, *Rev. Mod. Phys.*, **22**, 291.

Middleton, R., and Tai, C. T., 1951, *Proc. Phys. Soc.* A, **64**, 801.

Rasmussen, V. K., Hornyak, W. F., and Lauritsen, T., 1949, *Phys. Rev.*, **76**, 581.

Rotblat, J., Burrows, H. B., and Powell, C. F., 1951, *Proc. Roy. Soc.* A, in the press.

Schuster, N. A., and Pake, G. E., 1951, *Phys. Rev.*, **81**, 886.

LETTERS TO THE EDITOR

Ionization in Oxygen by μ-Mesons

We report here preliminary results of measurements of the ionization by μ-mesons in oxygen as a function of meson momentum. These show the expected logarithmic increase of ionization in the relativistic domain, in agreement with the recent measurements of Becker *et al.* (in process of publication) in krypton, and further give some indication of the onset of the polarization effects treated theoretically by Fermi (1940), Wick (1943) and Halpern and Hall (1948), which have already been observed in condensed material by Bowen and Roser (1951).

The region of high momentum ($p > 2 \times 10^{10}$ ev/c), where the polarization effect in a gas at normal pressure may be expected to become large, is the subject of work still in progress.

The present data are based on drop counts in a cloud chamber along the trajectory of μ-mesons, the momenta of which are determined in the Manchester magnetic spectrograph (see Hyams *et al.* 1950). The detailed precautions necessary in such measurements will be discussed elsewhere; briefly, the counts were made in oxygen and a water–alcohol condensant, maintained before expansion at atmospheric pressure and at a steady temperature of $20 \pm 1^{\circ}$ c, on the positive column of field separated tracks for which the condensation efficiency on the negative ions was high enough to ensure complete condensation on the positive ions. The results given in the table are based on the exclusion of large energy transfers leading to clusters of more than 30 ion-pairs, but other criteria of exclusion have been considered and the results are not sensitive to the precise procedure adopted. The standard error of the specific ionization, given in columns (5) and (6) of the table, is that obtained directly from the spread of values among the various tracks of each momentum range measurement. This spread is in good agreement with that calculated on the assumption that the distribution of secondary ionization corresponds to Rutherford scattering in the primary encounters.

The group of lowest momentum tabulated falls outside the efficient range of spectrograph; the particles used in this group were therefore selected as having a range in lead between 15 and 35 cm.

Table

(1)	(2)	(3)	(4)	(5)	(6)
$3–6\times10^{8}$	33	474·5	19,028	$40{\cdot}4\pm0{\cdot}8$	$44{\cdot}9\pm0{\cdot}9$
$6–10\times10^{8}$	9	140·2	6,237	$44{\cdot}4\pm1{\cdot}0$	$49{\cdot}6\pm1{\cdot}1$
$1–2\times10^{9}$	22	329·1	14,493	$44{\cdot}7\pm1{\cdot}2$	$49{\cdot}9\pm1{\cdot}3$
$2–3\times10^{9}$	16	241·5	11,321	$47{\cdot}6\pm1{\cdot}2$	$52{\cdot}8\pm1{\cdot}3$
$3–4\times10^{9}$	22	356·2	17,774	$49{\cdot}9\pm0{\cdot}9$	$55{\cdot}6\pm1{\cdot}0$
$4–10\times10^{9}$	14	235·1	12,427	$53{\cdot}0\pm1{\cdot}3$	$58{\cdot}8\pm1{\cdot}4$
$\sim1{\cdot}5\times10^{10}$	12	196·1	10,327	$52{\cdot}8\pm1{\cdot}1$	$58{\cdot}6\pm1{\cdot}2$
$\sim3\times10^{10}$	5	85·1	4,641	$55{\cdot}1\pm2{\cdot}8$	$60{\cdot}9\pm3{\cdot}1$

(1) Momentum range (ev/c); (2) number of tracks; (3) total track length (cm); (4) total number of drops on positive ions; (5) mean ionization per cm (observed); (6) mean ionization per cm (reduced to pure O_2, S.T.P.).

In the table the last column gives the ionization reduced to oxygen at standard pressure and temperature and also includes a correction (of the order of +4%) for the overlapping of the drop images.

The experimental values are compared with those given by the Bloch (1933) relation in the figure, where the experimental points and the theoretical curve are fitted at 2×10^{9} ev/c. The normalization of the curves yields a mean energy expenditure per ion-pair produced of $31{\cdot}0\pm0{\cdot}8$ ev. There is no significant discrepancy between the form of the theoretical curve and the observations below about 10^{10} ev/c; the last two experimental points, which refer to meson groups of higher mean momentum, appear, however, to fall significantly below the Bloch curve. A crude calculation to the approximation used by Fermi shows that the onset of polarization should take place at about 10^{10} ev/c.

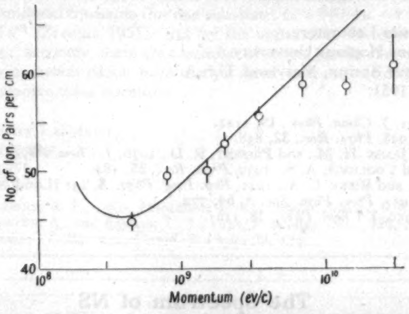

The Physical Laboratories,
University of Manchester.
16th October 1951.

S. K. Ghosh.
G. M. D. B. Jones.
J. G. Wilson.

Bloch, F., 1933, *Ann. Phys., Lpz.*, **16**, 285.
Bowen, T., and Roser, F. X., 1951, *Phys. Rev.*, **83**, 689.
Fermi, E., 1940, *Phys. Rev.*, **57**, 485.
Halpern, O., and Hall, H., 1948, *Phys. Rev.*, **73**, 477.
Hyams, B. D., Mylroi, M. G., Owen, B. G., and Wilson, J. G., 1950, *Proc. Phys. Soc.* **A**, **63**, 1053.
Wick, G. C., 1943, *Nuovo Cim.* (9), **1**, 302.

On Vibrational Transition Probabilities in Electronic Transitions

In a recent paper in this journal, Pillow (1951) has shown how distorted harmonic oscillator wave functions may be utilized to obtain vibrational transition probabilities in electronic transitions. According to Pillow, the vibrational transition probabilities obtained from these distorted harmonic oscillator wave functions are in good agreement, at least for low vibrational levels and for molecules with small anharmonicity, with those calculated from the appropriate Morse anharmonic wave function. The advantage claimed for this method is that it obviates the large amount of tedious calculation which is required to obtain the exact Morse wave function.

There is, however, another point which should not be overlooked in all these calculations. In computing the vibrational transition probabilities from the overlap integral of the vibrational wave functions, one makes the tacit assumption that the electronic moment integral $R_e = \int \psi_e' M \psi_e'' d\tau$ is independent of the internuclear distance r (Condon 1928). That this is not the case has been shown by explicit calculations of electronic transition probabilities and oscillator strengths as a function of internuclear distance (Coolidge, James and Present 1936, James and Coolidge 1939, Mulliken and Rieke 1941, Bates 1951). Whether this variation of R_e with r has any marked influence on the value of the vibrational transition probabilities has not yet been investigated in any detail. The only work along these lines of which the author is aware (Shuler 1950) seems to indicate that, at least for OH($^2\Sigma^+ \rightarrow {}^2\Pi$), the variation of R_e with r is a more important factor in the calculation of vibrational transition probabilities than is the use of more exact wave functions.

Until some additional information is available on this point, or unless one can take explicit account of this variation of R_e with r in a particular case, one probably should not place too much reliance on the numerical results of any calculation of vibrational transition probabilities in electronic transitions, regardless of how well the mechanical anharmonicity may have been taken into account.

Applied Physics Laboratory,
The Johns Hopkins University,
Silver Spring, Maryland, U.S.A.
9th October 1951.

Kurt E. Shuler.

Bates, R. D., 1951, *J. Chem. Phys.*, **19**, 1122.
Condon, E. U., 1928, *Phys. Rev.*, **32**, 858.
Coolidge, A. S., James, H. M., and Present, R. D., 1936, *J. Chem. Phys.*, **4**, 193.
James, H. M., and Coolidge, A. S., 1939, *Phys. Rev.*, **55**, 184.
Mulliken, R. S., and Rieke, C. A., 1941, *Rep. Prog. Phys.*, **8**, 231 (London : Physical Society).
Pillow, M. E., 1951, *Proc. Phys. Soc.* A, **64**, 772.
Shuler, K. E., 1950, *J. Chem. Phys.*, **18**, 1221.

The Spectrum of NS

A rotational analysis of the γ-system of NS, which was first observed by Fowler and Bakker (1932), has recently been given by Zeeman (1951). We had independently carried out an analysis of the same bands, though from spectrograms of much lower dispersion than used by Zeeman (Hilger large quartz Littrow instrument as against the 6th, 8th and 9th orders of a 21-ft. grating). Our results are in good agreement with his, and it is perhaps not without interest to note that the value of our primary constant, B'_0, namely 0·8283, differs from Zeeman's value, $0{\cdot}8267_0$, by only 0·2%.

However, apart from confirming Zeeman's results, we can add a little to the published data on this molecule. As already reported (Barrow 1950), the 0,0 and 1,0 bands of this system have been obtained in absorption. This seems to be the first time that any band with $v' > 0$ in the γ-system has been recorded. The measurements are given in the table. The values of $\Delta G'_{0,1}$ are $1386._2$ and $1387._5$ cm^{-1}. A very rough value of $x_e'\omega_e'$ can be obtained by assuming that the value of x_e' is the same as for the ground state. This gives

$x_e'\omega_e' \sim 8._{75}$ and $\omega_e' \sim 1403._5$ cm^{-1}. It may be noted that this new value of ω_e' gives, with $D=4B^3/\omega^2$, $D'=1{\cdot}16\times10^{-6}$, in poor agreement with Zeeman's experimental figure of $0{\cdot}77\times10^{-6}$. The use of the value $D'=1{\cdot}16\times10^{-6}$ together with Zeeman's values of $\Delta_2F'(K)$ would probably lead to a slightly improved determination of B_0', but the change would be very small, and it has not been thought worth while to do the calculations.

The facts about the other known system of NS, the β-system, are, in contrast, rather obscure. The transition has generally been considered to be $^2\Pi$–$^2\Pi$ by analogy with the β-system of NO. However, all our attempts at a rotational analysis from the low-dispersion plates on this basis have failed. But it has been possible to produce a partial analysis of the 2,0, 1,0, 0,0 and 0,1 bands on the assumption that each sub-band possesses a strong Q-branch. Confirmation comes from the agreement of the combination differences, $\Delta_1F''(J)$ as obtained from these bands with those got from Zeeman's measurements of the γ-system.

Table. Band-Heads in the Absorption Spectrum of NS

Head	Intensity	λ_{air} (Å)	ν_{vac} (cm^{-1})
0, 0 ^{0}P	1	2317·27	43139·1
P_2	3	15·98	165·0
P_1	2	05·28	365·3
Q_1	3	04·16	386·4
1, 0 P_2	2	2243·91	44551·2
Q_1	2	32·75	773·9

Note: These are the only bands of NS so far observed in absorption.

This, together with the fact that the apparent doublet separation in the β-bands differs considerably from that in the bands of the $^2\Sigma^+$–$^2\Pi$ system, leads us to conclude that the transition may be $^2\Delta$–$^2\Pi$ rather than $^2\Pi$–$^2\Pi$. Preliminary values of B for the upper state are: $B_v'=0{\cdot}694_5-0{\cdot}005_4(v'+\frac{1}{2})$.

Several other features of the ultra-violet spectrum of NS invite inquiry. First, the existence of perturbations in the upper state of the β-bands is suggested both by the anomalous behaviour of its vibrational constants (for one sub-state, $G'=940{\cdot}4u'-4{\cdot}8u'^2$; for the other, $G'=962{\cdot}0u'-8{\cdot}65u'^2$ (Zeeman 1951)) and by the appearance of some of the unanalysed rotational structure; secondly, there are a number of strong bands observed both by Fowler and Bakker and by ourselves which have not yet been assigned. Further work with high dispersion should resolve these questions.

Physical Chemistry Laboratory,
Oxford University.
20th October 1951.

R. F. Barrow.
A. R. Downie.
R. K. Laird.

Barrow, R. F., 1950, *Discussions of the Faraday Society*, **9**, 81.
Fowler, A., and Bakker, C. J., 1932, *Proc. Roy. Soc.*, **136**, 28.
Zeeman, P. B., 1951, *Canad. J. Phys.*, **29**, 174.

On θ Values in the Resistance of Metals

Blackman (1951) has recently pointed out that the θ values obtained from electrical resistance data are not directly related to the values obtained from specific heat data, since only longitudinal phonons interact with the electrons, at least at low temperatures. He has calculated values θ_L relating to that part of the specific heat which arises from the longitudinal phonons, that is in calculating θ_L he used the velocity of longitudinal waves, which in turn is obtained from the elastic constants.

However, an additional complication occurs in that the values of θ derived from the elastic constants relate only to the low-frequency phonon spectrum, and are related to the specific heat at low temperatures (T^3 region). The value of θ_M, associated with the maximum frequency in the Debye approximation (i.e. assuming the existence of a sharp cut-off frequency) and determining the specific heat at higher temperatures, is somewhat lower owing to the decrease of the phase velocity of the phonons with increasing frequency.

In the case of a linear chain, the ratio of the high-frequency velocity to the low-frequency velocity, and hence the ratio of the two θ values, would be $\pi/2 \sim 1{\cdot}57$, and for a three-dimensional lattice the value would probably be similar.

This dispersion of the phonon phase velocity is verified in the thermal conductivity of dielectric solids, treated elsewhere by the author (Klemens 1951). The θ value of quartz derived from the low temperature specific heat is 290° K. The value of θ which has to be substituted into the formula for the resistance due to *Umklapp* processes in order to fit the observed temperature dependence at liquid-hydrogen temperatures is about 170° K, for in this context θ refers to the maximum frequency of the transverse phonons.

In the case of electrical resistance, θ is determined by the relation between the resistance at temperatures T_1 greater than θ, and T_2 very much less than θ. At high temperatures the resistance is proportional to the total number of phonons present, i.e.

$$R \propto \int_0^{\omega_M} N(\omega)\omega^2\,d\omega \propto T^3 \int_0^{\theta_M/T} \frac{x^2\,dx}{(e^x-1)} \propto \theta_M^2 T. \qquad \ldots\ldots (1)$$

At low temperatures the resistance is due to a diffusion of electrons around the Fermi sphere in small steps proportional to ω^2. Hence

$$R \propto \int_0^{\omega_M} N(\omega)\omega^4\,d\omega \propto T^5 \int_0^{\theta_M/T} \frac{x^4\,dx}{(e^x-1)}. \qquad \ldots\ldots (2)$$

Both forms can be combined, when taking note of the appropriate multiplicative constant, by means of the Bloch–Grüneisen interpolation formula

$$R \propto T^5 \int_0^{\theta/T} \frac{x^5\,dx}{(e^x-1)(1-e^{-x})}. \qquad \ldots\ldots (3)$$

If $T_1 > \theta \gg T_2$,

$$\frac{R_2}{R_1} = 497{\cdot}6 \left(\frac{T_2}{\theta}\right)^4 \frac{T_2}{T_1}. \qquad \ldots\ldots (4)$$

If θ_R is the value obtained by fitting the resistance at high and low temperatures to (4), then, considering (1), we get $\theta_R = (\theta_L \theta_M)^{1/2} \simeq \theta_L (2/\pi)^{1/2} = 0{\cdot}8\theta_L$. It can be seen from the values tabulated that this explains, at least in part, the disagreement pointed out by Blackman between θ_L and θ_R.

Metal	Na	Li	Cu
θ_L	260	530	505
θ_R	202	260	330
$0{\cdot}8\,\theta_L$	208	425	404

There is considerable uncertainty in the value of θ_M, since the relation $\theta_M = 0{\cdot}8\,\theta_L$ applies only to a linear chain. Consequently one cannot expect close agreement. But in the case of Li, where the disagreement is considerable, the electrical resistance cannot be described by means of a single θ_R (MacDonald and Mendelssohn 1950), from which it follows that the Debye approximation is not a good description of the phonon spectrum. At higher temperatures one must choose $\theta_R \sim 360$° K to fit the observed resistance of Li.

The above considerations also explain why the θ value derived from the low-temperature specific heat, which is always less than θ_L, agrees often with θ_R, which must also be less than θ_L. But it is clear that in view of the many uncertainties involved it will be difficult to correlate the θ values obtained from the specific heat and from the resistivity.

Division of Physics,
Commonwealth Scientific and Industrial Research Organization,
Sydney, Australia.
1st November 1951.

P. G. Klemens.

Blackman, M., 1951, *Proc. Phys. Soc.* A, **64,** 681.
Klemens, P. G., 1951, *Proc. Roy. Soc.* A, **208,** 108.
MacDonald, D. K. C., and Mendelssohn, K., 1950, *Proc. Roy. Soc.* **A, 202,** 103.

Neutrons from the Spontaneous Fission of Thorium

The purpose of this letter is to resolve a point regarding the number of neutrons emitted in the spontaneous fission of thorium. The early work of Pose (1943) as reported by Segrè (1951) appears to give a value for ν, the average number of neutrons emitted per fission, of between 5 and 6. This is considerably greater than that obtained, for example, in the slow neutron induced fission of ^{235}U for which ν is $2{\cdot}5 \pm 0{\cdot}1$ (Atomics 1951).

The neutron emission from the spontaneous fission of uranium has been observed by several authors (Segrè 1951). Littler (1952) obtained a value of $59{\cdot}5 \pm 3{\cdot}3$ neutrons per gramme per hour for uranium, and coupling this with Segrè's value of the spontaneous fission rate of natural uranium (due to ^{238}U content) of $24{\cdot}8 \pm 0{\cdot}9$ per gramme per hour we obtain $\nu_U = 2{\cdot}4 \pm 0{\cdot}2$. This agrees well with the value of ν for neutron induced fission.

It seemed worth while to redetermine the number of neutrons emitted in the spontaneous fission of thorium to see if, in fact, the high figure for ν of Pose was correct. A slow neutron detector had been built similar to, but less sensitive than, one suggested by M. Goldhaber (private communication). Our apparatus consisted of a cube (of side 70 cm) of paraffin wax with a central cylindrical hole. Eight proportional counters, filled with $^{10}BF_3$ and coupled in parallel, were embedded symmetrically in the wax around the axis of the hole and the output pulses from these counters were fed to a head and main amplifier and then into a discriminator and scaler. The absolute sensitivity of the arrangement for detecting neutrons from a calibrated radium–beryllium source was about 1%. However, an accurate calibration of the sensitivity was unnecessary since, in this experiment, we simply compare the neutron emissions from known masses of uranium and thorium metal under identical geometrical conditions. The only assumption made is that the energy spectrum of the neutrons emitted in the spontaneous fission of the two nuclides is approximately the same. A cadmium cylinder was placed in the central hole of the wax and into this, in turn, were put the same number of uranium and thorium rods. The purpose of the cadmium was to eliminate any effects which might be caused by slow neutrons re-entering the uranium and causing neutron induced fissions. (With thorium such an effect is not possible.)

The apparatus was housed in a laboratory which was remote from neutron sources and the background counting rate of the neutron counters was low, being about 1 count per minute for all the eight counters. The counting rates obtained with uranium and thorium are given in the following table:

	Metal present		Background			
Wt. of metal	Total counts*	Time (min.)	Counts	Time (min.)	True counts per min.	Count/kg of metal
U 33·6 kg	4567	15	460	460	303±4·5	9·03 ±0·13
Th 23·8 kg	1219	505			1·42±0·09	0·060±0·004

* including background.

From this we see that the ratio of the neutron emissions from uranium and thorium is 153 ± 10, and since the ratio of the spontaneous fission rates of uranium and thorium is (Segrè 1951) 164 ± 13 we can say that the value of ν for thorium is, within the statistics, the same as that for uranium, i.e. $\nu_{Th}/\nu_U = 1{\cdot}07 \pm 0{\cdot}10$. This confirms then that Pose's figure of ν for thorium is too high.

We have satisfied ourselves that the contribution of neutrons due to (α, n) reactions with light element impurities in the uranium and thorium are negligible in this experiment. It is possible that Pose's determination may have been incorrect because of some impurities in the thorium used. For example, a uranium content about 1% by weight could account for the observed neutron emission.

Atomic Energy Research Establishment,
Harwell, Didcot, Berks.
14th November 1951.

F. R. Barclay.
W. Galbraith.
W. J. Whitehouse.

Atomics, 1951, **2,** No. 1, 15.
Littler, D. J., 1952, *Proc. Phys. Soc.* A, **65,** in the press.
Pose, H., 1943, *Z. Phys.*, **121,** 293.
Segrè, E., 1951, *Atomic Energy Commission Declassified Report* No. 3149.

Comparison of Geiger and Proportional Counters for Intensity Measurements in X-ray Diffraction

In a recent investigation with a counter spectrometer of the x-ray scattering from proteins, the need arose for as pure a monochromatic x-ray beam as possible without either the severe loss of available intensity entailed by the use of a plane crystal monochromator or the extra labour involved in a double scan with balanced filters. In particular, an estimate was required of that fraction of the detected radiation which was of a wavelength other than the characteristic Kα rays from the copper target.

A calcite cleavage slip was mounted on the spectrometer and the x-ray spectrum was investigated, using as a detecting device in turn a Geiger counter and a proportional counter. The latter was used in conjunction with a high gain linear amplifier and a single-channel pulse analyser adjusted so that only quanta corresponding to a narrow band of wavelengths centred on the Kα line were detected. The resulting curves are shown in fig. 1. Curve A is the intensity distribution observed with a Geiger counter and curve B that with the proportional counter, a nickel filter being mounted in front of the counter in each case in order to reduce the intensity of the Kβ line. Curve C is the intensity distribution at the x-ray tube window derived from curves A and B by correcting for the wavelength variation of the absorption in the intervening air, the nickel filter, the counter window and the counter gas. All three curves are also corrected for the variation of the reflection coefficient of calcite with wavelength (Compton and Allison 1935). For the sake of comparison the curves are plotted so as to make the intensity in the Kα line the same in each case. The total intensities in the two characteristic lines and in the continuous spectrum are compared in the table. It should be noted here that the sealed-off copper target x-ray tube was almost new and that it was operated at 30 kv d.c. In an older tube in which the target and the windows have become contaminated by tungsten, or in a self-rectifying tube operated from an a.c. supply, the ratio of energy in the continuous spectrum to that in the Kα line would be expected to be higher.

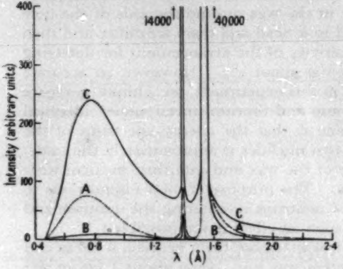

Fig. 1

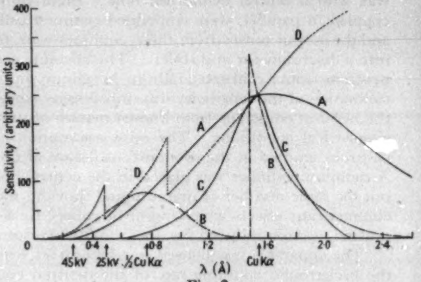

Fig. 2

	Spectrum	Geiger counter	Prop. counter
α	100	100	100
β	13·3	0·09	0·067
Continuous	18·5	3·5	0·9

The response of the conventional argon-filled Geiger counter to x-radiation of different wavelengths was calculated from published data (*Internationale Tabellen*, 1935) on the absorption coefficients of the filling and of the window (curve A, fig. 2). It will be seen that the addition of a β-filter materially improves this response curve for the case of the copper lines (curve B). The curve, however, still shows appreciable sensitivity to the first harmonic, $\lambda/2$ of CuKα, which may give rise to spurious effects. This sensitivity relative to the Kα wavelength cannot be appreciably reduced by the use of filters. A slight improvement can be effected by operating the x-ray tube at a lower voltage with consequent loss of available intensity. The short wavelength limit of the continuous spectrum is marked in fig. 2 for two different excitation voltages.

While the employment of filtered radiation combined with operation of the tube at a comparatively low voltage is adequate for many purposes, a very great improvement is achieved by substituting the proportional counter with appropriate circuits for the Geiger counter. Its response to any particular characteristic wavelength employed can be made as sharp as required. However, since the bias curve shows a spread about the centre of the selected channel, very sharp discrimination involves considerable loss of sensitivity to the Kα radiation. Fig. 2 curve C shows the response curve without nickel filter of the proportional counter used for a channel width of 3 volts when the centre of the channel at 28·5 volts corresponded to the Kα line, the external amplification being 10^6. Under these conditions approximately 50% of the Kα quanta absorbed in the counter were detected. This amount of discrimination reduces the sensitivity to the $\lambda/2$ harmonic to less than 5% of that for the Kα line itself. *The non X-ray background of the counter is then about 1 count/minute.*

The response curves for the counters may be compared with that for double-emulsion non-screen X-ray film shown in fig. 2 curve D, calculated on the basis of data given by Bromley and Herz (1950).

The proportional counter used in these experiments was specially constructed for this purpose by Messrs. 20th Century Electronics Ltd. It had a length of 10 cm and a diameter of 5 cm. Its cathode was Aquadag coated on the glass walls. Radiation entered the counter normal to its axis through a berosilicate glass bubble window. The counter was filled with argon to a pressure of one atmosphere, about 8% of ethyl alcohol being added to stabilize the gas amplification. The cathode was operated at −1750 volts, the 0·005-in. diameter tungsten wire being connected directly to the first grid of the pre-amplifier. The gas amplification under these conditions was about 10^3. The stability of the device when operated with a well-regulated power supply was in every way comparable with that of an externally quenched Geiger counter.

In those cases where monochromatization by crystal reflection is still necessary, a proportional counter offers great advantages over a Geiger counter in that its sensitivity to the $\lambda/2$ harmonic of the characteristic radiation can be made negligible and in that its background counting rate is about one-twentieth of that of a Geiger counter of comparable X-ray sensitivity.

The Royal Institution,
21 Albemarle Street,
London, W. 1.
15th November 1951.

U. W. Arndt.
D. P. Riley.

Bromley, D., and Herz, R. H., 1950, *Proc. Phys. Soc.* B, **63**, 90.
Compton, A. H., and Allison, S. K., 1935, *X-Rays in Theory and Experiment* (New York: D. Van Nostrand Company Inc.).
Internationale Tabellen zur Bestimmung von Kristallstrukturen, 1935, Vol. II (Berlin: Gebr. Borntraeger).

REVIEWS OF BOOKS

Advanced Dynamics, by E. Howard Smart. Vol. I, pp. xi+419; Vol. II, pp. xi+420. (London: Macmillan, 1951.) 40*s.* each volume.

The two volumes of the work under review embody the substance of lectures given by the late Mr. E. Howard Smart, sometime Head of the Department of Mathematics at Birkbeck College, and they are obviously the work of a man of wide and varied experience as a teacher and examiner. One of the most useful features of the work is the range and number of examples which are solved in detail to illustrate general principles and theorems; these examples form a substantial proportion of the text, and they make the work very valuable to a student who is forced to grapple with the difficulties of dynamics without much help from a teacher or supervisor. The two volumes could, for example, be recommended without hesitation to a physicist who feels his lack of knowledge of the subject, and who is, at the same time, forced to remedy this state of affairs by his own unaided efforts.

The scope of the work may be judged from the headings of the chapters. Volume I : Introductory, Fundamental dynamical principles, Rectilinear motion of a particle, Accelerations parallel to rectangular axes, Radial and transversal accelerations (central forces), Free motion under the law of inverse square, Constrained motion in two dimensions, Motion in a resisting medium, Motion of a chain in two dimensions, Motion of a particle in three dimensions; Volume II : Moments and products of inertia, Plane kinematics, D'Alembert's principle and the equations of motion, Two-dimensional motion of a rigid body (finite forces), Two-dimensional motion of a rigid body (impulsive forces), Dimensions and dynamical similarity, Motion in three dimensions, Lagrange's equations, Motion under no forces, Motion of a top or gyrostat, Hamilton's equations : general theorems on impulses, etc., Theory of small oscillations.

The work is obviously written from the standpoint of a mathematician and mainly, one suspects, with an eye on the syllabus of certain specific examinations. For a physicist, one result of these restrictions is a weakness in the treatment of those parts of the subject where physics and applied mathematics meet, and by way of illustration one may quote the disappointing chapter in Volume II on Dimensions and dynamical similarity. A second result is the omission of certain topics which are important to physicists; for example, whilst there is an exhaustive treatment of the small oscillations of a conservative system about a configuration of equilibrium, there is no mention of oscillations of finite amplitude or of non-linear oscillations.

On opening these books one is immediately struck by the absence of Clarendon type, due to the fact that the subject is treated almost entirely by resolution into Cartesian components, vector methods being ignored. This is not the place to marshal the case for and against the vector treatment of dynamics; it is sufficient to record that this work offers neither apology nor explanation for omitting the use of vector methods, and, as a physicist, the reviewer is not unsympathetic to this standpoint, if it were only because vector equations have to be translated into Cartesian language before they can be used in experimental physics.

R. M. D.

Integraltafel. Erster Teil : Unbestimmte Integral ; Zweiter Teil : Bestimmte Integrale, by W. GRÖBNER and N. HOFREITER. Pp. viii + 166 ; vi + 204. (Vienna and Innsbruck : Springer-Verlag, 1949 ; 1950.) 31*s*. ; 41*s*.

These two volumes should find their way into most reference libraries. The authors have taken advantage of earlier tables of integrals in making their compilation, and both the results taken from these and new results have all been independently checked.

Volume I contains indefinite integrals, which are presented in three groups according to the form of the integrands. These are rational functions, irrational algebraic functions and transcendental functions. In appropriate cases alternative forms are given, for example in ascending and descending powers of the variable respectively.

Volume II contains definite integrals listed according to the same arrangement as that adopted for indefinite integrals in the first volume.

The formulae and text have been photographed from a hand-written copy; although in German the script will be easily legible to the English reader. It is almost inevitable that some errors should occur in a collection of this size : the authors themselves quote three for volume I at the beginning of their second volume.

Every specialist will note some omissions from his own field, but this is understandable and needs no excuse. Nevertheless it is a little surprising to note, for example, that no indefinite integrals involving Bessel functions (of which there is a number of importance) are listed.

These criticisms will not detract from the obvious worth of a collection of this kind. Both the authors and the publishers are to be congratulated on it.

H. H. HOPKINS.

Dielectric Breakdown of Solids, by S. WHITEHEAD. (Monographs on the Physics and Chemistry of Materials.) Pp. xv+271. (Oxford: Clarendon Press, 1951.) 25*s*.

About twenty years ago Dr. Whitehead published his first treatise on dielectric breakdown. Since that time so much progress has been made both experimentally, under the leadership of Von Hippel and of the author and his colleagues, and theoretically, mainly by Von Hippel and Fröhlich, that the author has now produced an entirely new book on the subject.

Dielectric breakdown is a phenomenon of great practical importance and it has great theoretical interest. There are at least three distinct types: intrinsic breakdown takes place almost instantaneously if the electric field reaches a level at which an electronic equilibrium is no longer possible; thermal breakdown is due to the heat developed in the dielectric as Joule heat or by dielectric losses; and discharges outside the dielectric or in small cavities inside can weaken it chemically or thermally to the point of breakdown. It is the burden of Dr. Whitehead's book to set out these types, to show and to illustrate how the dielectric strength in its different aspects is measured, to summarize the results obtained and to explain the theoretical background and the detailed theories and finally to assess the importance of the different aspects of breakdown and the future trends of practice and research. In addition a discussion is given of the variation with time of dielectric strength due to diffusion and slow chemical processes.

This task is even more formidable than it may appear at first sight. The author tries to reduce to a compass of about 250 pages the contents of about 200 original papers, the scope of which includes subtle experimenting and fundamental theoretical analysis of electronic processes in dielectrics; and as original papers are, these days, usually already condensed almost beyond the limit of comprehensibility, the book makes very heavy demands on the reader's acumen. Details concerning experimental arrangements are scanty and the reader needs a great deal of imagination to get an idea how measurements are actually made and how the results given in diagrams are obtained. Even the plates showing photographs of faulty dielectrics are barely explained. The mathematical theories are given an appreciable portion of the space available; but the story is so involved that only readers with a good knowledge of the original literature may be able to follow.

The book will be warmly welcomed by those specially interested in dielectric breakdown as a clearly laid out summary of the subject written from a very high level. It is further an important book of reference for scientists interested in electronic processes in solids. It will give the reader readily an idea of the state of the subject, to the extent to which a much shorter review article could. But it will yield its full contents only to those who are prepared for a great deal of additional study. W. E.

Tensor Analysis for Physicists, by J. A. SCHOUTEN. Pp. x+275. (Oxford: Clarendon Press, 1951.) 30*s*.

This is no easy introduction to the subject of tensor analysis. The outlook of the author is that of a mathematician, and, though he is trying to write for physicists, he cannot, in the nature of things, share their outlook. As a consequence, the first part of the book will appear to many to be forbiddingly difficult, though in fact it only wants perseverance to grasp any of the ideas used. The later part of the book, where the general methods of tensor analysis are applied in turn to elasticity, classical dynamics, relativity and quantum mechanics, will be found in some ways easier to read than the earlier parts.

Much of the difficulty felt in reading work expressed in tensorial form is due to the unfamiliarity of the notation; Professor Schouten uses very clear and unambiguous symbolism, but one which makes considerable demands on the attention of the reader, who has to remember, for example, to distinguish between roman and italic numerals, as well as letters.

The book is exceptionally well produced, and is a valuable reference work to be included in any serious library of physical works. J. H. A.

CONTENTS FOR SECTION B

PAGE
Editorial 1
Prof. F. L. HOPWOOD. Water Bells 2
Dr. H. O. W. RICHARDSON. The Use of Current Sheets in the Design of Magnets to give Bounded Fields of Required Form, free from Edge Distortion . . . 5
Dr. H. O. W. RICHARDSON. The Extension of the Electrolytic Tank Method to the Study of Magnetic Fields due to Iron-clad Current Sheets in Three Dimensions 15
Dr. B. SZIGETI. On the Torsional Vibrations of Long Chain Molecules. . . . 19
Dr. N. R. TAWDE and Dr. N. RAMANATHAN. Fluorescence of Dyestuff Solutions: Viscosity and Temperature Effects 33
Dr. G. KLEIN. Optical Transmission of Certain Colloidal Solutions under Relaxation Conditions 40
Dr. R. C. FAUST. An Interferometric Method of Studying Local Variations in the Refractive Indices of a Solid 48
Dr. T. S. MOSS. Optical Properties of Tellurium in the Infra-Red 62
Mr. J. N. EASTABROOK and Dr. A. J. C. WILSON. The Diffraction of X-Rays by Distorted-Crystal Aggregates: III—Remarks on the Interpretation of the Fourier Coefficients 67
Mr. J. S. PRESTON and Mr. G. W. GORDON-SMITH. A New Determination of the Luminance Factor of Magnesium Oxide 76

Letters to the Editor:

Mr. D. J. C. YATES. A Note on some Proposed Equations of State for the Expansion of Rigid Porous Solids on the Adsorption of Gases and Vapours 80
Reviews of Books 82
Contents for Section A 86
Abstracts for Section A 87

ABSTRACTS FOR SECTION B

Water Bells, by F. L. HOPWOOD.

ABSTRACT. The author shows that when water is discharged through an annular slit above a plane water surface, the sealed 'water bells' thus formed exhibit some novel and remarkable properties not hitherto described. The primitive water bell is a dome-shaped bubble whose dimensions increase with increased rates of flow. If this is perforated with a finger the maximum diameter of the bell suddenly doubles itself. On continuously reducing the flow the expanded bubble contracts and assumes an alternating sequence of stable and semi-stable forms of great beauty. All these, when perforated, *contract* slightly. The semi-stable forms have the general appearance of a hyperboloid surmounted by a saucer-shaped depression with the annular slit at the bottom. On inflating an expanded bubble by a slow stream of small air bubbles, semi-stable forms similar to the above are produced, but possessing an additional inflection in their contours. During these changes the maximum differences of pressure do not exceed one-tenth of a millimetre of water above or below atmospheric pressure. The author shows how the apparatus can easily be modified to produce enclosing water bells. It may also be adapted to produce sonic and ultrasonic underwater vibrations.

The Use of Current Sheets in the Design of Magnets to give Bounded Fields of Required Form, free from Edge Distortion, by H. O. W. RICHARDSON.

ABSTRACT. The use of current sheets to produce static magnetic fields of required form, with freedom from edge or fringing distortion and with no stray flux, is discussed. Two types of magnet winding are considered. The first, or field-terminating type, encloses a tube of force and serves as a sharp boundary to the field. The second, or iron-shrouded

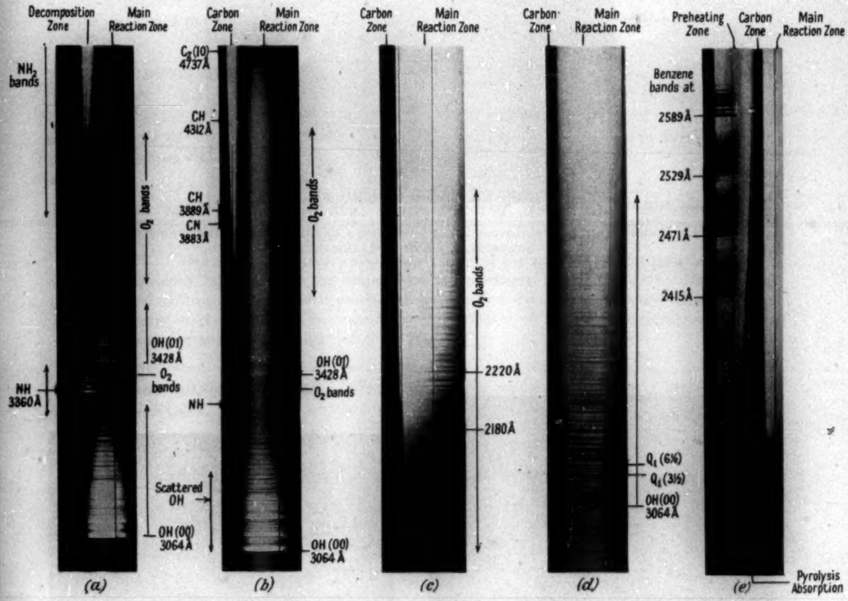
Decomposition Zone
Main Reaction Zone
NH$_2$ bands
O$_2$ bands
OH(01) 3428Å
O$_2$ bands
NH 3360Å
Scattered OH
OH(00) 3064Å
(a)
Carbon Zone
Main Reaction Zone
C$_2$(10) 4737Å
CH 4312Å
CH 3889Å
CN 3883Å
O$_2$ bands
NH
OH(01) 3428Å
O$_2$ bands
OH(00) 3064Å
(b)
Carbon Zone
Main Reaction Zone
O$_2$ bands
2220Å
2180Å
(c)
Carbon Zone
Main Reaction Zone
Q$_1$(6½)
Q$_1$(3½)
OH(00) 3064Å
(d)
Preheating Zone
Carbon Zone
Main Reaction Zone
Benzene bands at
2589Å
2529Å
2471Å
2415Å
Pyrolysis Absorption
(e)

Fig. 4. (*a*) NH_3–O_2 flame, emission (medium Hilger, zenith plate); (*b*) C_2H_4–O_2 flame, emission (medium Hilger, zenith plate); (*c*) C_2H_4–O_2 flame, absorption (medium Hilger, Q1 plate); (*d*) C_2H_4–O_2 flame, absorption (Hilger E1, process plate); (*e*) CH_4–C_6H_6–O_2 flame, absorption (medium Hilger, zenith plate).

Fig. 1. Pattern from a KBr cleavage face, upon which a thin layer of silver chloride has been evaporated. KBr [001] azimuth.

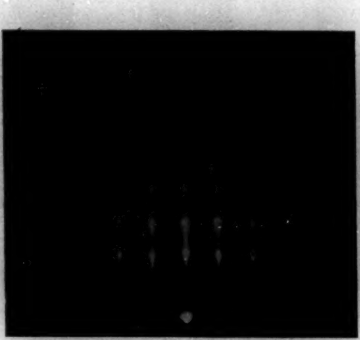

Fig. 3. Oriented TlCl on a KBr cleavage face. TlCl has an abnormal NaCl type structure. KBr [001] azimuth.

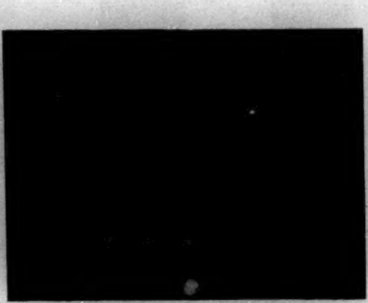

Fig. 4. TlCl layer on a mica cleavage face. Mica [010] azimuth.

type, is wound against the inner surface of an iron shroud and, with a suitable distribution of turns, can generate any required shape of field in the iron enclosure. In both types stray field can be avoided if the iron return-path is infinitely permeable, or if it is covered with an 'anti-reluctance' winding.

A discussion is given of (*a*) the uniform field, (*b*) the field whose lines of force are coaxial circles, (*c*) the synchrotron field, and (*d*) the prolate spheroidal field, whose lines are confocal ellipses.

The Extension of the Electrolytic Tank Method to the Study of Magnetic Fields due to Iron-clad Current Sheets in Three Dimensions, by H. O. W. RICHARDSON.

ABSTRACT. An application of the electrolytic tank method to plot the magnetic fields of a current sheet is described. In general, three-dimensional fields due to currents can be plotted, provided that the current is close to the surface of a piece of permeable iron.

On the Torsional Vibrations of Long Chain Molecules, by B. SZIGETI.

ABSTRACT. Simplified models are discussed for long chain molecules in which all units are equal except for one which is heavier than the others. Certain general conclusions are reached for the vibrations of such molecules. The results will be applied to the out-of-plane or torsional vibrations of long chain ketones in a following paper.

Fluorescence of Dyestuff Solutions: Viscosity and Temperature Effects, by N. R. TAWDE and N. RAMANATHAN.

ABSTRACT. The effect of viscosity and temperature of the medium on the polarization of the fluorescent light emitted by some dyestuff solutions when excited by linearly polarized monochromatic light is investigated by the visual and photoelectric methods. The variations in the polarization caused by temperature are found to depend on the concentration and molecular weight of the dyestuff.

Optical Transmission of Certain Colloidal Solutions under Relaxation Conditions, by G. KLEIN.

ABSTRACT. Formulae are derived for the variation in time of transmission of light through dilute colloidal solutions of uniaxial particles which are initially orientated by an external electric or magnetic field from the instant the field is removed. Two cases are considered: (i) particles opaque and large compared with the wavelength of light, and (ii) metallic particles small compared with the wavelength.

An Interferometric Method of Studying Local Variations in the Refractive Indices of a Solid, by R. C. FAUST.

ABSTRACT. Many small transparent solids possess local variations in their refractive indices that cannot be detected by the standard immersion methods. This difficulty has been overcome by placing the immersed solid between the two parallel, metal-coated plates of an interferometer illuminated at normal incidence by a parallel beam of white light. The immersion liquid is so chosen that its dispersion curve intersects that of the solid at some wavelength within the visible spectrum. An image of the immersed specimen is then projected on to the slit of a spectrometer, whereupon one can observe coloured fringes of equal chromatic order (channelled spectra). These fringes generally suffer a displacement on crossing from the liquid to the liquid–solid region of the interferometer; this displacement does, however, vanish at that wavelength at which the refractive index of the liquid equals that of the solid. The method is equally applicable to both isotropic and birefringent specimens, the index measurements under favourable conditions being accurate to within $\pm 0{\cdot}0001$.

The paper is illustrated by several examples, particular reference being made to the possibility of studying the skin effect in rayon fibres.

Optical Properties of Tellurium in the Infra-Red, by T. S. Moss.

ABSTRACT. The refractive index and absorption constant of tellurium layers have been measured in the near infra-red. The refractive index has been measured over the wavelength range 3 μ to 11 μ. The value extrapolated to long wavelengths is found to be 4·8; this is much higher than any other known refractive index. Absorption measurements were made for wavelengths 1 μ to 3 μ: the absorption constant is $2{\cdot}2\times10^5$ cm^{-1} at 1·0 μ, falling rapidly with increasing wavelength. Transmission measurements on bulk specimens are possible at wavelengths greater than 3·3 μ.

The Diffraction of X-Rays by Distorted-Crystal Aggregates: III—Remarks on the Interpretation of the Fourier Coefficients, by J. N. Eastabrook and A. J. C. Wilson.

ABSTRACT. The line profile of the *h*th order reflection from a set of lattice planes is known to be given by a Fourier series with coefficients $A(h, m)=N(m)J(h, m)$. The function $N(m)$ depends on the particle shapes and sizes, and $J(h, m)$ depends on the state of strain. Neither can be completely determined from the experimental Fourier coefficients for a single value of h. They have, however, different behaviours for small m, and $A(h, m)$ has an unambiguous interpretation in this region only: its initial slope gives the mean particle thickness, and its initial curvature sets a lower limit to the mean-square strain. The practical value of this interpretation is subject to two limitations: (i) the initial shape of the $A(h, m)$ curve depends on the ' tail ' of the line profile, (ii) if the crystals are large enough to contain several regions of compression and extension, probability theory shows that $J(m)$ is likely to be approximately proportional to $\exp\{-\text{const.}\ |m|\}$ for m large. Extrapolation to small m could then tend to give fictitiously small values for both particle size and strain.

The problem of obtaining the greatest possible amount of information from observed line profiles of all orders is discussed. Usually only a few orders can be measured, and the information obtainable is less, but in three special cases the Fourier coefficients of two lines can yield all information obtainable from the full set.

A New Determination of the Luminance Factor of Magnesium Oxide, by J. S. Preston and G. W. Gordon-Smith.

ABSTRACT. A simple, direct, and absolute method of reflectometry is described, avoiding the use of the inverse square law, and overcoming several of the drawbacks of the selenium photovoltaic cell which is used for the measurements. These advantages are secured through the use of calibrated apertures and certain integrating properties of the cell. The result obtained for the luminance factor for white light of an MgO smoked layer 1 mm thick was 1·01 for normal incidence and 45° view.